INTERNATIONAL SCHOOL FOR ADVANCED STUDIES

CONDENSED MATTER THEORY SECTOR

Non-local correlation in Density Functional Theory

Thesis submmitted for the degree of Doctor Philosophiæ
Academic Year 2011/2012

CANDIDATE
Riccardo Sabatini

SUPERVISOR
Prof. Stefano de Gironcoli

December 2012

SISSA - Via Bonomea 265, 34136 Trieste - ITALY

Contents

Chapter 1

Introduction

In the lest 40 years Density Functional Theory has proven to be a powerful theoretical approach to describe very heterogeneous classes of materials. Proposed back in the mid 60's by P. Hohenberg and W. Kohn[1], even in its simplest form, the Local Density Approximation[2] and the Local Spin Density Approximation[3], this theory has been remarkably successful in describing a wide range of *hard* materials, from closed packed metals to ionic crystals and semiconductors[4], and with more sophisticated approaches, such as the Generalized Gradient Approximation[5], this theory has given results in very good agreement with experiments in molecular systems, supported materials[6], surfaces[7] and complex polar systems such as ice and solutions[8].

Thanks to several efficient techniques to solve the quantum mechanical problem defined by DFT, such as plane-wave, pseudo-potentials approaches and Car-Parrinello dynamics, and thanks to the ever growing computing power now available, modern software implementations of DFT are able to address problems once considered out of reach for this technique, such as long molecular dynamics and extended systems comprising several hundreds atoms and thousands of interacting electrons[9].

In spite of its remarkable successes, among the shortcoming of this theory the treatment of non-local correlations, and dispersion interaction in general, seems to be one of the most important open issues to be addressed. Commonly named "van der Waals" forces[10], dispersion interaction is an ever present binding mechanism in

weakly bonded materials, from biological systems to rare-gas molecules. Arising from the interactions of charge fluctuations among separated chunks of matter, van der Waals forces are on the edge between classical physics and quantum effects. Dipoles generated by instantaneous charge fluctuations, due to quantum mechanical zero-point energy vibrations or thermal fluctuations, interact as classical electromagnetic dipoles with a typical $1/R^{-6}$ long range decay.

This is an inherently non-local effect that cannot be accounted for by local (LDA) or semi-local (GGA) approximations. The theoretical approach, in principle exact, to handle this kind of interaction has been developed starting from the Adiabatic-Connection Fluctuation-Dissipation Theorem[11], but even in its simplest practical application, where called Random Phase Approximation[12] (RPA) is used to simplify the treatment, the calculations are so computationally demanding that only very small test cases can be addressed in a non self-consistent way.

To overcome these limitations in recent years several solutions have been proposed, from parametrized density functionals[13, 14] to semi-empirical atomic pair-wise potentials[15], obtaining some good results[16] in specific kind of materials, but introducing a level of empiricism that deviates from the ab-initio and universal approach of the DFT.

Very recently a theoretical breakthrough has been achieved in the field of non-local interaction in DFT, with the definition of a new class of seamless non-local functionals specifically designed to handle long-range correlation. Derived from previous works of Andersson, Langreth and Lundqvist (ALL) [17] and Richardson and Ashcroft (RA)[18], the non-local functional form proposed by Langreth and coworkers[19], usually called vdW-DF, and its evolutions, such as vdW-DF2 [20], offers a robust, computationally inexpensive and very accurate method to handle dispersion interaction in an *ab-initio* approach. This non-local functionals has already been used with remarkable results in several systems, from biological interacting molecules[21], to water systems[22] and carbonaceous materials[23] reaching in several cases the accuracy level of highly accurate, and computations very expensive, theoretical quantum chemistry methods.

In this thesis we're presenting some extension and improvements of the non-local density functional approach, with the objective of building a complete set of theoretical "tools", and computational implementations, to exploit at best this powerful new scheme for soft matter applications.

1.1 Outline of the thesis

After a very short theoretical summary in Chap. 2 and Chap. 3, necessary to correctly frame the non-local density functional approach and to understand both its power and limitations, the first work we present in Chap. 4 address the implementation of stress in non-local density functionals. As an essential tool in structure prediction and characterization, thanks to the stress implementation it's possible to study, in an efficient way, the behavior of structures described by non-local functionals under pressure. As an example we report an interesting study on aminoacid crystals, a perfect benchmark considering that the molecular packing force holding together the entire crystal is mainly due to dispersion interaction between molecules.

In Chap. 5 we present a second contribution, a revision of Vydrov and Van Voorhis "VV10" density functional[24]. In 2010 these authors proposed a new flavor of non-local functional, commonly called VV10, with remarkable accuracy with respect to quantum chemistry results, and that performs better than any other non-local functional available since then. Unfortunately, due to some technical details we'll explain in the following chapters, this new functional is computationally very demanding, a property that limits its usability in practical cases. To overcome this limitation we present a modified functional form, very similar to the original VV10 definition, but such that it can be integrated in an efficient way. This new functional, called rVV10, is shown to perform as accurate as the original VV10 implementation in all the test cases, giving consistently better results than any other non-local functional in plane waves.

The final development we present, in Chap. 6, is the incorporation of non-local xc density functionals in Density Functional Perturbation Theory [25]. The ability to

correctly predict vibrational properties in soft matter is an essential feature for the understanding of many biological mechanisms, from DNA conformational changes and melting [26, 27] to odor sensing in humans[28]. DFPT is an efficient theoretical framework that allows to calculate phonon frequencies, in the linear response regime, without the need of supercells as instead required by the "frozen phonon" approach. We present an extension to DFPT for non-local functional, implemented in Quantum ESPRESSO [29] both for vdW-DF type functionals and the newly proposed rVV10, and we test this new tool in the first fully *ab-initio* prediction of soft-phonons in graphite.

To conclude, in App. A we present a computational tool developed in SISSA in the last years, Moka (MOdeling pacKage for Atomistic simulations). This Java based, open source, modeler has been build primarily to target very specific needs in atomistic simulations: high-throughput and massively parallel task handling. With a Graphical User Interface (GUI) and a Python scripting engine, this software is an ideal tool and execution daemon to interact both with a single laptop and a High Performance Computing (HPC) cluster in an effortless way. Released as a lab project of the Quantum ESPRESSO Foundation it's now available to anyone interested through the QE-Forge home page http://qe-forge.org.

Chapter 2

Theoretical framework

In this chapter we introduce shortly all the main theoretical concepts and approximations necessary to put in context our original contributions that we'll show in the following chapters. Our goal is twofold: we want both to give the necessary elements for a clear comprehension, and to explain some critical aspects that motivated our work.

2.1 Density functional theory

Before introducing density functional theory, it's useful to start with a very common approximation that help us to greatly reduce the complexity of a real atomistic problem, called the Born-Oppenheimer approximation[30]. Considering the large mass difference between protons and electrons, a useful simplification consists in treating the two problems, nuclear and electronic, as decoupled systems. In physical terms, this means considering the time scale for electron excitations (the inverse of their bandwidth) much smaller than the typical one for the ions (the inverse of the phonon frequency). With this in mind, one can describe the electronic problem considering the ions at rest, and the total wavefunction of the system became a product of two: one describing the ions and one the electrons[1].

Now, only the (complex) electronic problem remains. This is a quantum many

[1]The electronic wavefunction depends on the atomic positions only as parameters of the equation.

body problem, where the electron-electron interactions cannot be decoupled in single particle contributions and the exact solution is far too complicated to be solved exactly even for the most simple cases. The conceptual breakthrough of density functional theory lays exactly in the original definition of the electronic problem[1]: instead of working with complicated correlated wavefunctions, Hohenberg and Kohn showed that the ground state properties of the system can be defined in terms of the electronic groundstate charge density minimizing the functional

$$E\left[n\left(\mathbf{r}\right)\right] = F\left[n\left(\mathbf{r}\right)\right] + \int V_{ext}\left(\mathbf{r}\right) n\left(\mathbf{r}\right) d\mathbf{r} \tag{2.1}$$

where V_{ext} stands for the external potential, and the electronic density is defined such that its integral in all space equals the number of electron in the system

$$\int n\left(\mathbf{r}\right) d\mathbf{r} = N \tag{2.2}$$

Up to now the formulation is exact, but the functional $F[n(\mathbf{r})]$ is not known and the problem still cannot be solved. To overcome this limitation Kohn and Sham[2] proposed that the charge density n of the system can be obtained solving an auxiliary problem of non-interacting electrons, described by a set of single particle orthonormal wavefunctions $\psi_i\left(\mathbf{r}\right)$ with energy ϵ_i. In this framework the charge density is equal to

$$n\left(\mathbf{r}\right) = 2\sum_{n=1}^{N/2} \left|\psi_i\left(\mathbf{r}\right)\right|^2 \tag{2.3}$$

In the Kohn and Sham formulation the unknown functional $F[n(\mathbf{r})]$ is decomposed in three parts, as shown here

$$F\left[n\left(\mathbf{r}\right)\right] = T_0\left[n\left(\mathbf{r}\right)\right] + \frac{1}{2}\int \frac{n\left(\mathbf{r}\right) n\left(\mathbf{r}'\right)}{\left|\mathbf{r}-\mathbf{r}'\right|} d\mathbf{r} d\mathbf{r}' + E_{xc}\left[n\left(\mathbf{r}\right)\right] \tag{2.4}$$

$$T_0\left[n\left(\mathbf{r}\right)\right] = -2\frac{\hbar^2}{2m}\sum_{n=1}^{N/2} \int \psi_i^*\left(\mathbf{r}\right) \frac{\partial^2 \psi_i}{\partial \mathbf{r}^2} d\mathbf{r} \tag{2.5}$$

where E_{xc} is the exchange and correlation (xc) term, T_0 is the non-interacting

electron kinetic energy and the integral represents the Hartree term, describing the classical electrostatic Coulomb interaction. All the many-body complexity of electron-electron interaction is now contained in the single term $E_{xc}[n(\mathbf{r})]$ representing a small fraction of the entire energy contribution, a condition that suggests how its approximations will hopefully be less significant for the full problem.

The search for the ground state of a system is now stated as a minimization problem for the functional over the charge distribution, defined by the non-interacting electron wave functions. Similarly to the Hartree-Fock approach it's simple to build a set of non-linear equations, 2.6, 2.7 and 2.8, where the single particle wave functions ψ_i take the name of Kohn-Sham (KS) wave functions.

$$H_{KS}\psi_i(\mathbf{r}) = \left[-\frac{\hbar^2}{2m}\frac{\partial^2}{\partial \mathbf{r}^2} + V_{KS}(\mathbf{r})\right]\psi_i(\mathbf{r}) = \epsilon_i\psi_i(\mathbf{r}) \tag{2.6}$$

with

$$V_{KS}(\mathbf{r}) = V_{ext}(\mathbf{r}) + e^2\int\frac{n(\mathbf{r}')}{|\mathbf{r}-\mathbf{r}'|}d\mathbf{r}' + v_{xc}(\mathbf{r}) \tag{2.7}$$

$$v_{xc}(\mathbf{r}) = \frac{\delta E_{xc}[n]}{dn(\mathbf{r})} \tag{2.8}$$

The solution of this problem has to be defined self-consistently since the potential V_{KS} depends on the charge density itself. The ground state energy is the objective of the minimization and is defined in Eq. 2.9, where E_N represents the electrostatic energy due to the lattice.

$$\begin{aligned} E(\{\mathbf{R}\}) = {} & T_0[n(\mathbf{r})] + \frac{e^2}{2}\int\frac{n(\mathbf{r})\,n(\mathbf{r}')}{|\mathbf{r}-\mathbf{r}'|}d\mathbf{r}d\mathbf{r}' + E_{xc}[n(\mathbf{r})] \\ & - \int V_{ext}(\mathbf{r})\,n(\mathbf{r})\,d\mathbf{r} + E_N(\{\mathbf{R}\}) \end{aligned} \tag{2.9}$$

Once the ground state energy is obtained, and hence the ground state charge distribution defined, several important properties can be derived in a simple way. For example, being the DFT defined as a variational problems, we can apply the Hellmann-Feynman theorem to obtain the forces acting on each atom m with a simple

functional derivative

$$F_{x_m} = -\frac{\partial E}{\partial x_m} = -\langle\psi|\frac{\partial \hat{H}}{\partial x_m}|\psi\rangle \tag{2.10}$$

2.2 Exchange and correlation approximations

As we said before, all the complexity of the many-body electron-electron interaction is now contained in the exchange and correlations E_{xc} functional. It's clear that the goodness of a density functional theory calculation is directly connected to which kind of E_{xc} form we adopt, and in the last decades several candidates have been proposed.

The very first class of exchange and correlations functionals dates back in 1965, and it's based on a very strong approximations, the so called Local Density Approximation[31, 32]. In this formulation the xc energy of a real system it's considered to behave locally as in an uniform (homogeneous) electron gas (HEG) having the same density. The functional form is expressed in a simple way by

$$E_{xc}^{LDA}\left[n\left(\mathbf{r}\right)\right] = \int \epsilon_{xc}^{hom}\left(n\left(\mathbf{r}\right)\right) n\left(\mathbf{r}\right) d\mathbf{r} \tag{2.11}$$

where ϵ_{xc}^{LDA} is the exchange and correlation energy density per particle in an homogeneous electron gas of density $n(\mathbf{r})$. Several flavors of LDA have been proposed in history, with the main differences based on how the ϵ_{xc}^{LDA} is parametrized but he most accurate ones are parametrization based on very accurate Quantum Monte Carlo simulations and can be considered basically exact. From the energy functional it's possible to derive the potential to be used in the self-consistent KS problem, reported here

$$v_{xc}^{LDA}\left(\mathbf{r}\right) = \frac{\delta E_{xc}^{LDA}[n]}{\delta\left(\mathbf{r}\right)} = \left.\frac{\partial F_{xc}[n]}{\delta n}\right|_{n=n(\mathbf{r})} \tag{2.12}$$

The LDA approximation, despite the strong simplification for the complex electronic interactions problem, was a remarkable success for many practical applications. Clearly, LDA works best when the charge distribution can be roughly approximated

as homogeneous in the system, and for many materials this proves to be a reasonable condition. From metallic bulks[33] to semiconductors[4], LDA even today is used with very good agreement to experimental values, an impressive result for such a simple approximation.

Nevertheless, when the charge distribution is more localized, for example in strong covalent bindings, or where the local approximation is not enough, as with dispersion interactions, the LDA in not enough to describe the system and more sophisticated approximations are needed. To overcome this shortcomings, a new class of functionals have been proposed during the years, designed to account as well for local variations of the charge, a semi-local approach called Generalized Gradient Approximation. In this case the exchange and correlations functional depends not only on the charge, but on the gradient of the charge as well, and the functionals are generally defined in this form

$$E_{xc}^{GGA}\left[n\left(\mathbf{r}\right),\nabla n\left(\mathbf{r}\right)\right]=\int\epsilon_{xc}^{GGA}\left(n\left(\mathbf{r}\right),\left|\nabla n\left(\mathbf{r}\right)\right|\right)n\left(\mathbf{r}\right)d\mathbf{r} \tag{2.13}$$

where the corresponding potential can be expressed as

$$v_{xc}^{GGA}\left(\mathbf{r}\right)=\frac{\delta E_{xc}^{GGA}[n]}{\delta n\left(\mathbf{r}\right)}=\left(\frac{\partial F_{xc}[n]}{\partial n}-\sum_{\alpha=1}^{3}\partial_{\alpha}\left(\frac{\partial F_{xc}[n]}{\partial\left(\partial_{\alpha}n\right)}\right)\right)\Bigg|_{n=n(\mathbf{r})} \tag{2.14}$$

Here $F_{xc}\left(n,\left|\nabla n\right|\right)=\epsilon_{xc}^{GGA}\left(n\left(\mathbf{r}\right),\left|\nabla n\left(\mathbf{r}\right)\right|\right)$ and ∂_{α} stands for the αth component of the gradient. This new approximation solves part of the critical issues found with LDA and has been successfully applied on surfaces, molecules and covalent bonded solids. Many different forms for $\epsilon_{xc}^{GGA}\left(n\left(\mathbf{r}\right),\left|\nabla n\left(\mathbf{r}\right)\right|\right)$ have been proposes, the most common being the PBE[5] one, but even the GGA suffers a very fundamental problems: it's still a semi-local approximation that by construction does not account for long-range interactions.

2.2.1 Adiabatic connection formula

There is anyway another approach, exact in principle, to define the complicated exchange and correlation functional, derived independently by Langreth and Perdew[34], and by Gunnarsson and Lundqvist[35] usually called *Adiabatic Connection Formula*. The idea consists in defining E_{xc} functional starting from a non interacting system and then slowing re-introducing the interaction in an adiabatic way.

Let's consider a fictitious systems of N electrons where Coulomb interaction between the particles v_{int} is modulated by a parameter λ with $(0 \leq \lambda \leq 1)$, immersed in an external local potential $v_{ext}^{\lambda}(\mathbf{r})$ such that $n_\lambda = n$. The full hamiltonian of the systems is then

$$H_\lambda = v_{ext}^{\lambda}(\mathbf{r}) + \lambda v_{int} \tag{2.15}$$

In the limit of $\lambda = 0$ the system is exactly a Kohn-Sham system of non-interacting electrons, and the external potential became $v_{ext}^{\lambda=0} = v_{KS} = v_{ext} + v_H + v_{xc}$. We can now study the variation of the energy with respect to λ, and thanks to the Hellmann-Feynman theory we can define this variation as

$$\frac{\partial E(\lambda)}{\partial \lambda} = \frac{\partial}{\partial \lambda}\langle \Psi^\lambda | H_\lambda | \Psi^\lambda \rangle = \langle \Psi^\lambda | v_{int} | \Psi^\lambda \rangle + \langle \Psi^\lambda | \frac{\partial v_{ext}^{\lambda}}{\partial \lambda} | \Psi^\lambda \rangle \tag{2.16}$$

where Ψ^λ is the ground state of H_λ. Integrating this equation over λ we obtain

$$E_{\lambda=1} = E_{\lambda=0} + \int_0^1 d\lambda \langle \Psi^\lambda | v_{int} | \Psi^\lambda \rangle + \int_0^1 d\lambda n(\mathbf{r}) \frac{\partial}{\partial \lambda} \left[v_{ext}(\mathbf{r}) - v_{KS}(\mathbf{r}) \right] \tag{2.17}$$

where $v_{KS}(\mathbf{r}) = v_{ext} + v_H + v_{xc}$. With this results we can finally define the exchange and correlation functional E_xc as

$$E_{xc} = \int_0^1 d\lambda \left(\langle \Psi^\lambda | v_{int} | \Psi^\lambda \rangle - E_H \right) \tag{2.18}$$

which is customary written as[35]

$$E_{xc} = \frac{1}{2} \int d^3r \frac{n(\mathbf{r}) n_{xc}(\mathbf{r}, \mathbf{r}')}{|\mathbf{r} - \mathbf{r}'|} \tag{2.19}$$

where $n_{xc}(\mathbf{r}, \mathbf{r}')$ in known as the exchange-correlation hole[35]. This xc-hole represents the conditional probability of the charge, or, better stated, the probability of finding an electron at r' given that there is one at r. In the physical sense represents the "hole" that an electrons "digs" for itself in the surrounding density. Another expression, using the pair density function $n_2(\mathbf{r}, \mathbf{r}')$ for the exchange-correlation hole is usually given as $n_{xc}(\mathbf{r}, \mathbf{r}') = n_2(\mathbf{r}, \mathbf{r}')/n(\mathbf{r}) - n(\mathbf{r}')$.

This formulation, exact in principle, is the starting point for a powerful and accurate approach called Random Phase Approximation, an method known to account for long-range correlation effects, but so computationally expensive that its practical use even today is limited to very small systems. This will be discussed in detail in Chap. 3.

2.3 Phonons with Density Functional Perturbation Theory

In Chap.6 we'll show our work on phonons calculations with non-local functionals, and in this section we want to review very shortly the theoretical concepts needed to understand the derivation we'll present.

There are several approaches on how to calculate vibrations frequencies, "frozen phonon" techniques, molecular dynamics time averages over trajectories or Density Functional Perturbation Theory (DFPT)[25]. While the first two do not need any theoretical extension on basic DFT, they're both very expensive and require either big supercells or long molecular dynamics simulations.

DFPT[25] is an elegant theoretical development that allows us to calculate linear response properties of system to an external perturbation, starting from the ground state solution of the Kohn-Sham problem. In DFPT the responses to perturbations of different wavelengths are decoupled, allowing us to calculate phonon frequencies

at any wave vectors $\mathbf{q}$ without the use of supercells and with a computational cost independent of the phonon wavelength.

Before introducing DFPT, we review some very basic equations that define the phonon problem. For a system near its equilibrium geometry, the harmonic approximation applies and the nuclear Hamiltonian reduces to the Hamiltonian of a system of independent harmonic oscillators, called normal modes. Normal mode frequencies, ω, and displacement patterns, U_α for the αth Cartesian component of the Ith atom, are determined by the secular equation

$$\sum_{J,\beta} \left(C_{IJ}^{\alpha\beta} - M_I \omega^2 \delta_{IJ} \delta_{\alpha\beta} \right) U^\beta = 0 \tag{2.20}$$

where $C_{IJ}^{\alpha\beta}$ is the interatomic force constant (IFC) matrix element defined by

$$C_{IJ}^{\alpha\beta} = \frac{\partial^2 E(\mathbf{R})}{\partial R_I^\alpha \partial R_J^\beta} = -\frac{\partial F_I^\alpha}{\partial R_J^\beta} \tag{2.21}$$

Remembering that in DFT we can apply Hellmann-Feynman theorem, forces can be calculated with a simple derivation of the functional energy Eq.2.9 with respect to the atomic positions

$$-F_I = +\frac{\partial E}{\partial R_I} = \int n(\mathbf{r}) \frac{\partial V_{ext}(\mathbf{r})}{\partial \mathbf{R}_I} \mathrm{d}\mathbf{r} + \int \frac{\delta E(\{\mathbf{R}\})}{\delta n(\mathbf{r})} \frac{\partial n(\mathbf{r})}{\partial \mathbf{R}_I} \mathrm{d}\mathbf{r} + \frac{\partial E_N(\{\mathbf{R}\})}{\partial \mathbf{R}_I} \tag{2.22}$$

where the second term vanishes being in a minimum of the energy with respect to the charge distribution. We can now derive an explicit expression for IFC, differentiating the forces with respect to the nuclear coordinate

$$\frac{\partial^2 E(\{\mathbf{R}\})}{\partial \mathbf{R}_I^\alpha \partial \mathbf{R}_J^\beta} = \int \frac{\partial n(\mathbf{r})}{\partial \mathbf{R}_J^\beta} \frac{\partial V_{ext}(\mathbf{r})}{\partial \mathbf{R}_I^\alpha} \mathrm{d}\mathbf{r} + \delta_{IJ} \int n(\mathbf{r}) \frac{\partial^2 V_{ext}(\mathbf{r})}{\partial \mathbf{R}_I^\alpha \partial \mathbf{R}_J^\beta} + \frac{\partial^2 E_N(\{\mathbf{R}\})}{\partial \mathbf{R}_I^\alpha \partial \mathbf{R}_J^\beta} \tag{2.23}$$

To obtain the IFC not only the ground state charge is needed, but also it's linear variation with respect to the nuclei displacement. This can be obtained with a linear

variation of the KS equation for the density in (Eq.2.3)

$$\frac{\partial n(\mathbf{r})}{\partial \mathbf{R}_I} = 4\mathrm{Re}\sum_{n=1}^{N/2} \psi_n^*(\mathbf{r}) \frac{\partial \psi_n(\mathbf{r})}{\partial \mathbf{R}_I} \tag{2.24}$$

and the derivatives of the KS wave functions are similarly obtained with a linear variation of Eq.2.6, resulting in

$$\left(H_{KS} - \epsilon_n\right) \frac{\partial \psi_n(\mathbf{r})}{\partial \mathbf{R}_I} = -\left(\frac{\partial V_{KS}(\mathbf{r})}{\partial \mathbf{R}_I} - \frac{\partial \epsilon_n}{\partial \mathbf{R}_I}\right) \psi_n(\mathbf{r}) \tag{2.25}$$

with

$$\frac{\partial V_{KS}(\mathbf{r})}{\partial \mathbf{R}_I} = \frac{\partial V_{ext}(\mathbf{r})}{\partial \mathbf{R}_I} + e^2 \int \frac{1}{|\mathbf{r} - \mathbf{r}'|} \frac{\partial n(\mathbf{r}')}{\partial \mathbf{R}_I} \mathrm{d}\mathbf{r} + \int \frac{\delta v_{xc}(\mathbf{r})}{\delta n(\mathbf{r}')} \frac{\partial n(\mathbf{r}')}{\partial \mathbf{R}_I} \mathrm{d}\mathbf{r} \tag{2.26}$$

The set of equations Eq.2.24, Eq.2.25 and Eq.2.26 defines another self consistent problem, very similar to the KS one, that is the essence of the DFPT technique. From the ground state energy a linear variation of the charge is calculated for a specific mode (defined by a set of nuclear translations), the linear variations of the wavefunctions can be calculated and the potential updated. This process can iterate until preferred precision is achieved, and the IFC matrix finally calculated.

Chapter 3

Non-local correlation

In this chapter we present some detailed theoretical advancement to handle dispersion interaction in density functional theory. We'll introduce rapidly the random phase approximation and we'll review other common methods to account for dispersion interactions in DFT. In the last section we'll introduce a fundamental breakthrough achieved in very recent years with the formulation of non-local functionals. We'll discuss some important details of these new functionals, presenting an efficient interpolation scheme recently proposed. This chapter will be of fundamental importance to understand all the original contribution we'll discuss later, all of them based on non-local functional theory.

3.1 The failure of local functionals

To better understand why local and semilocal functionals fail to predict the correct long-range behavior, it's worthwhile to introduce a very simple picture of vdW interactions between two separated neutral spherical atoms A and B.

In this scheme the atoms separation $R >> d$ is much larger than the atomic size d, a limit that ensure that the corresponding wavefunctions are not overlapping[1], and atoms are described by dipolar polarizabilities equals to α_A and α_B respectively.

[1] As we'll see later, this limit will be an important reference for the non-local functionals previously mentioned

The zero-point motion of the electrons in these atoms can generate an instantaneous dipole in one of them, the first one A, with intensity d_A. This dipole will induce a charge reconfiguration in the second atom, generating a new dipole of the order $d_B = \alpha_B d_A R^{-3}$. The non-retarded Coulomb interaction energy between this two dipoles has a nonzero average value that can be estimated[36] as

$$E = -C_6^{AB} R^{-6}, \qquad C_6^{AB} = K\hbar\omega_0 \alpha_A \alpha_B \tag{3.1}$$

where C_6, called the "Hamaker constant", is a commonly studies quantity to asses the importance of dispersion interactions (the dimensionless constant K is not specifiable from this qualitative argument). Even with this very simple electromagnetic model we recollect an important feature of the vdW interaction: the long range dependence goes as R^{-6}. Qualitatively this can be understood as arising from two actions of the dipolar field, proportional to R^{-3}, suggesting that this approach needs a second-order perturbations theory, as we'll see later.

Now let's focus on how previously explained DFT functionals can cope with this kind of interactions. The electrostatic field of the two separated neutral atoms decays exponentially with distance, and this is the reason why this term in DFT cannot account for the long-range vdW interactions.

For the exchange and correlation term, things can be better analyzed using the correlation hole density previously introduces (the correlation part of Eq.2.19). The induced dipole on the second atom in the picture above is represented by a very distant part of the correlations hole density $n_c(\mathbf{r}'|\mathbf{r})$, it's in fact a conditional probability: only if an electron is found at a specific $\mathbf{r}$, thus generating the dipole d_A, the charge distortion on the second atom B at $\mathbf{r}'$ it's possible.

Since both the LDA and GGA are mean-field approaches, where the charge is considered always in a local (or semi-local) approximations, the only long-range "tail" they can predict it's when a distortion of the density of each atom is present, a distortion described in both theories to decay exponentially with separation, falling in the same problem of the electrostatic term discussed before. In conclusion LDA

and GGA are focused on the environment of a single point in space, an approximation that holds for short range correlations but fails for the long-range ones, as in the case of the vdW interactions.

3.2 The limitations of RPA

As briefly discusses before, there is an *ab-initio* way to handle the complex E_{xc} term, that we'll briefly introduce here. Thanks to the adiabatic connection formula of Eq.2.18, all the many-body electron problem can be represented by a single term, the xc hole $n_{xc}(\mathbf{r}, \mathbf{r}')$. To obtain a usable definition for the energy, we need an approximation for the hole, or similarly for the pair-density function.

A robust relation that (partially) solves this issue is found in the fluctuation-dissipation theorem[37], that applied in conjunction to the adiabatic connection formula is most commonly addressed as Adiabatic-Connection Fluctuation-Dissipation Theory [38] (ACFDT). In this section we'll introduce very rapidly this approach, which is much more complicated and needs several mathematical steps to be fully justified, we point the reader to the recent literature for more insights[39, 12].

To obtain the RPA energy functions expression, we first introduce the time-dependent density response $\delta n(\mathbf{r}, t)$ to an applied potential $\delta v(\mathbf{r}, t)$, formally given by the first-order Taylor expansion

$$\delta n(\mathbf{r}, t) = \int d^3 r \, \chi(\mathbf{r}, \mathbf{r}'; t - t') \delta v(\mathbf{r}, t) \tag{3.2}$$

In the last equation $\chi(\mathbf{r}, \mathbf{r}'; t - t') = \delta n(\mathbf{r}, t)/\delta v(\mathbf{r}, t)$ is the many-body linear response kernel of the system, a conceptually simple quantity that can be directly compared with experiments since the response $\delta n(\mathbf{r}, t)$ is in fact a measurable property. Now, the relation between the Fourier component of the linear response kernel $\chi(\mathbf{r}, \mathbf{r}'; \omega)$ and the pair-density $n_2(\mathbf{r}, \mathbf{r}')$ is given by the fluctuation-dissipation theorem, here reported

$$\oint_C \frac{d\omega}{2\pi i}\chi(\mathbf{r},\mathbf{r}';\omega) = n_2(\mathbf{r},\mathbf{r}') - n(\mathbf{r})n(\mathbf{r}') + \delta^3(\mathbf{r}-\mathbf{r}')n(\mathbf{r}) \tag{3.3}$$

With the aid of the ACFDT, the equation defining the exchange and correlation functional E_{xc} obtained with Eq.2.18 can be expressed as [2]

$$E_{xc} = -\int_0^1 d\lambda \int_0^\infty \frac{du}{2\pi}\mathrm{Tr}\left[\chi_\lambda(iu)V\right] - E_{self} \tag{3.4}$$

where $V(\mathbf{r},\mathbf{r}') = 1/|\mathbf{r}-\mathbf{r}'|$, E_{self} is the Coulomb self-energy of all the electrons and where χ_λ is the response function with coupling strength λ. The Random Phase Approximation assumes that the λ dependence of χ_λ only comes from the electrostatic response of the system without any *xc* contribution to the response. This lets us express the RPA exchange and correlation functional as

$$E_{xc} = \int_0^\infty \frac{du}{2\pi}\mathrm{Tr}\left[\ln(1-\tilde{\chi}(iu)V)\right] - E_{self} \tag{3.5}$$

RPA has demonstrated to account correctly for long range interactions, and coupled to a short range local approximation such as LDA, as proposed by Kurth and Perdew[40], is one of the most sophisticated *ab-initio* method today available in DFT to handle this kind of interactions. Unfortunately, although correct in principle, the computational effort is so demanding that its practical use is severely limited.

The only applications even nowadays consist in non-self consistent addition to the ground state energy, obtained either by LDA or Exact Exchange (in this case the approach usually takes the name of EXX/RPA) applied only to very small systems.

3.3 Other approaches

Due to the complexity of the fully *ab-initio* treatment, in the last years several approximations and techniques have been proposed to handle non-local correlation and long-range interactions, mostly requiring some empiricism to be added to the calcu-

[2] As said, several technical details are omitted in the derivation, but the conceptual argumentation it's sufficient to grasp the fundamental logic of the theory.

	Corrections	R^{-6}	Empiricism	Cost
Parametrized DF	$V = V_{KS}$	No	Medium	Low
1ePOT	$V = V_{KS} + V_{1e}$	No	High	Low
DFT-D	$E = E_{KS} + E_{pair}$	Yes	Medium	Low
vdW-DF	$V = V_{KS} + V_{nl}$	Yes	Low	Medium

Table 3.1: Few characteristics (see text) of the different DFT methods to handle non-local correlation and dispersion interactions discusses in the chapter.

lations.

The most common techniques used today can be categorized in four classes, depending on how they are integrated in DFT framework, as reported in Tab.3.3. In this section we'll review very briefly the first three of them, and in the next one we'll focus on vdW-DF, a recent development that will be the starting point for the works presented in this thesis.

Parametrized density functionals

Modern highly parametrized density functionals, such as hybrid functionals[14] or meta-GGA[41] functionals, are a class of xc-functionals where several contributions such as LDA, GGA or Hartree-Fock (HF) are summed together with specific relative weights. The idea is that by tuning the different repulsive and attractive contributions in these functionals parts we can "emulate" the medium-range non-local dispersion interactions without any new term other than the usual ones already present in density functional calculations.

There exists a very dense "forest" of these parametrized density functionals in literature, and we'll show just some selected examples to let the reader have the feeling for this methodology. Defining the HF exchange energy functional as

$$E_x^{\mathrm{HF}} = \frac{1}{2}\sum_{i,j}\int\int \psi_i^*(\mathbf{r_1})\psi_j^*(\mathbf{r_1})\frac{1}{r_{12}}\psi_i(\mathbf{r_2})\psi_j(\mathbf{r_2})d\mathbf{r_1}d\mathbf{r_2} \tag{3.6}$$

hybrid functionals are defined as a mixture of LDA and GGA with some Hartree-

Fock contribution. A very famous example is the Becke, 3-parameter, Lee-Yang-Parr [42] (B3LYP) functionals, defined as

$$E_{xc}^{\mathrm{B3LYP}} = E_{xc}^{\mathrm{LDA}} + a_0(E_x^{\mathrm{HF}} - E_x^{\mathrm{LDA}}) + a_x(E_x^{\mathrm{GGA}} - E_x^{\mathrm{LDA}}) + a_c(E_c^{\mathrm{GGA}} - E_c^{\mathrm{LDA}}) \quad (3.7)$$

where a_0, a_x and a_c have been defined by fitting the results on a set of atomization energies, ionization potentials, proton affinities, and total atomic energies. Other important examples are the X3LYP[43], HSE[44] and the original Becke implementation[14]. Another subclass of hybrid functionals, the meta-hybrid GGA, where the ϵ_{xc} depends also on the non-interacting kinetic energy density $\tau_S(\mathbf{r}) = 1/2\sum_{i\mathbf{k}} |\nabla\phi_{i\mathbf{k}}(\mathbf{r})|^{\mathbf{2}}$ includes the Tao-Perdew-Staroverov-Scuseria[45] (TPSSh), the mPW1PW parameterizations proposed by Adamo and Barone [46] and all the M06[47] suite of functionals.

These functionals can give good results in several systems, such as DNA bases[48], rare-gas complexes [49], water complexes [49] and many others [50]. Nevertheless these approaches fails in a non-systematic way in many other examples where dispersion interaction is important, giving inaccurate asymptotic behavior for large internuclear separations. The highly specific correct results are thus arising from the fortuitous correct balance of HF and GGA/LDA contributions for the specific case, and not from the ability to correctly describe the non-local interactions.

DFT-D: DFT plus dispersion

The idea behind DFT-D is to treat the complex many-body dispersion interactions problem out of the DFT framework using a semi-classical approximation. This method is not defined as a density functional acting on the electronic charge of the system, but a correction to the total energy calculated using the nuclei's relative distances and some semi-empirical parameters.

For DFT-D as well several different approximations have been proposed, but the general formalism can be summarized in the following equation

$$E_{\text{disp}}^{DFT-D} = -\sum_{AB}\sum_{n=6,8,10...} s_n \frac{C_n^{AB}}{R_{AB}^n} f_{damp}(R_{AB}) \tag{3.8}$$

where the sum is over all atom pairs in the system, C_{AB} denotes the averaged dispersion coefficient of order n (n = 6, 8, 10, . . .) for atom pair AB and R_{AB} is their internuclear distance and finally s_n is the global GGA scaling factor. For $n >= 6$ the asymptotic behavior is correctly described by this approximation, and in order to avoid double counting and singularities for small R a damping function f_{damp} is used, where the shape and cut-off radius is a matter of active research[51, 52]. In these methods both the C_n and the damping function parameters are calculated with quantum chemistry methods on selected atomic configurations and used in DFT calculations depending on the chemical environment of the selected atoms.

Some of the most widely used implementations are the DFT-D3 method proposed by Gimme[16] (where the DFT-D3 is the most recent refinement of DFT-D2), the TS-vdW from Tkatchenko and Scheffler[53] and the dipole-exchange hole model (XDM) of Becke and Johnson[54]. These modern implementations have been successfully tested in very different environments, from biological molecules to π-stacked systems, showing very consistent results and good transferability.

A very recent improvement based on this approach, that partially solves the empiricity added to the calculation, has been proposed by Silvestrelli [55] where all the parameters necessary to define Eq. 3.8 are calculated starting from the Maximally Localized Wannier function (MLWF) formalism. In his approach WF are calculated starting from the ground state energy of a semi-local DFT calculation and then used to derive necessary cutoffs and C_6 parameters in an *ab-initio* approach.

In all this methods non-local correlation is correctly embedded in the calculations, by construction of the C_n parameters, but added to the DFT scheme in a non-self consistent way that does not suite well the theory in general. In fact, the ground state charge distribution obtained with this methods does not contain any information on the non-local correlation present in the system [3], a problems that strongly limits its

[3] As some authors noted the non-local correlation is supposed to affect very little the ground state charge distribution, but any DFT extension based on energy derivatives in DFT-D calculation could

use to extract more sophisticated electronic properties of the system studied.

One-Electron Corrections

Inspired by the very good performances of the DFT-D methods another approach proposed in literature is the 1ePOT, consisting in the definition of single-atom potentials to be added to the full V_{KS}. In this way the dispersion interaction behavior will be included in the total charge in a self consistent way, in principle a much more flexible and extensible approach than DFT-D.

Dispersion-corrected atom-centered potentials (DCACP) proposed first by von Lilienfeld [56], and implemented as atomic pseudo potential for core electrons, has been demonstrated to perform rather well for noble gas dimers, argon-benzene complexes and several other systems. Some new implementations[57, 58] based on DCACP showed good results on the entire set S22 but no reported case for bigger intermolecular system, or more complex bindings, are reported.

Even if this method achieved some success, and it's more coherent with the DFT framework, it's still a semi empirical approximation that asymptotically do not show the correct R^{-6} behavior (graphite sheets are underbonded by 20% in DCACP). Moreover the definition of parameters necessary to define a single atomic potential require such long and tedious human effort that only potentials of very few elements are now available.

3.4 Non-local functionals

The last approach we present in this (short) theoretical review of dispersion interaction it's a breakthrough, presented in its final derivation by Dion and colleagues in 2004 [19], that will be the focus of the works we'll present in the following chapters. To better understand the physical meaning of this approximation, we have to go back to the simple example presented in Cap.3.1, where we introduced in a qualitative way

not be defined as a simple functional derivative.

the long-range interaction energy among separated neutral atoms[4].

It's in fact possible to derive a precise quantitative formula for the interaction energy previously discussed, the second order dispersion interactions energy $E^{(2)}$

$$E^{(2)} = -\frac{3\hbar}{\pi}\int_0^\infty \mathrm{d}u \int_A \mathrm{d}^3 r \int_B \mathrm{d}^3 r' \frac{\alpha(\mathbf{r}, \mathrm{i}u)\alpha(\mathbf{r}', \mathrm{i}u)}{|\mathbf{r}-\mathbf{r}'|^6} \tag{3.9}$$

where A and B are the integration domains centered on the separated (non-overlapping) interacting neutral atoms, or fragments in a more general picture. To obtain this simple form we had to approximate the polarizability response tensor $\alpha_{ij}(\mathbf{r}, \mathbf{r}', iu)$ (approximated to α in the simple qualitative example shown before) to a local and isotropic form by assuming $\alpha_{ij}(\mathbf{r}, \mathbf{r}', iu) = \delta_{ij}\alpha(\mathbf{r}, iu)\delta(\mathbf{r}-\mathbf{r}')$. This local polarizability density is connected to an experimentally measurable quantity, the average dynamic polarizability, as

$$\bar{\alpha}(\mathrm{i}u) = \int \mathrm{d}^3 r\, \alpha(\mathbf{r}, \mathrm{i}u) \tag{3.10}$$

and, since the f-sum rule requires that $\lim_{u\to\infty} \bar{\alpha}(\mathrm{i}u) = Ne^2/mu^2$ with N the total number of electrons in the system, $\alpha(\mathbf{r}, \mathrm{i}u)$ is usually expressed as

$$\alpha(\mathbf{r}, \mathrm{i}u) = \frac{e^2}{m}\frac{n(\mathbf{r})}{\omega_0^2(\mathbf{r}) + u^2} \tag{3.11}$$

Substituting this last expression in Eq.3.9 we obtain a very useful equation for the dispersion interaction energy

$$E^{(2)} = -\frac{3\hbar e^4}{2m^2}\int_A d^3 r \int_B d^3 r' \frac{n(\mathbf{r})n(\mathbf{r}')}{\omega_0(\mathbf{r})\omega_0(\mathbf{r}')[\omega_0(\mathbf{r}) + \omega_0(\mathbf{r}')]\,|\mathbf{r}-\mathbf{r}'|^6} \tag{3.12}$$

In this equation ω_0 plays a fundamental role since the peculiar physics of polarizability for a specific implementation is all contained in this term. In fact different local polarizability models, and different ω_0, are the sole difference between the long-range behavior for all the non-local functionals we'll present soon. Also, when the interacting fragments are far apart, the term $|\mathbf{r}-\mathbf{r}'|^6$ can be carried out of the inte-

[4]For the following derivations we refer the reader to the elegant treatment proposed by Vydrov and Van Voorhis in Ref [59].

gral, giving the correct long range shape R^{-6}, and defining the remaining part of the equation as the expression for the C_6^{AB} coefficient in Eq.3.1.

In this context Dion and colleagues proposed a new kind of non-local functionals E_c^{nl}, defined as an additional correction to the local or semilocal approximation for correlation in E_{xc}. The complete definition for $E_c = E_c^{LDA/GGA} + E_c^{nl}$ is then

$$E_c^{nl} = \frac{\hbar}{2} \int \mathrm{d}^3 r \int \mathrm{d}^3 r' n(\mathbf{r}) \Phi(\mathbf{r}, \mathbf{r}') n(\mathbf{r}') \tag{3.13}$$

The $E_c^{LDA/GGA}$ part, chosen to give exact results in the uniform electron gas, handles the short range correlations while E_c^{nl} is the fully non-local functional that describes the long-range dispersion, designed to vanish in the uniform electron density (such that double counting is avoided with the short range term). In Eq.3.13 the kernel $\Phi(\mathbf{r}, \mathbf{r}')$, symmetric for $\mathbf{r}$ and $\mathbf{r}'$, is defined such that

$$\lim_{R \to \infty} : \Phi = -\frac{3\, e^4}{2m^2 \omega_0(\mathbf{r}) \omega_0(\mathbf{r}') [\omega_0(\mathbf{r}) + \omega_0(\mathbf{r}')] \left|\mathbf{r} - \mathbf{r}'\right|^6} \tag{3.14}$$

where $R = |\mathbf{r} - \mathbf{r}'|$. This reduce the entire non-local functional E_c^{nl} to Eq.3.12, which is the correct way to describe long-range correlation interactions. E_c^{nl} is a universal functional that does not depend on any empirical value, contrary to the other approaches previously introduced in Sec.3.3.

The magnitude of this non-local correlation term is typically small; in most cases it's only on the order of 1–2% of the overall exchange-correlation energy. Nevertheless, its contribution is often vital and can have significant effects. For example, many simple molecular dimers do not bind without it [60]. And even in crystals, as we'll see later in Chap.4 this small effect can result in completely different groundstate crystal structures [61].

Finally the contribution of the non-local correlation term to the Kohn-Sham effective potential [62] is obtained by taking the functional derivative of the corresponding energy with respect to the density for a general point

$$v_c^{nl}(\mathbf{r}) = \int n(\mathbf{r}') \, \frac{\partial \left(n\Phi\right)}{\partial n} \, d\mathbf{r}' - \sum_\alpha \nabla_\alpha \left\{ \frac{\nabla_\alpha n}{|\nabla n|} \int n(\mathbf{r}') \, \frac{\partial \left(n\Phi\right)}{\partial |\nabla n|} \, d\mathbf{r}' \right\}. \tag{3.15}$$

Notice that this expression reduces to the well known one appropriate for a local or semilocal functional [63] if the explicit $\mathbf{r} - \mathbf{r}'$ dependence in the non-local kernel is reduced to a delta function, thus transforming the non-local functional into a local one

$$\frac{\sqrt{nn'}}{2}\,\Phi(n, n', |\nabla n|, |\nabla n'|, |\mathbf{r} - \mathbf{r}'|) \longrightarrow F_c^{\mathrm{LDA/GGA}}(\sqrt{nn'}, \sqrt{|\nabla n||\nabla n'|})\,\delta(\mathbf{r} - \mathbf{r}')\ . \tag{3.16}$$

Polarizatin models

Since from the original implementation of Dion and colleagues in 2004 several new non-local functionals with the form shown in Eq.3.13 have been proposed, the most commons of them being vdW-DF2, a revision of the original vdW-DF by the same authors, vdW-DF-09 a revision from Vydrov and Van Vhooris of the original vdW-DF and VV09, with its final evolution VV10, both proposed by Vydrov and Van Vhooris.

In this implementations we find very different kernels Φ, and we refer the reader to the original papers for all the details, but in the long range $R \to \infty$ they all can be expressed by the equations Eq.3.14. Using this similarity we can compare the different functionals by the definition of ω_0 they use, in fact the only possible difference in the long-range approximation; in Tab.3.4 we report the specific expression of ω_0 for implementations cited before [5].

In the table are reported, aside to the ω_0 implementations, the Mean Absolute Relative Errors on two different benchmarks sets. The C_6 is a set of 34 C_6 coefficient of closed-shell species, where the value calculated with Eq.3.14 is compared to quantum chemistry values[64] while the S22[65] is a very famous database of molecular configurations where the inter-molecular binding energy calculated self-consistently with each functional is compared to CCSD results[65].

While the differences resulting for the set S22 are more complicated to understand (the interplay of the short-range DFT and the non-local functional it's hard

[5] The original implementation of vdW-DF is different from the one exposes here, but as discussed in Ref. [59], it can easily be reformulated in this form.

	Definition of ω_0	MARE C_6	MARE S22
vdW-DF	$\frac{9\hbar}{8\pi m}\left[k_F\left(1+\mu s^2\right)\frac{4\pi}{3e^2}\epsilon_c^{LDA}\right]$; $\mu = 0.09434$	18.5%	25.96%
vdW-DF2	$\frac{9\hbar}{8\pi m}\left[k_F\left(1+\mu s^2\right)\frac{4\pi}{3e^2}\epsilon_c^{LDA}\right]$; $\mu = 0.20963$	60.9%	14.72%
VV10	$\sqrt{\frac{\omega_p^2}{3}+C\frac{\hbar^2}{m^2}\left\lvert\frac{\nabla n}{n}\right\rvert^4}$; $C = 0.0089$	10.7%	4.42%

Table 3.2: Definition of ω_0 for several non-local density functional definitions discusses in the chapter.

to disentangle), the differences present in the C_6 calculations are only due to the ω_0 chosen in each implementation and this gives some qualitative insight on the physics the different functionals can describe (at least in the long-range regime).

It's clear that the VV10 implementation give much better results, and not surprisingly the ω_0 used in this expression correctly describe also very simple cases, such as "jellyum" spheres, correctly predicting the uniform electron gas results to be $\omega_0 = \omega_p/\sqrt{3}$, where ω_p is the plasma frequency (proposed by Nesbet[66]). VV10 functional is today the best performing non-local functional implementation and our work to extend this approach will be shown in the following chapters.

3.4.1 Interpolation scheme

The general equation defining non-local functionals proposed by Dion et. al. unfortunately requires a very demanding calculation, a six dimensional integral in real space, something that can severely compromise its practical use, especially for DFT plane-wave approaches.

To overcome this difficulty Román-Pérez and Soler (RPS) [67] introduced for the original vdW-DF functional a very efficient integration scheme based on the fact that vdW-DF kernel Φ depends on density and density gradient in the two spatial points only through an auxiliary function $q(\mathbf{r}) = q(n(\mathbf{r}), |\nabla n(\mathbf{r})|)$ whose specific form in vdW-DF is not relevant here.

Exploiting this feature in their approach the kernel is computed on a two dimensional grid of fixed q values and any needed value in the integral is then obtained by interpolation:

$$\Phi(q, q', |\mathbf{r} - \mathbf{r}'|) \approx \sum_{ij} P_i(q)\ \Phi(q_i, q_j, |\mathbf{r} - \mathbf{r}'|)\ P_j(q')\ , \tag{3.17}$$

where the interpolating functions $P_i(q)$ are defined such that $P_i(q_j) = \delta_{ij}$ on a sufficiently dense grid of q's. The double spatial integrals appearing in the vdW-DF functional can then be computed as a series of convolutions that are most efficiently evaluated in reciprocal space, as for instance in

$$\begin{aligned} E_c^{nl} &= \frac{1}{2} \iint n n'\ \Phi(q, q', |\mathbf{r} - \mathbf{r}'|)\ d\mathbf{r} d\mathbf{r}' \\ &= \frac{\Omega}{2} \sum_{ij} \sum_{\mathbf{G}} \theta_i^*(\mathbf{G})\ \Phi(q_i, q_j, |\mathbf{G}|)\ \theta_j(\mathbf{G}) \\ &= \frac{\Omega}{2} \sum_{j} \sum_{\mathbf{G}} u_j^*(\mathbf{G})\ \theta_j(\mathbf{G})\ , \end{aligned} \tag{3.18}$$

where Ω is the crystal cell volume, $\Phi(q_i, q_j, |\mathbf{G}|)$ and $\theta_i(\mathbf{G})$ are the Fourier transform of the real space valued functions $\Phi(q_i, q_j, |\mathbf{r}|)$ and $\theta_i(\mathbf{r}) = n(\mathbf{r}) P_i(q(n(\mathbf{r}), |\nabla n(\mathbf{r})|))$, respectively, and the auxiliary function $u_j(\mathbf{G}) = \sum_i \theta_i(\mathbf{G}) \Phi(q_i, q_j, |\mathbf{G}|)$ is further introduced. With this expression it's simple to derive the the non-local potential, defined as $v_{nl} = \partial(E_c^{nl}/\partial n)/\Delta\Omega$ and reported in the following equation

$$v^{nl} = \sum_{\alpha} \left[u_\alpha \frac{\partial \Theta_\alpha}{\partial n} \right] \sum_e \partial_e \left[\sum_\alpha u_\alpha \left(\frac{\partial \Theta_\alpha}{\partial |\nabla n|} \frac{1}{|\nabla n|} \right) \partial_e n \right] \tag{3.19}$$

The non-local correlation energy can be calculated as a sum of convolutions most efficiently evaluated in reciprocal space. A grid of radial $\Phi\left(q_i, q_j, R\right)$ including a few tens of q's in each direction is typically needed for an accurate evaluation, making the time spent in this operation larger than the one needed for standard LDA/GGA potential evaluation but marginal in comparison with the time spent in the rest of the calculation even for small systems.

This approach, first developed for the vdW-DF functional, can be in principle ap-

plied to any non-local functional whose kernel depends on density and density gradient in the two spatial points only through an auxiliary function $q(\mathbf{r}) = q(n(\mathbf{r}), |\nabla n(\mathbf{r})|)$. For each implementations the q functions and the kernel table will have different formulations, but the RPS interpolation scheme will hold. As we'll see VV10 cannot be formulated in this way, and in Chap.5 we present a revision of the functional to overcome this limitation, the rVV10.

3.4.2 Limitations

Even though the non-local functional approach demonstrated to be a powerful and accurate approximation of the complex dispersion interactions problem, it has some important limitations and shortcoming that still need to be addressed in future research.

First of all the E_{nl} is build to account for two-body contributions, a leap forward to the usual local and semilocal approaches, but it still neglects the non additive many-body contributions that in some cases can be quite significant[68].

Then, in the large distance limit the non-local energy is expressed by the second order energy Eq.3.12. This approximation is known to have some important limitations for extended systems[69], such as metallic fragments or interacting surfaces and more investigations are needed in this cases. Later in this thesis we report calculations in graphite, showing good results for the inter-layer binding energies, but more complicated case can probably be underestimated by this approach.

To conclude, each non-local functional implementations needs a short-range description for the correlations, given by LDA or GGA. As explained before there are tens of different "flavors" of these functionals and the interplay between the short-range part and the non-local one is still a matter of active research. While the long-range limit of these functionals is known, in the overlapping regime double counting could produce sensible errors in the energy and reduce the predictive power of the total functional.

Chapter 4

Stress in non-local functionals

In this chapter we extend the non-local functionals theory and derive the corresponding stress tensor in a fashion similar to LDA and GGA, which allows for a straightforward implementation in any electronic structure code. We then apply our methodology on vdW-DF implementations to investigate the structural evolution of amino acid crystals of glycine and L-alanine under pressure up to 10 GPa—with and without van der Waals interactions—and find that for an accurate description of intermolecular interactions and phase transitions in these systems, the inclusion of van der Waals interactions is crucial.

4.1 Stress implementations

Stress is an essential tool in structure prediction and characterization, giving the ability to study, in an efficient way, the behavior of materials under pressure, predict structural phases and possible phase transitions.

The general formulation of the stress tensor $\sigma_{\alpha\beta}$ is defined as the derivative of the energy over the strain tensor $\epsilon_{\alpha\beta}$

$$\sigma_{\alpha\beta} = -\frac{1}{\Omega}\frac{\partial E}{\partial \epsilon_{\alpha\beta}} \tag{4.1}$$

As explained in the previous chapters, in DFT the energy is defined as a functional

of the electronic charge, and to calculate the stress we need to take derivatives of the energy functional for each component of Eq.2.1. In recent years stress implementations for all the DFT energy functionals have been developed, and in Appendix B we report derivation for LDA and GGA. The new non-local functional is defined as an additional contribution to the E_{xc} energy functional and thus an extension of the stress derivation is necessary.

To calculate the stress contribution we apply a simple procedure proposed by Nielsen and Martin[70], consisting in a set of expansions for the charge, wavefunctions and their derivatives, and a rigid rescaling. Calculations are straightforward but a little involved, and we give all the details in Appendix B. The stress derivation for the general non-local functional form is reported in Eq.B.15, but a more useful equation is the derivation for the efficient Román-Pérez and Soler (RPS) energy formulations of Eq.3.18, where the stress results to be

$$\begin{aligned}\sigma_{c\ \alpha\beta}^{nl} = & \frac{1}{\Omega}\left[E_c^{nl} - \int_\Omega n\ v_c^{nl}\ d\mathbf{r}\right]\delta_{\alpha\beta} \\ & - \sum_j \int u_j(\mathbf{r})\ n\ \frac{\partial P_j}{\partial q}\ \frac{\partial q}{\partial|\nabla n|}\ \frac{\nabla_\alpha n \nabla_\beta n}{|\nabla n|}\ d\mathbf{r} \\ & - \frac{1}{2}\sum_{ij}\sum_G \frac{G_\alpha G_\beta}{|\mathbf{G}|}\ \frac{\partial\Phi\left(q_i, q_j, |\mathbf{G}|\right)}{\partial|\mathbf{G}|}\ \theta_i^*(\mathbf{G})\ \theta_j(\mathbf{G})\ .\end{aligned} \tag{4.2}$$

The above formula has been implemented in the PWscf code of the QUANTUM ESPRESSO distribution [71] that efficiently solves Kohn-Sham self-consistent equations in a plane-wave pseudo-potential formalism. Numerical tests in simple benzene and methane crystals confirmed that the stress tensor computed in this way agrees perfectly (well within 0.01 GPa) with the numerical derivative, the residual discrepancy to be attributed to discretization error in the latter.

4.2 Background on glycine and L-alanine

Structural evolution of amino acid crystals under pressure constitutes a suitable case to test the adequacy of vdW-DF variants using our implementation of stress calculation. In particular, Glycine, the smallest amino acid, crystallizes in various molecular orientations, and is studied extensively in the literature, yet questions about its high pressure phases are still open. Alanine, the smallest naturally occurring chiral amino acid, constitutes a good test case where there is recent ongoing debate about a phase transition driven by pressure.

Glycine and alanine are among the simplest amino acids, yet their structural evolution under pressure displays a rich phenomenology that has been studied extensively in the literature and constitute an ideal test set for vdW-aware functionals [72, 73, 74, 75, 76, 77, 78, 79, 80, 81, 82, 83, 84, 85, 86, 87].

Glycine, $H_3N^+CH_2COO^-$ in its zwitterionic form, has three polymorphs under ambient conditions: α (Z'=4), β (Z'=2), and γ (Z'=3) [72, 73, 74], the most stable one being the γ phase. [75] The evaporation of aqueous solutions yields the α phase. Crystallization of glycine from water/ethanol solutions, instead, results in the β phase. At ambient conditions, the order of stability is $\gamma > \alpha > \beta$ [75, 76]. The γ phase transforms to the α phase upon heating, at around 170 °C, depending on the thermal history of the sample [75, 77]. High humidity drives a phase transition from α to γ phase [75, 78]. The β phase, metastable in dry air, rapidly transforms to α or γ phases in the presence of moisture at room temperature [75, 79].

Under pressure, the α phase is found to be stable up to 23 GPa, the β phase is shown to undergo a phase transition to the δ phase at 0.76 GPa. Two independent experimental studies showed that the γ phase transforms to a new glycine phase called ϵ, starting from 1.9 or 2.74 GPa. The experimental studies by Boldyreva and co-workers [80] resulted in a proposed structure for the ϵ phase based on the data obtained at 7.85 GPa. An alternative model for this phase is given by the work of Dawson and co-workers [81] at 4.3 GPa. In our study, we model the ϵ phase based on the latter structure. All known phases of glycine crystals are monoclinic, with the

exception of the trigonal γ form.

L-alanine is the smallest naturally occurring chiral amino acid and has been studied extensively. It is found to crystallize in zwitterion form CH3CH($NH3^+$)COO^-, in an orthorhombic structure with space group $P2_12_12_1$ with more than one molecule in its asymmetric unit cell (Z'=4) [82, 83, 84]. Previous high-pressure, Raman-scattering experiments on L-alanine have indicated a structural phase transformation at about 2.3 GPa [85] and further synchrotron XRD experiments confirmed this transition and identified the new phase as tetragonal in symmetry [86]. Moreover, the same XRD experiments also suggested another transition, to a monoclinic phase at about 9 GPa. Both of these findings were questioned by Tumanov and co-workers as their Raman, X-ray, and optical microscopy did not confirm the previously suggested phase transitions. Instead, with increase in pressure, cell parameters a and c are found to accidentally equate at around 1.5–2 GPa, without changing the cell symmetry. A new phase, proposed to belong to a solvate of L-alanine, was observed at around 3.5 GPa[87].

4.3 Computational Details

Ab initio calculations are performed in the framework of density functional theory as implemented in the Quantum ESPRESSO distribution [71]. The exchange-correlation functionals used in our study include two popular GGA functionals and the fully non-local vdW-DF correlation functional combined with two flavors of GGA exchange proposed in the literature. The two GGA functionals considered are the standard Perdew-Burke-Ernzerhof (PBE) [88] functional and the Zhang-Yang revised-PBE (revPBE) [89] functional. In the work introducing vdW-DF [90] the exchange part of the revPBE functional was selected to be combined with the fully non-local correlation term, based on the observation that more standard GGAs predict substantial binding in rare gas dimers from exchange alone, a feature absent for exact Hartree-Fock exchange and described correctly by revPBE exchange. A further refinement of revPBE exchange, named c09x, was subsequently developed by Cooper

[23] to be used in conjunction with the non-local vdW-DF correlation. The resulting vdW-DF-c09x [23] functional was found to be superior to the original vdW-DF (revPBE) functional on the benchmark S22 [65] database of weakly bound molecules. Both the original vdW-DF (revPBE) [90] functional and its refinement vdW-DF-c09x [23] are considered here.

The accuracy of the q-points grid involved in the Román-Pérez and Soler interpolation [67] of the vdW-DF kernel has been carefully checked and the standard 20-point grid was confirmed to be adequate. Results obtained with a denser 30-point grid did not change significantly: less than 0.1 mRy the energy per molecule, less than 10^{-3} eV/Åforces on atoms and less than 10^{-3} GPa the stress tensor.

Ultrasoft pseudopotentials from the PSLibrary project [91] are used without further modification. A kinetic energy cutoff of 80 Ry and a charge density cutoff of 560 Ry are used to achieve pressure convergence within less than 0.1 GPa. Monkhorst-Pack [92] k-point grids of $4\times2\times4$ / $3\times3\times3$ / $3\times3\times3$ / $2\times3\times3$ / $3\times3\times3$ are used for α, β, γ, δ, and ϵ phases of glycine, respectively. For alanine, an $8\times8\times4$, grid is found sufficient. With this setting, a tight convergence of less than 0.1 mRy in total energy is achieved. The cell parameters and atomic positions are fully optimized. Vibrational zero-point motion and finite temperature effects are non included.

4.4 Results at Ambient Pressure

Glycine

Our optimized lattice parameters a, b, c, and β calculated at ambient pressure for the three monoclinic stable phases α, β, and γ are given in Table 4.1. Also listed are experimental values determined for these structures.

Calculated volumes are found to be sensitive to the exchange-correlation functionals used. On average, PBE is found to overestimate the volumes by +10.7%, revPBE by +30.4%, vdW-DF (with revPBE exchange) by +9.1%, and vdW-DF-c09x is found to underestimate the volume by 4.3%. The difference between the strongly overestimated volume obtained with revPBE and the improved volume estimate obtained

XC	a (Å)	b (Å)	c (Å)	β (°)	mol/cell	vol/mol (Å^3)
α-glycine						
PBE	5.203	12.717	5.476	109.6	4	85.32
revPBE	5.359	14.000	5.525	109.4	4	97.76
vdW-DF (revPBE)	5.244	12.289	5.570	111.1	4	83.74
vdW-DF-c09x	5.034	11.567	5.449	112.9	4	73.06
Exp. Ref.[93]	5.083	11.820	5.460	111.9	4	76.0
β-glycine						
PBE	5.167	6.768	5.411	112.0	2	87.75
revPBE	5.414	8.231	5.546	120.0	2	106.98
vdW-DF (revPBE)	5.216	6.410	5.503	112.5	2	85.03
vdW-DF-c09x	5.017	5.990	5.399	113.9	2	74.20
Exp. Ref.[75]	5.094	6.286	5.383	113.2	2	79.2
γ-glycine						
PBE	7.252	7.251	5.520	90	3	83.81
revPBE	7.868	7.854	5.496	90*	3	97.94
vdW-DF (revPBE)	7.236	7.235	5.590	90	3	84.46
vdW-DF-c09x	6.892	6.892	5.459	90	3	74.84
Exp. Ref.[94]	6.975	6.975	5.437	90	3	76.9

Table 4.1: Optimized cell parameters at zero pressure for glycine phases that are stable under ambient conditions.

with vdW-DF reveals the beneficial effect of including long-range correlations. We can see that the vdW-aware c09x functional consistently underestimates the experimental volume outside the typical GGA behavior and gives the closest results to experiment. Concerning the individual lattice parameters and monoclinic angle, we can see that revPBE in particular provides a poor description of the crystal shape, but inclusion of non-local correlations in vdW-DF significantly improve the situation. From our results, it is evident that crystal densities and shapes are strongly dependent on the choice of XC functional.

Next, we explore the performance of these functionals in reproducing the structure of the single molecules in the crystal. In Table 4.2, we compare the bond lengths and torsion angle for α glycine at ambient pressure. In terms of bond lengths, all functionals describe the molecule reasonably well, within a 2% range from experimental values for bonds not involving hydrogen atoms, and 6% for bonds with hydrogen atoms. We can notice that in general atom-atom distances are overestimated within

bonds	PBE	revPBE	vdW-DF (revPBE)	vdW-DF-c09x	Exp. Ref. [93]
C1–O1	1.26	1.27	1.27	1.27	1.25
C1–O2	1.27	1.27	1.27	1.27	1.25
C2–N	1.49	1.50	1.51	1.48	1.48
C1–C2	1.53	1.55	1.55	1.53	1.52
C2–H1	1.10	1.10	1.09	1.10	1.05
C2–H2	1.09	1.09	1.09	1.10	1.04
N–H3	1.05	1.04	1.04	1.06	1.03
N–H4	1.07	1.07	1.06	1.07	1.09
N–H5	1.04	1.04	1.03	1.05	1.09
torsion					
N-C2-C1-O1	30.2	37.6	21.5	20.1	18.6

Table 4.2: Optimized bond lengths (Å) and torsion angle (°) for α glycine at zero pressure. The numbering of the atoms is given in the graphical representation at the bottom.

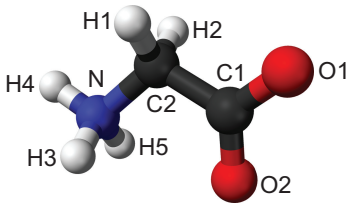

PBE and that this tendency is enhanced by revPBE, consistent with the observed volume behavior. Including long-range correlations in vdW-DF does not improve the description of bond lengths, at variance with the observed effect on volume. The effect of the XC functional becomes more apparent in the torsion angle where only vdW-including functionals show a very good agreement with the experiment. We observe the same general trend also for the other glycine phases, which are stable at ambient pressure.

Alanine

At ambient pressure, alanine molecules, bearing a net electric dipole, are aligned in chains along the c axis, packed in the ab plane so as to minimize electrostatic energy. In addition, a network of H-bonds exists, which are rigid along chains and rather flexible in the orthogonal plane. On this basis we can expect vdW interactions to be particularly important for the description of the lateral chain packing in the ab plane.

We report the optimized a, b, and c lattice parameters at ambient pressure for L-alanine in Table 4.3, together with the experimentally determined values[86, 87]. Similar to the case of glycine, we see that the calculated volume is sensitive to the choice of XC functional. While GGA functionals overestimate the volume, PBE by 8.1% and revPBE by 19%, the vdW-aware ones are able to describe the system with higher precision, vdW-DF overestimating the cell volume by 6% while vdW-DF-c09x underestimating it by 5%. The apparently better results for the crystal volume obtained with GGA functionals with respect to the glycine case is somewhat misleading, as cell shape is very badly described by these functionals. In fact, both GGA functionals strongly overestimate the a lattice parameter while underestimating b (and for revPBE also c), confirming the importance of the inclusion of dispersion forces for the aforementioned lateral chain packing. Indeed, the two vdW-aware functionals provide a more balanced, though not perfect, description of the crystal shape.

As in the case of glycine, all functionals are able to describe with reasonable accuracy the structure of the single molecule, as we can see in Table 4.4, where we

XC	a (Å)	b (Å)	c (Å)	volume (Å^3)
PBE	6.831	11.615	5.871	465.91
revPBE	7.241	11.939	5.525	512.64
vdW-DF (revPBE)	6.119	12.637	5.910	456.99
vdW-DF-c09x	5.886	12.055	5.781	410.17
Exp. Ref.[86]	6.102	12.339	5.780	425.13
Exp. Ref.[87]	6.049	12.345	5.780	431.6

Table 4.3: Optimized cell parameters at zero pressure for the L-alanine phase stable under ambient conditions.

bonds	PBE	revPBE	vdW-DF	c09x	Exp. Ref. [84]
C1–O1	1.26	1.26	1.26	1.26	1.24
C1–O2	1.28	1.28	1.28	1.28	1.26
C1–C2	1.54	1.55	1.56	1.53	1.53
C2–N	1.49	1.51	1.52	1.48	1.49
C2–C3	1.53	1.53	1.54	1.52	1.52
N–H1	1.04	1.04	1.04	1.05	1.03
N–H2	1.05	1.04	1.04	1.05	1.03
N–H3	1.06	1.05	1.05	1.07	1.05
C2–H4	1.10	1.10	1.10	1.10	1.09
C3–H5	1.09	1.10	1.10	1.10	1.08
C3–H6	1.09	1.09	1.10	1.10	1.08
C3–H7	1.10	1.10	1.10	1.10	1.08
torsion					
N–C2–C1–O1	17.0	19.5	20.0	17.2	18.7

Table 4.4: Optimized bond lengths (Å) and torsion angle (°) for L-alanine at zero pressure. The numbering of the atoms is given in the graphical representation at the bottom.

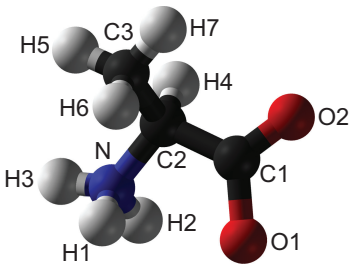

report the characteristic bond lengths for a single alanine molecule. All bonds are correctly described within a 2% range from experimental values, including C–H and N–H ones, and also the torsion angle does not vary significantly between the different XC functionals used and agrees well with experiment.

4.5 Results at High Pressure

Glycine

Addressing the relative stability of glycine polymorphs is difficult due to the very small energy differences between the phases (less than 1 kcal/mol). Calculated differences are also sensitive to the exchange-correlation functionals used. In Fig. 4-1 we report the enthalpy per molecule as a function of pressure, referenced with respect to the α phase, for all XC functionals employed.

At zero pressure, vdW-DF is the only functional that predicts the $\gamma > \alpha > \beta$ stability order correctly, while vdW-DF-c09x also shows very similar enthalpy for the γ and α phases. Since the energy differences are extremely small, we can regard these two functionals as performing equally well at zero pressure. For both functionals, the β phase is well separated from the α and γ phases as expected for a metastable state, however this is not observed for the PBE functional. We see that revPBE displays a highly erratic stability order both at zero pressure and at higher pressures.

The sharp increase in enthalpy for the β phase at 2.0 GPa with the revPBE functional is due to the reorganization of the hydrogen-bond network taking place from the 1.0 GPa configuration to the 3.0 GPa one. At 1.0 GPa, the two molecular layers in the unit cell are stacked on top of each other, so that linear hydrogen-bonds between molecules of the two layers are formed, normal to the layer plane. At 3.0 GPa, the layer stacking changes such that a molecule of the top layer sits in the void between two molecules of the lower layer, forming a trigonal hydrogen-bond network. The 2.0 GPa configuration is the transition point between these two, resulting in higher enthalpy. The on-top stacking at 1.0 GPa is only observed with the revPBE functional. Due to this and other anomalies in its enthalpy plot, we deduce that the

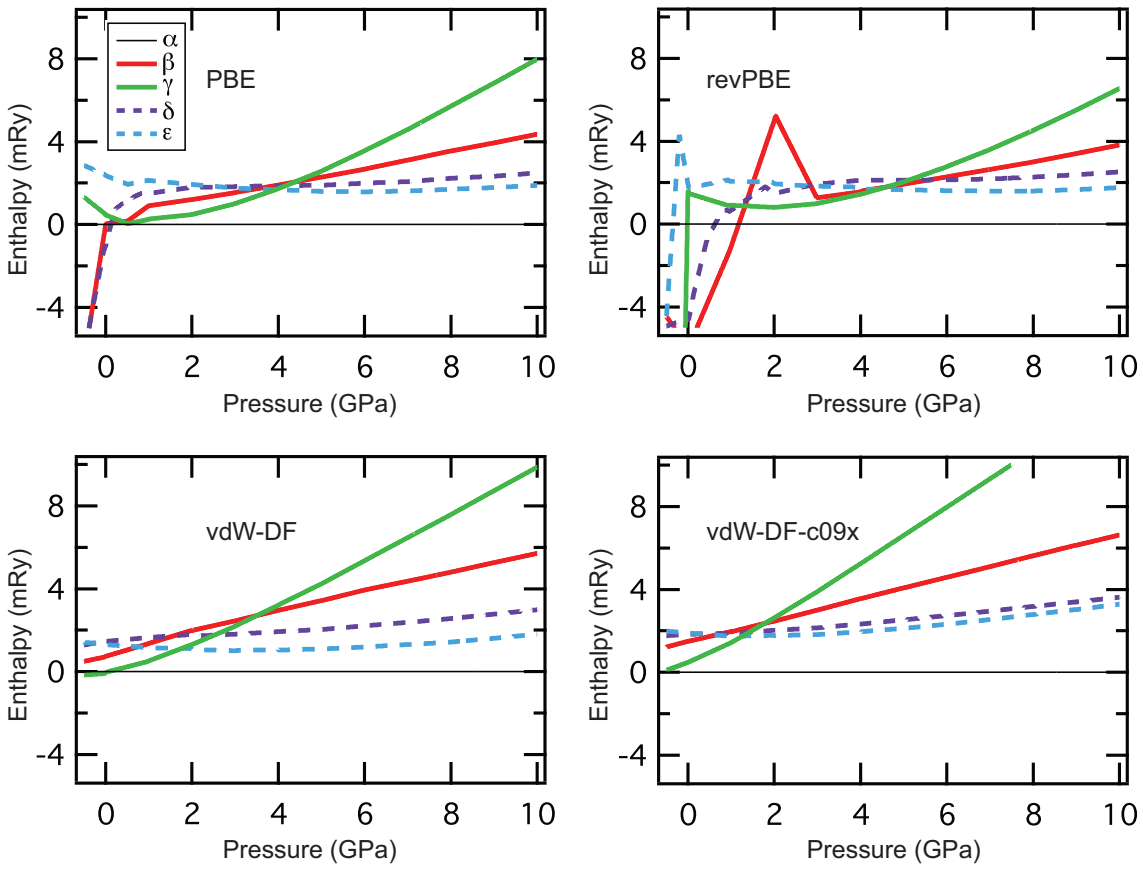

Figure 4-1: (color online) Enthalpy per molecule referenced with respect to the α phase as a function of pressure for all known phases of glycine up to 10 GPa, for all XC functionals considered. Calculations are performed with target pressure –0.5 GPa, 0 GPa, and up to 10 GPa in increments of 1 GPa. Additional calculations were performed for high-pressure phases at around ambient pressure for better convergence.

revPBE functional is not reliable and will not be discussed further.

In agreement with the experimental observations, the α phase is stable up to 10 GPa for PBE, vdW-DF, vdW-DF-c09x, and after 1.1 GPa also for revPBE. The phase transition from β to δ occurs experimentally at 0.76 GPa. The δ phase is calculated to be thermodynamically more stable than the β phase after around 4.0 GPa, 1.5 GPa, and 0.7 GPa for PBE, vdW-DF, and vdW-DF-c09x, respectively. Considering the precision of our calculations, the estimates from vdW-DF and vdW-DF-c09x are equally satisfactory, while PBE overestimates the transition point.

The phase transition of the γ polymorph is experimentally more complicated, as single crystals undergo a phase transition to a polycrystalline phase already at 1.9 GPa, but the identification of the ϵ phase could only be obtained at 4.3 GPa. Our calculations predict that the ϵ phase becomes thermodynamically more stable than the γ one at around 4.0 GPa, 1.8 GPa, and 1.2 GPa for PBE, vdW-DF, and vdW-DF-c09x, respectively. As in the case of the $\beta \rightarrow \delta$ transition, we can say that vdW-DF and vdW-DF-c09x perform equally well in predicting the single crystal transition of the γ form, while PBE overestimates the transition pressure. The stability order remains the same for all XC functionals at high pressures: $\alpha > \epsilon > \delta > \beta > \gamma$.

Our calculations show that energetics and structural properties are sensitive to the choice of XC functionals in the case of glycine crystals at ambient and higher pressures. Although for a more definite discussion of the relative stability of the different polymorphs inclusion of vibrational zero-point motion and finite temperature effects would be desirable, exchange-correlation functionals including van der Waals interactions result in better estimates for the stability order and crystal density than the functionals missing this contribution. For the stability order at ambient pressure and transition pressures, both vdW-aware functionals perform equally well and better than PBE and revPBE, suggesting that using vdW-aware XC functionals can greatly improve the energetics and structural properties of molecular crystals obtained by *ab initio* methods.

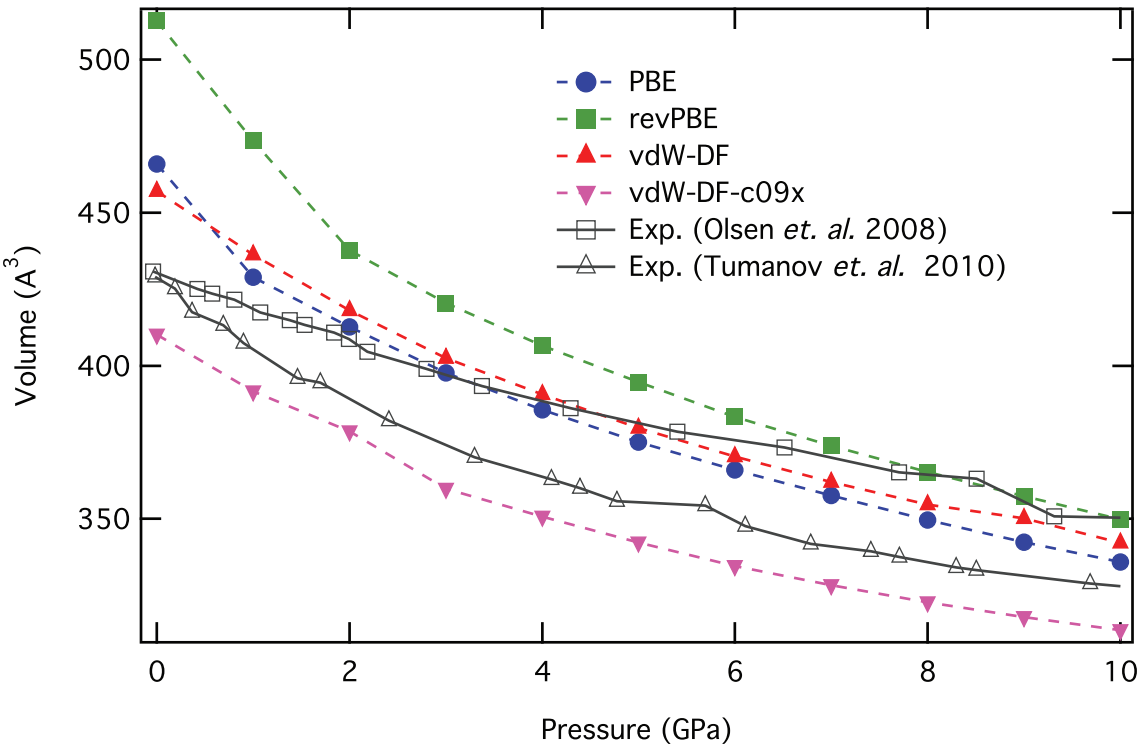

Figure 4-2: (color online) Cell volume as a function of pressure for L-alanine for all the XC functional considered. Experimental data from Refs.[86, 87] are also shown.

Alanine

As a final case, we address the ability of the new vdW-aware functionals to correctly describe the equation of state of L-alanine and to shed light on the ongoing controversy about a debated pressure-driven phase transition [85, 86, 87]. In Fig. 4-2, we report the cell volume as a function of pressure for the four functionals considered between 0 to 10 GPa, a range where three structural phase transitions have been reported.

The two available experimental volume sets [86, 87] agree at low pressure but significantly differ at higher pressure. At low pressure revPBE fails to describe correctly the crystal, grossly overestimating the volume, while at higher pressure, where long-range correlations likely play a less important role, the functional approaches experiments. As for the non-local functionals, vdW-DF-c09x underestimates the experimental volume at all pressures, while vdW-DF overestimates it at low pressure and falls midway within experiment uncertainty at higher pressures. PBE appears to give reasonably good results for the volume, close to vdW-DF ones at all pressures.

XC	B_0	B_0'
L-alanine		
PBE	11.2	7.32
revPBE	7.4	7.04
vdW-DF (revPBE)	17.8	4.32
vdW-DF-c09x	16.4	5.25
Exp. Ref.[86]	31.5±1.4	4.4±0.4
Exp. Ref.[87]	15.1±1.2	5.1±0.9

Table 4.5: L-alanine bulk modulus B_0 (GPa) and its pressure derivative B_0'. Experimental values from Ref. [87] were extracted by fitting experimental data.

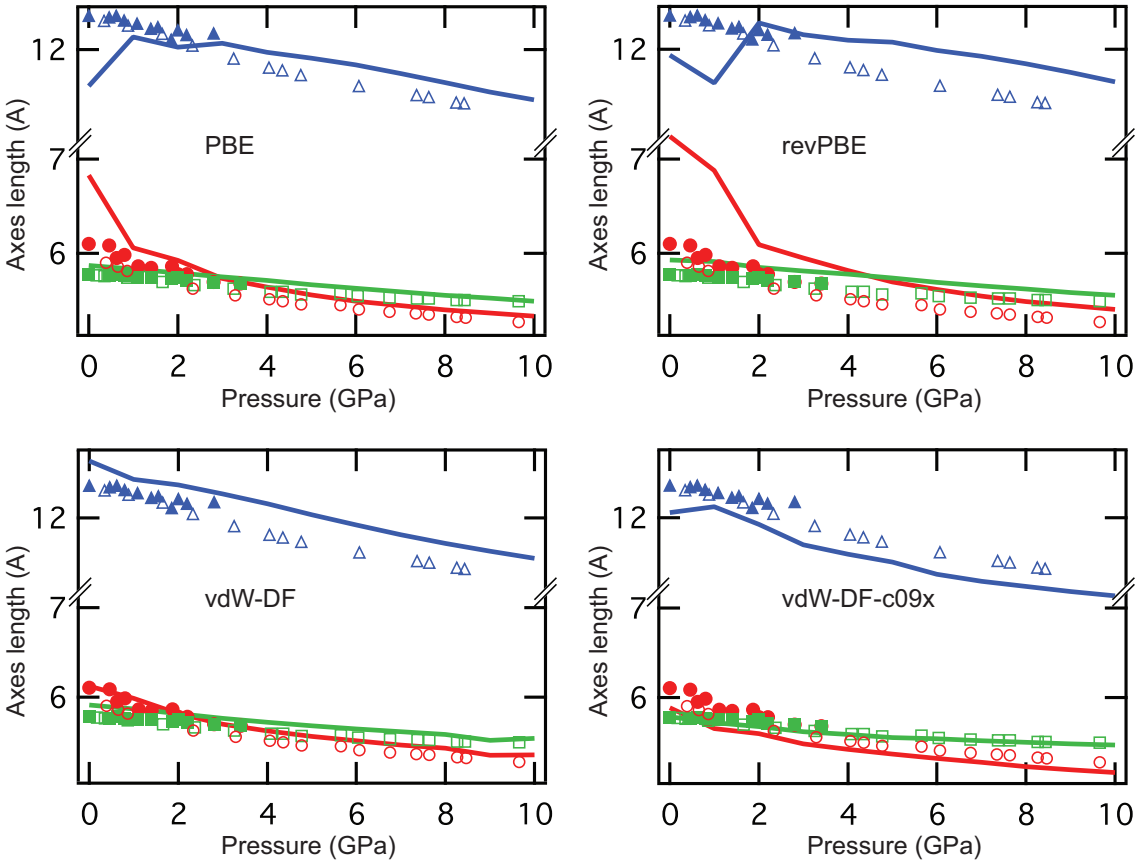

Figure 4-3: (color online) Crystal cell parameters a (red lines and circles), b (blue lines and triangles), and c (green lines and squares) of L-alanine as a function of pressure. Lines connect the calculated points. Experimental data from Ref.[86] and Ref.[87] are reported with full and open symbols, respectively.

A least-square fit of the data with the Birch-Murnaghan equation of state gives the equilibrium bulk modulus and its pressure derivative for each functional, reported in Table 4.5. As already evident from Fig. 4-2, compressibility from vdW-aware functionals agrees very well with the value that can be deduced from the experimental data in Ref. [87], while agreement is less good with Ref. [86]. In any case, both GGA functionals severely overestimate the compressibility of the system.

As already noted when discussing ambient pressure results, the small difference between PBE and vdW-DF volumes in L-alanine is misleading. In Fig. 4-3 we report the evolution of the a, b, and c cell parameters as a function of pressure, compared with experimental values. As could be expected, the c axis corresponds to the stiffer direction in the crystal and all functionals give a very reasonable description of its pressure dependence. It can be seen instead that PBE and revPBE values for the a and b lattice parameters are completely wrong at low pressure and approach the experimental values only at higher pressure, where weak van der Walls interactions become less important. The only functionals able to correctly describe the evolution of the cell geometry in the whole pressure range are the vdW-aware ones.

Experimental data from Ref. [86], reported with full symbols, show the signature of the experimentally observed transition, from orthorhombic to tetragonal, at 2.3 GPa where a and c become equal. Experimental data from Ref. [87], reported with open symbols, indicate instead an accidental crossing between these two quantities that interchange at higher pressure.

Our calculations with vdW-aware functionals support this interpretation, with the original vdW-DF giving the best results.

4.6 Remarks

Our calculations show that consideration of vdW-aware XC functionals can greatly improve the description of the energetics and structural properties of molecular crystals from first principles. In the case of glycine, functionals including van der Waals interactions result in better estimates for the stability order of the different poly-

morphs and crystal density than the functionals missing this contribution. Both flavors of vdW-aware functionals perform equally well and significantly better than PBE and revPBE.

In the case of L-alanine only vdW-aware functionals deliver individual cell parameters that evolve correctly with pressure, while GGA results are qualitatively wrong. The equation of state agrees reasonably well with some recent experiment, less so with another one. The bulk modulus is much improved compared with GGA results.

In conclusion, while our results confirm that vdW-DF functionals allow a significant step forward in the first-principle description of soft matter, they also show that significant room for improvement still remains.

Chapter 5

Revised VV10

In this chapter we introduce a simple revision of the VV10 non-local density functional by Vydrov and Van Voorhis [24]. Unlike the original functional our modification allows non-local correlation energy and its derivatives to be efficiently evaluated in a plane wave framework along the lines pioneered by Román-Pérez and Soler (RPS) [95]. Our revised functional maintains the outstanding precision of the original VV10 in non covalently bonded complexes and performs well in representative covalent, ionic and metallic solids.

5.1 VV10 limitations

As we previously discusses, the VV10 implementation by Vydrov and Van Voorhis showed to be a remarkably accurate in calculations of C_6 coefficients and on the set S22 intermolecular binding energies, composed of small biological interacting molecules.

Based on previous works by the same authors [96, 97], VV10 functional is defined by the very simple analytic form for the non-local kernel in Eq. 3.13

$$\Phi^{VV10}(\mathbf{r},\mathbf{r}') = -\frac{3e^4}{2m^2}\frac{1}{gg'(g+g')} \tag{5.1}$$

where $g = \omega_0(\mathbf{r})R^2 + k(\mathbf{r})$, and similarly $g' = \omega_0(\mathbf{r}')R^2 + k(\mathbf{r}')$, with $R = |\mathbf{r} - \mathbf{r}'|$. In these expressions $\omega_0 = \sqrt{\omega_g^2 + \frac{\omega_p^2}{3}}$, where $\omega_p^2 = 4\pi ne^2/m$ is the plasma frequency

and $\omega_g^2 = C(\hbar^2/m^2)\left|\frac{\nabla n}{n}\right|^4$ is the so-called local band gap with C=0.0093 as discussed in Ref. [24]. The term $k = 3b(\omega_p/k_s^2) = 3\pi b\left(\frac{n}{9\pi}\right)^{\frac{1}{6}}$, where k_s is the Thomas-Fermi screening wavevector, controls the short range damping of the R^{-6} divergence in the kernel and depends on an empirically determined parameter b. We refer the reader to the original work [24] for further details.

Unfortunately the VV10 kernel, Eq. 5.1, depends separately on densities and density gradients in $\mathbf{r}$ and $\mathbf{r}'$ and a direct extension of RPS procedure to perform 4-dimensional interpolation would still be very computationally demanding.

5.2 rVV10: a simple revision

To address this problem we analyze in some details the analytic behavior of the VV10 kernel. It is useful to introduce the auxiliary function $z(\mathbf{r}) = \frac{\omega_0(\mathbf{r})}{k(\mathbf{r})}R^2 + 1$ such that $g(\mathbf{r}) = k(\mathbf{r})z(\mathbf{r})$ and the original VV10 kernel can be rewitten as:

$$\Phi^{VV10}(\mathrm{r},\mathrm{r}') = -\frac{3e^4}{2m^2}\frac{1}{k^{\frac{3}{2}}k'^{\frac{3}{2}}}\frac{1}{zz'\left(\sqrt{\frac{k}{k'}}z + \sqrt{\frac{k'}{k}}z'\right)} \tag{5.2}$$

where we can identify three ingredients: $k^{\frac{3}{2}}(\mathbf{r})$ and $k'^{\frac{3}{2}}(\mathbf{r}')$, that enter as simple multiplicative factors to the densities in Eq. 3.13, $z(\mathbf{r})$ and $z(\mathbf{r}')$, that depend on the ratio of ω_0 and k but not separatly on the two, and the ratio $\sqrt{k/k'}$ that depends on the density on both grid points, $\mathbf{r}$ and $\mathbf{r}'$. This last term is the one that prevents VV10 kernel to be put in a form suitable to be treated by the RPS procedure.

We implemented the VV10 functional in the PWSCF code of the Quantum ESPRESSO distribution [71], performing explicitly the calculation in real space and we focused our attention on the behavior of the ratio $\sqrt{k/k'}$. We run our tests on several molecular configurations taken from the S22 set of non-covalently bonded complexes [65]. In Fig.5-1 we analyze $\sqrt{k/k'}$ obtained for the water dimer configuration, very similar results were obtained in the analysis of the other test cases.

In the upper panel of Fig. 5-1 we show the values of $\sqrt{k/k'}$ as a function of the distance between the two points $R = |\mathbf{r} - \mathbf{r}'|$. Only points whose charge density

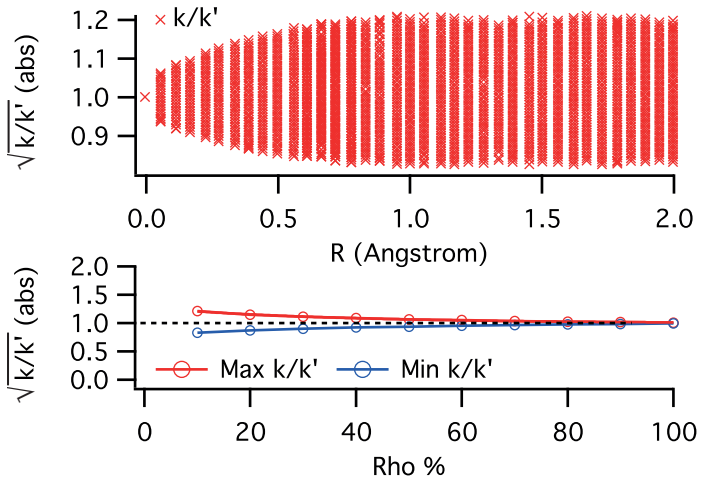

Figure 5-1: $\sqrt{k/k'}$ ratio analysis in the water dimer configuration included in the S22 set, similar results are obtained in other cases we analyzed. (*top*) $\sqrt{k/k'}$ values as a function of the R distance, showing a very narrow dispersion around 1. (*bottom*) $\sqrt{k/k'}$ values as a function of the percentage of interacting charge (w.r.t. the max charge in the system). The red curve show the maximum value if the ration, while the blue curve the minimum.

exceeds 10 % of the maximum value in the system are included in the plot. From this analysis we can see that $\sqrt{k/k'}$ takes values in a very narrow range centered around 1. The maximum deviation from unit decreases with decreasing distance and collapses of course to one for $\mathbf{r} = \mathbf{r}'$. For clarity only a small part of the entire R dependence is shown but the range of values is basically stable beyond $R = 1$ Å.

The range of possible values mildly depends on the charge cutoff used in the calculation. In the lower panel of Fig. 5-1 we report the maximum and minimum value of the $\sqrt{k/k'}$ ratio as a function of the minimum charge density included in the calculation, expressed in percentage of the maximum charge density in the system. We see immediately that only for points involving very small charges the ratio can deviate significatly from one. Combining the information from the two panels we can conclude that $\sqrt{k/k'}$ can differ from unit only when involving interacting charge densities are far apart from each other and such that at least one is very small. But even in this situation the deviation of the ratio from unit contributes very little to the integral since the kernel is multiplied by the product of the two charge densities.

Moreover for large R all the z factors in the denominator in Eq. 5.2 tend to be large.

With this in mind, it is natural to introduce an approximation where the ratio $\sqrt{k/k'}$ is dropped in Eq. 5.2 and we propose a revised VV10 kernel (rVV10) that reads

$$\Phi^{rVV10} = -\frac{3e^4}{2m^2} \frac{1}{(qR^2+1)(q'R^2+1)(qR^2+q'R^2+2)} \tag{5.3}$$

where we have defined q and q' as $q(\mathbf{r}) = \omega_0(n(\mathbf{r}), |\nabla n(\mathbf{r})|)/k(n(\mathbf{r}))$, and similarly for $\mathbf{r}'$, and we have removed from the kernel definition the factors $1/k^{\frac{3}{2}}$ and $1/k'^{\frac{3}{2}}$ that will be directly multiplied to the corresponding densities.

This new form allows us to apply the RPS interpolation scheme in reciprocal space in the evaluation of the integral that reads

$$E_c^{nl} = \frac{\hbar}{2}\Omega \sum_{ij} \sum_{\mathbf{G}} \tilde{\theta}_i^*(\mathbf{G}) \tilde{\Phi}^{rVV10}(q_i, q_j, |\mathbf{G}|) \tilde{\theta}_j(\mathbf{G}) \tag{5.4}$$

where $\tilde{\Phi}^{rVV10}(q_i, q_j, |\mathbf{G}|)$ are the Fourier transforms of the rVV10 kernel evaluated on a bidimensional grid of q values and $\tilde{\theta}_i(\mathbf{G})$ are the Fourier transforms of $\theta_i(\mathbf{r}) = n(\mathbf{r})P_i(q(\mathbf{r}))/k^{\frac{3}{2}}(\mathbf{r})$, where $P_i(q)$ are the same interpolating polinomials introduced in Ref. [67].

We implemented the new functional in the Quantum ESPRESSO distribution [71] including the self-consistent evaluation of the corresponding correlation potential [98] as well as the evaluation of forces and stress tensor [99].

We have found that a logarithmic mesh of 20 q points is enough to correctly interpolate the kernel Φ^{rVV10}, and we used the saturation scheme proposed in RPS [67]. With this setup the evaluation of the exchange and correlation energy and potential becomes 400 times more expensive than for a standard semilocal functional. Accounting for up to 30-50% of the total calculation time in a few electron system it is totally negligible for larger system with many electrons per cell and/or many k-points.

Following the original VV10 functional definition, the full XC energy is defined as $E_{xc}^{rVV10} = E_x^{rPW86} + E_c^{LDA} + E_{c-nl}^{rVV10}$ where E_x^{rPW86} stands for the refitted Perdew-Wang exchange functional [**?**] and E_c^{LDA} is the Local density approximation for correlation

according to the Perdew and Wang [7] parametrization.

5.3 Benchmarks on set S22 and selected materials

As a first benchmark we compare [1] our revised functional and the original VV10 on the S22 molecular set obtaining very similar binding energies, with differences not exceeding 0.85 kcal/mole in the worst case.

As mentioned earlier the VV10 functional contains an empirical parameter b that has been determined by minimizing the mean square deviation of the calculated molecular binding energies of the full S22 set from their quantum chemistry [100] reference value. By following the same strategy we reoptimized the b parameter for the present functional obtainig a value $b = 6.3$ not far from the original value of $b = 5.9$, giving confidence that the proposed modification does not significantly impact the physical behavior of the functional.

In Tab.5.1 we report the binding energies (in kcal/mol) for each element of the set S22 comparing the results obtained for rVV10 functional both with the optimized b value and the original one taken from the original VV10 implementation, the original VV10 results [24], the vdW-DF2 and results obtained with the PBE-D3 [16] approach. Molecular structures are from Ref. [65] and quantum chemistry reference binding energies are from Ref. [100] for all systems except adeninethymine complexes, for which the values from Ref. [101] are used. In Fig.5-2 we report a commonly used visualization to compare S22 results build with the data in Tab.5.1.

From inspection of these results one can see that the main effect of the functional modification in rVV10 is to slightly but systematically increase the molecular binding energy in S22 complexes and that the optimization of b effectively compensate for this effect and indeed, for all configurations, rVV10 gives almost identical results to the original VV10 ones, with a maximal difference of 0.16 kcal/mol. Notice that this

[1] We used ultrasoft pseudopotentials input data from the PSLibrary project [91], generated with the density functionals suggested in [24]. A kinetic energy cutoff of 80 Ry and a charge density cutoff of 560 Ry are used to achieve good energy convergence and we used a periodic cubic cell of $20\mathring{A}$ to ensure the molecules were far apart from their periodic replicas.

Complex	rVV10 ($b = 6.3$)	rVV10 ($b = 5.9$)	VV10	Ref	vdW-DF2	PBE-D3
Hydrogen-bonded						
NH3 dimer	3.44	3.51	3.43	3.15	2.97	3.59
H2O dimer	5.56	5.63	5.50	5.00	4.78	5.82
Formic acid dimer	20.07	20.29	19.96	18.75	16.77	19.83
Formamide dimer	16.71	16.91	16.71	16.06	14.43	16.56
Uracil dimer pl.	20.99	21.23	21.10	20.64	18.69	20.83
2-pyridone-						
2-aminopyridine	18.14	18.40	18.05	16.94	15.37	18.12
Adeninethymine WC	17.35	17.63	17.42	16.74	14.74	17.35
Dispersion-bound						
CH4 dimer	0.50	0.55	0.50	0.53	0.68	0.82
C2H4 dimer	1.43	1.54	1.42	1.48	1.32	1.62
BenzeneCH4	1.46	1.59	1.45	1.45	1.29	1.60
Benzene dimer p.	2.74	3.12	2.71	2.66	2.15	2.49
Pyrazine dimer	4.09	4.49	4.02	4.26	3.30	3.61
Uracil dimer s.	9.70	10.28	9.70	9.78	8.76	9.15
Indolebenzene	4.55	5.11	4.54	4.52	3.44	3.77
Adeninethymine	11.44	12.27	11.42	11.66	9.58	10.00
Mixed complexes						
C2H4C2H2	1.69	1.75	1.68	1.50	1.53	1.90
BenzeneH2O	3.35	3.48	3.31	3.28	2.80	3.94
BenzeneNH3	2.31	2.44	2.28	2.32	1.99	2.67
BenzeneHCN	4.33	4.49	4.30	4.54	3.55	4.52
Benzene dimer (t-s.)	2.59	2.79	2.54	2.72	2.06	2.69
Indolebenzene	5.34	5.63	5.27	5.63	4.20	5.56
Phenol dimer	7.15	7.41	6.99	7.10	5.97	6.94
MARE (Hydrogen-b.)	6.30 %	7.78 %	6.03 %	-	8.78 %	7.25%
MARE (Dispersion-b.)	2.57 %	7.83 %	2.57 %	-	18.00 %	16.68%
MARE (Mixed comp.)	4.40 %	5.09 %	4.93 %	-	16.89 %	9.56%
MARE	4.34 %	6.94 %	4.42 %	-	14.72 %	11.41%

Table 5.1: Binding energies (in kcal/mol) for each element of the set S22 used in the preparation of Fig. 2 of our manuscript. Molecular structures are from Ref. [65] and quantum chemistry reference binding energies are from Ref. [100] for all systems except adeninethymine complexes, for which the values from Ref. [101] are used.

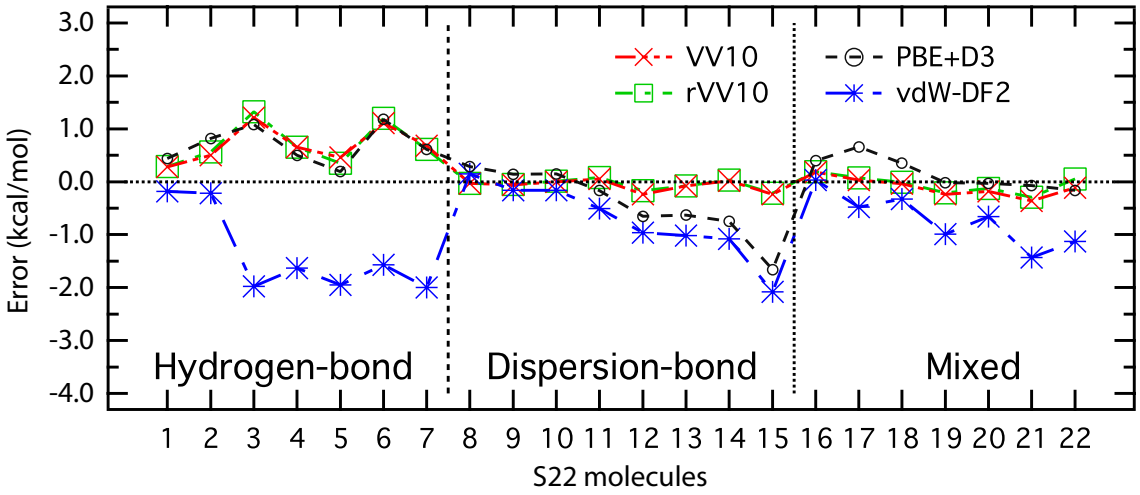

Figure 5-2: Binding energies differences (in kcal/mol) for the S22 test set. Molecular structures are from [65] and reference binding energies are from [100] for all systems except adeninethymine complexes, for which the values from [101] are used. VV10 and vdW-DF2 results are reproduced from [24], PBE-D3 results from [16]. rVV10 results are obtained using the rVV10 implementation in Quantum ESPRESSO. Positive (negative) values mean overbinding (underbinding) w.r.t. the reference values. Numerical values for all these data are reported in Tab. 5.1.

value is an order of magnitude smaller than the maximum difference between rVV10 and the quantum chemistry benchmark (1.79 kcal/mol for 2-pyridone2-aminopyridine complex) as well as between VV10 and the benchmark (1.89 kcal/mol, for the same complex). This confirms the soundness of our approximation and gives confidence on its robustness. Both rVV10 and the original VV10 perform much better than vdW-DF2, the best performing functional of his family on the S22 set [102].

To further compare the ability of VV10 and rVV10 to describe non-local interaction we report in Fig.5.3, a comparison of their MARE in each sub-group of the S22 set with the recently published results obtained for several other techniques such as EXX-cRPA, MP2, PBE-D3 and TS-vdW (all these values are reproduced from Ref. [103]). From this comparison the high accuracy of the VV10 and rVV10 results, as well as their overall similarity is evident.

Another natural system where to test non-local correlation functionals are rare gas dimer binding energies. In Fig. 5-4 we report Argon dimer binding energy as a function of interatomic separation for the rVV10 functional, the original VV10

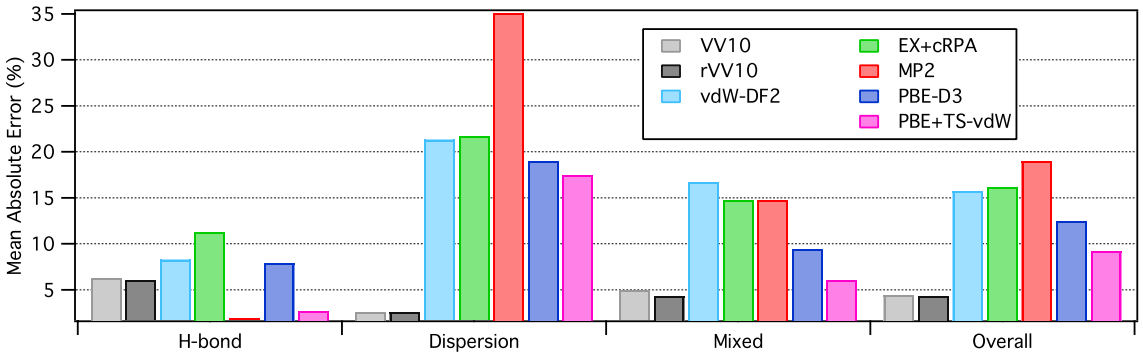

Figure 5-3: A comparison of the original VV10 and rVV10 MARE in each sub-group of the S22 set with the recently published results obtained for several other techniques such as EXX-cRPA, MP2, PBE-D3 and TS-vdW (all these values are reproduced from Ref. [103]).

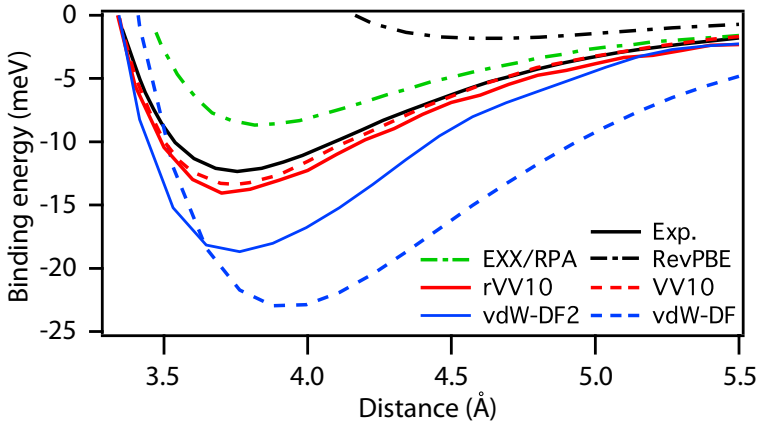

Figure 5-4: Binding energy curves for Ar dimer obtained with different DFT functionals and compared with the experimental curve from [105]. For completeness the EXX/RPA calculation from [104] is also reported.

and compare them with reference calculations with other functionals and techniques [104]. Again the agreement between the two functionals and the experiment [105] is impressive and reassuring.

A further important requirement for a new functional is its ability to maintain the high quality of results that can be obtained with GGA in solids and hard matter. To this purpose we selected some simple materials representative of different binding behaviors, namely bulk Cu, Al, Si, C (in the diamond structure) and NaCl, and tested the performance of rVV10 functional for them. In table Tab.5.2 we report the calculated equilibrium lattice parameter and the bulk modulus for these materials

Complex	vdW-DF2	rVV10	PBE	Ref
Lattice constants (Å)				
Cu	3.76	3.68	3.65	3.60
Al	4.08	4.02	4.04	4.02
Si	5.52	5.48	5.46	5.42
C (diamond)	3.61	3.58	3.57	3.54
NaCl	5.69	5.59	5.70	5.57
Bulk moduli (GPa)				
Cu	97.0	124.6	139	142.0
Al	60.1	79.0	78.6	79.4
Si	79.6	86.5	88.3	99.2
C (diamond)	395.0	424.4	429	443.0
NaCl	26.0	27.9	22.8	26.6

Table 5.2: Lattice constants in Å and bulk moduli in GPa of different solids calculated with rVV10 and vdW-DF2 compared with experimental values.

and compare them with experiment. For completeness also results obtained with vdW-DF2 (from [106]) and PBE are included.

In all systems the quality of rVV10 results is very good, comparable if not better than PBE, and our revised functional outperforms vdW-DF2 that has a general tendency to overestimate lattice parameters and to underestimate bulk moduli.

As a final test case we considered Graphite, whose interlayer separation and binding energy are notoriously difficult to describe within standard density functional theory, even using the non-local correlation functional now available (vdW-DF, vdW-DF2 and similar). Our results from a complete optimization of the cell with rVV10 functional not only gives both the in-plane lattice parameter and the interlayer separation in perfect agreement with the experiment ($a = 2.46$ Å, $c = 3.36$ Å for both) but also gives an inter-layer binding energy of 39 meV/atom in good agreement with a recent experimental determination of 31±2 meV/atom [107].

5.4 Remarks

The simple and sound modification of the VV10 non-local correlation functional we proposed allows an efficient implementation in a plane wave framework. We demonstrate that our revised VV10 functional maintains the excellent performance of the original functional in predicting interaction energies and inter monomer separation in non covalently bonded complexes, without deteriorating the accurate description of the structural properties of representative covalent, ionic and metallic solids.

Chapter 6

Phonons with non-local functionals

In this section we extend the formulation of density functional perturbation theory[25] (DFPT) to the vdW non-local functionals, allowing us to calculate phonon frequencies at arbitrary wave vectors $\mathbf{q}$ avoiding the use of supercells and with a workload that is essentially independent of the phonon wavelength. Numerical results for vdW-DF [19], vdW-DF2 [20] and rVV10 will be shown for graphite, compared with other theoretical approaches and experimental data where available.

6.1 DFPT extensions to non-local functionals

The ability to calculate vibrational frequencies in soft materials, where van der Waals (vdW) interaction is of critical importance, has been demonstrated to be a key issue in the understanding of several features both in solid states and biological matter. From DNA conformation changes and melting [26, 27], to the recently proposed phonon assisted tunneling mechanics at the base of human odor recognition[28], vibrational properties due to the non-local correlation are also a fundamental characteristic in solid state materials, such as rare-gas crystals[108, 109] and graphite[110], supported molecules [111] and many others.

There are in principle several techniques to calculate phonons in DFT, some of them requiring nothing more than the application of several DFT ground state calculations in different configurations. Within the frozen-phonons technique, for example,

the frequencies of selected phonon modes can be calculated from energy differences produced by infinitesimal, periodic, displacements of selected atoms from their original equilibrium position in the lattice. Using this technique, to obtain phonons frequencies at a generic $\mathbf{q}$ vector a supercell is required, having $\mathbf{q}$ as a reciprocal-lattice vector and whose linear dimensions to be at least of the order of $2\pi/\mathbf{q}$, a demanding computational requirement that limits the applicability of this method in many practical cases.

The use of DFPT to calculate vibrational properties is instead a very efficient approach, where the responses to perturbations of different wavelengths are decoupled, as shown in Eq.2.24, Eq.2.25 and Eq.2.26, allowing us to calculate phonon frequencies at arbitrary wave vectors $\mathbf{q}$ avoiding the use of supercells and with a workload that is essentially independent of the phonon wavelength,

Used in phonon calculations, the DFPT perturbation is defined by the displacement of an ion L in direction α from its equilibrium position, thus inducing a perturbation $\Delta^\lambda V_{SCF}$ in the electronic KS potential V_{SCF}, leading to a variation $\Delta^\lambda n(r)$ of the charge density ($\lambda \equiv L\alpha$). As we've seen the non-local potential v_{nl} of Eq.3.15 is a corrective addition to the exchange and correlation potential v_{xc}, and its variation $\Delta^\lambda v_{nl}$ must be added to $\Delta^\lambda v_{xc}$ when solving the DFPT equations [25].

In this section we'll start from the energy and potential formulation proposed by Román-Pérez and Soler in Eq.3.18 and Eq.3.19, an interpolation we've seen can be used for vdW-DF and all it's derivatives (vdW-DF2, vdW-DF-c09x, vdW-DF2-c09x and others) and now also to rVV10.

Depending on the specific implementation of the non-local functions, in the RPS scheme both the kernel $\Phi(q_i, q_j, |\mathbf{r} - \mathbf{r}'|)$ and the $\Theta(\mathbf{r})$ functions will have a different form but to keep the following derivation more general, from now on we'll consider $\Theta(\mathbf{r})$ to have the generic expression $\Theta(\mathbf{r}) = c\, n(\mathbf{r})^k P$, with $P(q)$ the interpolating functions. It's easy to check that in any of the aforementioned non-local functionals $\Theta(\mathbf{r})$ can be expressed by a suitable choice of k and c in the general form we introduced, and as we'll see in the next section there is no need to define any specific kernel $\Phi(q_i, q_j, |\mathbf{r} - \mathbf{r}'|)$.

The linear response of the non-local potentials $\Delta^\lambda v_{nl}$ implies several tedious but straightforward algebraic manipulations, but it can be expressed in a concise form as the sum of the linear response of each term present in Eq.3.19, namely $\Delta^\lambda v_{nl} = \Delta^\lambda b + \Delta^\lambda h$. The results for these variations is reported in the following equations

$$\begin{aligned}\Delta^\lambda b = &\sum_\alpha \left[\Delta^\lambda u_\alpha \frac{\partial \Theta_\alpha}{\partial n}\right] + \sum_\alpha \left[u_\alpha \frac{\partial^2 \Theta_\alpha}{\partial n^2}\Delta^\lambda n\right] + \\ &\sum_\alpha \left[u_\alpha \left(\frac{\partial}{\partial |\nabla n|}\left(\frac{\partial \Theta_\alpha}{\partial n}\right)\frac{1}{|\nabla n|}\right)\nabla n \cdot \nabla \Delta^\lambda n\right]\end{aligned} \tag{6.1}$$

$$\begin{aligned}\Delta^\lambda h = &\sum_e \partial_e \sum_\alpha \left\{\Delta^\lambda u_\alpha \left(\frac{\partial \Theta_\alpha}{\partial |\nabla n|}\frac{1}{|\nabla n|}\right)\partial_e n + \right. \\ &u_\alpha \left[\frac{\partial}{\partial n}\left(\frac{\partial \Theta_\alpha}{\partial |\nabla n|}\frac{1}{|\nabla n|}\right)\Delta n\right]\partial_e n + \\ &\left. u_\alpha \left[\frac{\partial}{\partial |\nabla n|}\left(\frac{\partial \Theta_\alpha}{\partial |\nabla n|}\frac{1}{|\nabla n|}\right)\frac{\nabla n \cdot \nabla \Delta^\lambda n}{|\nabla n|}\right]\partial_e n\right\} + \\ &\sum_e \partial_e \sum_\alpha \left[u_\alpha \left(\frac{\partial \Theta_\alpha}{\partial |\nabla n|}\frac{1}{|\nabla n|}\right)\right]\partial_e \Delta^\lambda n\end{aligned} \tag{6.2}$$

where

$$\Delta^\lambda u_\alpha = \sum_\beta \left[\frac{\partial \Theta_\beta}{\partial n}\Delta n + \left(\frac{\partial \Theta_\alpha}{\partial |\nabla n|}\frac{1}{|\nabla n|}\right)\nabla n \cdot \nabla \Delta^\lambda n\right]\Phi_{\alpha\beta} \tag{6.3}$$

Several derivatives of the $\Theta(\mathbf{r})$ functions are needed in Eq.6.1 and 6.2, and considering their q dependence, the complete equations are both involved and very different for each functional definition. We report in Appendix C all the detailed calculation both for vdW-DF type and rVV10 functionals, while in Eq.6.4 we report only the general derivation, common to all the implementations

$$
\begin{aligned}
\frac{\partial\Theta}{\partial n} &= c\,n^{k-1}\left[kP + \frac{\partial P}{\partial q_0}\frac{\partial q_0}{\partial q}\frac{\partial q}{\partial n}n\right] \\
\frac{\partial\Theta}{\partial|\nabla n|}\frac{1}{|\nabla n|} &= c\,n^{k-1}\left[\frac{\partial P}{\partial q_0}\frac{\partial q_0}{\partial q}\left(\frac{\partial q}{\partial|\nabla n|}\frac{n}{|\nabla n|}\right)\right] \\
\frac{\partial^2\Theta}{\partial n^2} &= c\,n^{k-2}\Bigg[(k-1)\,kP + (2k-1)\,\frac{\partial P}{\partial q_0}\frac{\partial q_0}{\partial q}\left(\frac{\partial q}{\partial n}n\right) + \\
&\quad \frac{\partial^2 P}{\partial q_0^2}\left(\frac{\partial q_0}{\partial q}\right)^2\left(\frac{\partial q}{\partial n}n\right)^2 + \\
&\quad \frac{\partial P}{\partial q_0}\frac{\partial^2 q_0}{\partial q^2}\left(\frac{\partial q}{\partial n}n\right)^2 + \\
&\quad \frac{\partial P}{\partial q_0}\frac{\partial q_0}{\partial q}\left(\frac{\partial}{\partial n}\left(\frac{\partial q}{\partial n}n\right)n\right)\Bigg] \\
\frac{\partial}{\partial|\nabla n|}\left(\frac{\partial\Theta}{\partial|\nabla n|}\frac{1}{|\nabla n|}\right)\frac{1}{|\nabla n|} &= c\,n^{k-2}\Bigg[\frac{\partial^2 P}{\partial q_0^2}\left(\frac{\partial q_0}{\partial q}\right)^2\left(\frac{\partial q}{\partial|\nabla n|}\frac{n}{|\nabla n|}\right)^2 + \\
&\quad \frac{\partial P}{\partial q_0}\frac{\partial^2 q_0}{\partial q^2}\left(\frac{\partial q}{\partial|\nabla n|}\frac{n}{|\nabla n|}\right)^2 + \\
&\quad \frac{\partial q_0}{\partial q}\left(\frac{\partial}{\partial|\nabla n|}\left(\frac{\partial q}{\partial|\nabla n|}\frac{n}{|\nabla n|}\right)\frac{n}{|\nabla n|}\right)\Bigg] \\
\frac{\partial}{\partial n}\left(\frac{\partial\Theta}{\partial|\nabla n|}\frac{1}{|\nabla n|}\right) &= c\,n^{k-2}\Bigg[(k-1)\,\frac{\partial P}{\partial q_0}\frac{\partial q_0}{\partial q}\frac{\partial q}{\partial|\nabla n|}\frac{n}{|\nabla n|} + \\
&\quad \frac{\partial^2 P}{\partial q_0^2}\left(\frac{\partial q_0}{\partial q}\right)^2\left(\frac{\partial q}{\partial|\nabla n|}\frac{n}{|\nabla n|}\right)^2 + \\
&\quad \frac{\partial P}{\partial q_0}\frac{\partial^2 q_0}{\partial q^2}\left(\frac{\partial q}{\partial|\nabla n|}\frac{n}{|\nabla n|}\right)^2 + \\
&\quad \frac{\partial P}{\partial q_0}\frac{\partial q_0}{\partial q}\left(\frac{\partial}{\partial n}\left(\frac{\partial q}{\partial|\nabla n|}\frac{n}{|\nabla n|}\right)n\right)\Bigg]
\end{aligned}
$$

Being the non-local potential defined as an addition to the exchange and correlation potential v_{xc} the extension of DFPT to non-local functional amounts simply to the definition and implementation of the variation $\Delta^\lambda v_{nl}$, to be added to $\Delta^\lambda v_{xc}$.

6.2 Phonons dispersion in graphite

The DFPT extension was implemented in the PHONON code of the QUANTUM ESPRESSO[71] package, with particular attention to the efficiency of the algorithm.

In fact it's important to remark that, following the RPS implementation, the kernel interpolation table $\Phi(q_i, q_j, |G|)$ is defined and stored in reciprocal space, while $\Theta_\alpha(\mathbf{r})$ functions, and all their derivatives, are defined in real space. This imply quite a convoluted procedure where first $\Theta_\alpha(\mathbf{r})$ and it's derivatives are computed in real space and stored in memory, then u_α and $\Delta^\lambda u_\alpha$ are calculated in reciprocal space and finally both $\Delta^\lambda b$ and $\Delta^\lambda h$ can be computed, where directions derivatives ∂_e have to be performed in reciprocal space, to be consistent with the potential. This computational effort is roughly of the same order of the potential, already tested to be a quite efficient implementation even for large systems.

We now discuss the phonon dispersion of graphite, obtained with this approach. Graphite is known to a be very interesting benchmark for DFT techniques, having in a simple and compact atomic configuration both strong covalent carbon-carbon bindings between in-plane atoms and weak Van der Waals interaction between different planes. There is an extensive literature regarding phonon dispersion in graphite, obtained both with finite differences methods[112, 113, 114, 115] and with DFPT[116, 117]. In these works LDA approximation showed to give better results compared with experimental data, outperforming the more sophisticated GGA. This difference originates from the ability of LDA to correctly predict the interlayer binding energy, while GGA underestimates it by over 30% [118]. This has been subject of discussion in previous works, and if a comparison between LDA and newly vdW-like functionals exists for the structural results, a comparison of vibrational frequencies between LDA and non-local functionals is still laking.

We present here phonon dispersions of graphite obtained both with LDA, and some of the most common non-local functionals previously mentioned. For all the calculation we used ultrasoft pseudopotentials from the PSLibrary project [91] without further modification. To achieve good energy convergence we used a kinetic energy cutoff of 80 Ry and a charge density cutoff of 560 Ry. We employ a 0.002-Ry Marzari-Vanderbilt smearing of the occupation around the Fermi level and to correctly integrate the crystal cell we used a Monkhorst-Pack[92] k-point grids of $24 \times 24 \times 12$. With this setting, a tight convergence of less than 0.01 mRy in total en-

ergy is achieved. The dynamical-matrix is calculated on a three-dimensional $6 \times 6 \times 4$ Monkhorst-Pack grid in the reciprocal space of the phonon wave-vector $\mathbf{q}$: from this, the dynamical matrix at any $\mathbf{q}$ is obtained by interpolation, imposing frequencies to obey the acoustic sum rule.

In Tab.6.1 we report the structural optimization, with parameters a and c, for all the functionals tested. As we can see vdW-DF type functionals underestimates by $4 \sim 6\%$ the interlayer binding energy, while LDA overestimates it of about 2%; rVV10 functional, inspired by the original VV10 approach, give the best results compared to experimental values. As shown further, this differences will be a key issue in the performance of a specific functional to correctly describe phonon dispersion.

It is worthwhile to discuss briefly why we did not included GGA calculations in this sections. As several works showed in the past years[119], GGA functionals are able to describe accurately only the in-plane covalent carbon-carbon bonds, while they overestimate separation among planes of more than 30%. In Fig. 6-1 we report calculations of ground state energy for a $1 \times 1 \times 1$ graphite cell as a function of both a (in-plane) and c (plane separation) parameters, done in Quantum ESPRESSO with both GGA (PBE) and vdW-DF functionals, and compared with experimental values (dashed black lines in the figure). From this analysis it's evident that, while in vdW-DF the minimum is well defined both for a and c, in GGA the minimization gives good results only for the in-plane parameter a, while the c minimum is both very far from the experimental results and hard to define due to the weak dependence of the energy with respect to the plane separation.

The GGA inability to recover the correct structural properties is a critical issue in phonons calculations, especially for the soft-phonons arising along the $\Gamma - A$ reciprocal directions. A common trick used to solve this GGA shortcoming is to force the experimental result for the planes separation, using the DFT optimal value only for the in-plane distance. This hybrid approach is not needed anymore with non-local functionals, where the correct planes separation emerges in a natural way, and in LDA, where due to some compensation of errors the inter-plane distance is correctly described as well. For this reason we decided to compare only these last two cases,

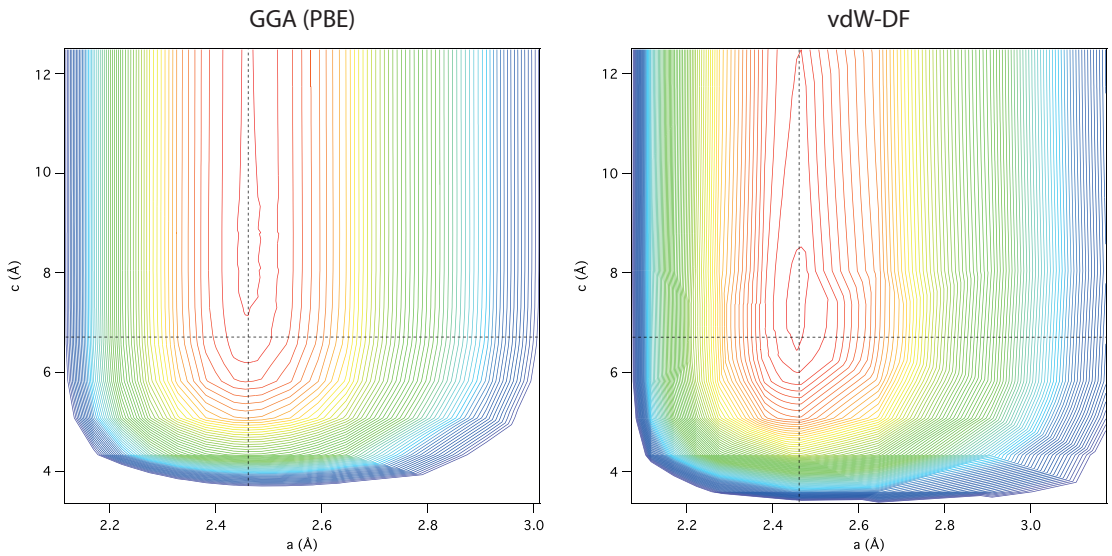

Figure 6-1: Graphite ground state energy as a function of a and c for GGA (PBE) functional and vdW-DF non-local functions. In both pictures the colors represent different energy values, from red (more negative) to blue (less negative), and the experimental value of both parameters is reported with a black dashed line. Absolute binding energies are not important for this analysis and are not reported. and

leaving the analysis of GGA results in previous works to the reader.

In Fig.6-2 we report the results obtained using the DFPT extension introduced for rVV10, vdW-DF and vdW-DF2. In this first figure we plotted the $\Gamma - K - M - \Gamma$ path, a very common choice for graphite represented in Fig. 6-2. The vibrational modes in this specific path are all due to displacements of atoms in the plane, where the strong covalent bonds are present. In general all the functionals describe with good accuracy the phonon dispersion along these directions, recovering almost all the features found in the experimental data. Among the non-local functionals the rVV10 is the best candidate for this system, while both vdW-DF and vdW-DF2 tend to underestimate the phonon frequencies in all the spectra. This is probably due to the small differences found in the structural characterization, resulting in a small systematic error. This difference is more pronounced in the higher frequencies, where the rVV10 significantly perform better than all the other approaches.

A more quantitative comparison can be drawn from the analysis of frequencies at high symmetry points of the cell, as reported in Tab.6.1. We analyzed specific frequencies at Γ, K and M for all the functionals, and compared them with exper-

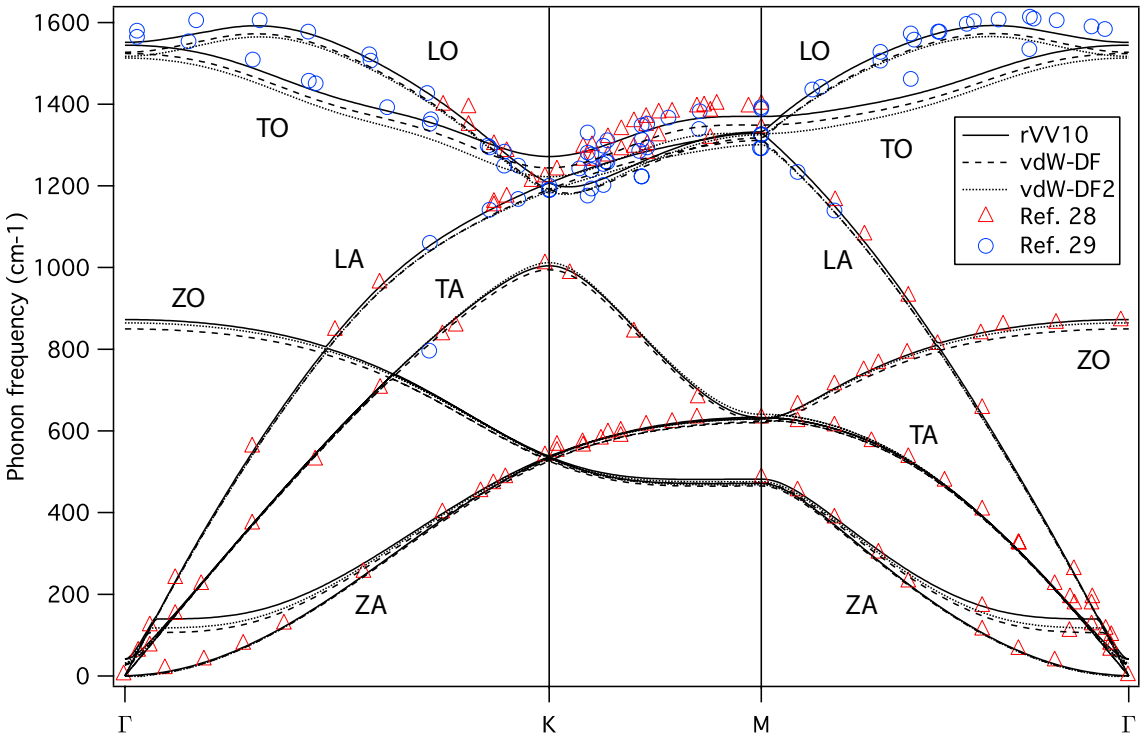

Figure 6-2: Phonon dispersion curves along the $\Gamma - K - M - \Gamma$ reciprocal space path for rVV10 (solid curve), vdW-DF (dotted curve) and vdW-DF2 (dashed curve) obtained with the DFPT extensions introduced in this work. Red circles [120] and blue triangles [121] show experimental results.

		LDA	vdW-DF	vdW-DF2	rVV10	Exp.
Structural optimization						
Opt. a (Å)		2.44	2.48	2.47	2.46	2.46
Opt. c (Å)		3.32	3.59	3.52	3.36	3.35
Phonon frequencies (cm^{-1})						
Γ	ZO	893	849	864	872	868
	LO/TO	1597	1527	1517	1551	1587
M	LA	1346	1311	1300	1328	1290
	LO	1368	1317	1324	1332	1323
	TO	1428	1348	1328	1368	1390
K	LO/LA	1238	1191	1186	1207	1194
	TO	1326	1244	1222	1271	1265
MAE		39.86	24.57	28.29	18.29	-
MAPE (%)		3.21	1.85	2.04	1.36	-

Table 6.1: Comparison of DFT-calculations of phonon frequencies (in cm^{-1}) at high-symmetry points in graphite for LDA, vdW-DF, vdW-DF2 and rVV10 obtained with DFPT. Structural properties (a and c) of graphite are also reported for reference and comparison. Mean Absolute Error and Mean Absolute Percentage Error with respect to experimental data is calculated on phonon frequencies, and reported at the bottom.

imental results. Quantitative results are in agreement with the previous comments: all the vdW-type functional underestimate vibrational frequencies in a systematic way, while rVV10 overestimates only some of them giving consistently better results; LDA frequencies instead are overestimated in all the points here compared. This results are not surprising if we compare them with the structural optimization for each functional: when the in-plane parameter a is overestimated all the vibrational frequencies are underestimated (vdW-DF and vdW-DF2), when instead a is underestimated all the frequencies are overestimated (LDA). rVV10 gives a very accurate structure definition, and the most accurate vibrational frequencies. In Tab.6.1 we report also the Mean Absolute Error (MAE) and Mean Absolute Percentage Error (MAPE), a very concise and clear measure on the goodness of the functionals here analyzed: LDA performs worst than all the non-local functionals in a significant way, while rVV10 results to be the most accurate. As we said LDA correctly describe the graphite for a fortuitous case, while the new non-local functionals, able to account for dispersion interaction by constructions, can reach mush better agreement with experimental results.

A final results we present here is the analysis of soft phonons in graphite. Soft phonons in this system are usually defined as the vibrational modes generating frequencies under the $400cm^{-1}$, and of particular interest are those present along the $\Gamma - A$ reciprocal space path, generated from the out-of-plane atoms displacements. In Fig.6-3 we reported calculations of soft phonons obtained using DFPT both with previously mentioned non-local functionals and the LDA approach, and in Tab. 6.2 we show the analysis for the high-symmetry point A.

All the non-local functionals describe in a good way the phonon dispersion of graphite even in this frequencies range, and while vdW-DF and vdW-DF2 underestimate a little the absolute value, rVV10 preforms best among the three recovering almost all the experimental values. An interesting case is represented by LDA calculations, giving unexpectedly remarkably good results with an absolute error of the order of the rVV10 functional. This fortuitous coincidence has been speculated by some authors [116] as an indicator of the fact that the interlayer binding mechanism

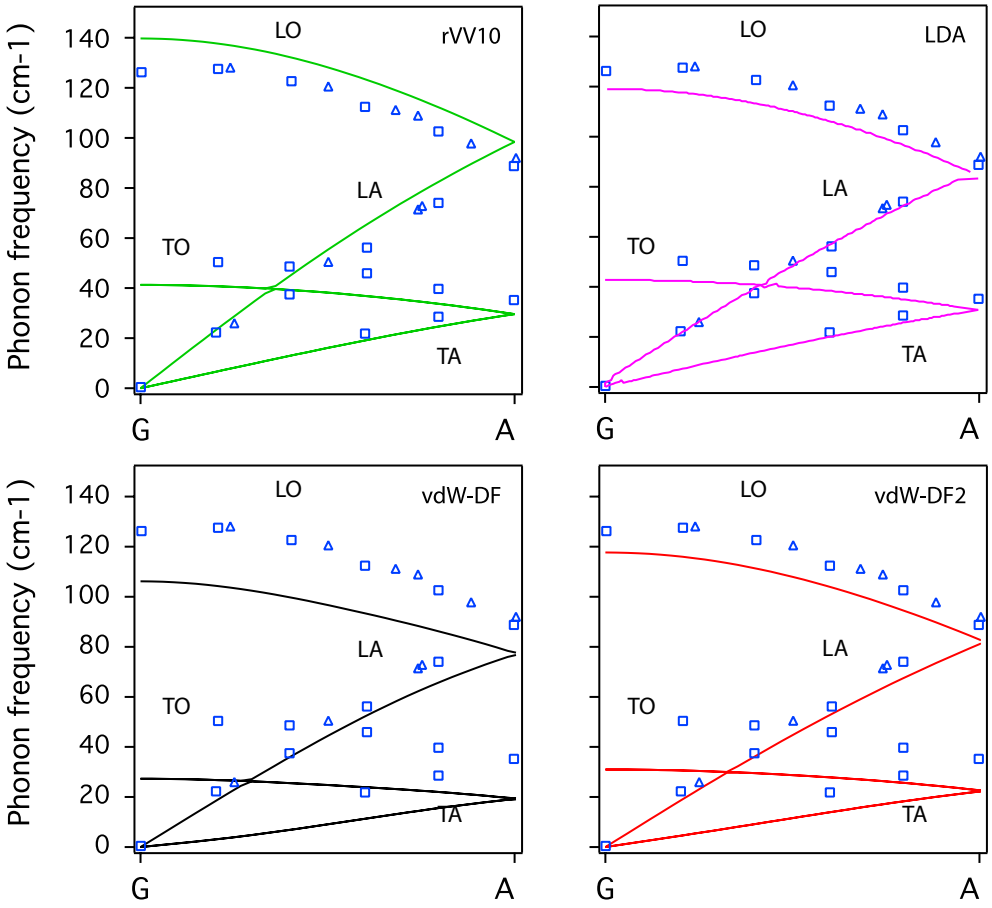

Figure 6-3: (color online) Phonon dispersion curves along the $\Gamma - A$ reciprocal space path for rVV10 (top-left, solid green), LDA (top-right, solid blue), vdW-DF (bottom-left, solid black) and vdW-DF2 (bottom-right, solid red) obtained with the DFPT extensions introduced in this work. Blue triangles [121] and blue circles [122] show experimental results.

		LDA	vdW-DF	vdW-DF2	rVV10	Exp.
Phonon frequencies (cm^{-1})						
A	TA/TO	30	20	22	29	35
	LA/LO	83	77	82	98	89
MAE		5.50	13.50	10.00	7.50	-
MAPE (%)		10.51	28.17	22.50	13.63	-

Table 6.2: Comparison of DFT-calculations of soft phonon frequencies (in cm^{-1}) at high-symmetry point A in graphite for LDA, vdW-DF, vdW-DF2 and rVV10 obtained with DFPT with Mean Absolute Error and Mean Absolute Percentage Error with respect to experimental data reported at the bottom.

could be due not only to dispersion interaction, but also to a small π-π overlapping between molecular orbitals. This aspects certainly needs more profound analysis, but the most probable explanation [123] is that this good results arises just from a peculiar cancellation of errors, not happening in other similar stacked systems.

6.3 Remarks

The DFPT theory extension we proposed allows an efficient calculations of phonon frequencies with non-local functionals, with a small computational cost and without the need of complex supercell calculations or long molecular dynamic runs. This development offers an important tool in the non-local Density Functional Theory, and a new class of studies of soft materials and biological systems are now available. We demonstrate that our extensions is able to work on most implementations of non-local functionals, deriving specific equations for vdW-DF and rVV10 types and finally we tested our implementation on a simple but sophisticated material, graphite, obtaining very good results compared to experimental values. In this work we also noticed the curious case of the ability of LDA to describe soft phonons in graphite, a subject that need further studies to be better understood.

Chapter 7

Conclusions

In this thesis we presented several extensions and developments in the field of non-local density functional theory. Starting from the general formalism proposed by Dion and co-workers, and thanks to the advancement in the field proposed by Román-Pérez and Soler, non-local functionals became a powerful and widely adopted approach to handle dispersions interaction. Proposed only very recently, this new formalism require a number of extensions or developments in order to make its use possible not only in ground state calculations but also in more complex applications.

The first extension we proposed in this thesis is the stress formulation for both the general functional form of Dion and the efficient implementation of RPS. Being defined as the derivative of the energy over the strain tensor, this extension consisted in the functional derivative of the new non-local energy functional to be added to the other terms composing the total energy functional. This implementation has been encoded in the Quantum-ESPRESSO code only for the RPS formulation being the most efficient and used implementation in plane-waves and thanks to the stress it's now possible to approach efficiently structural optimization and characterization of materials under pressure.

We reported an interesting study where the stress implementation was of fundamental importance, where two aminoacid crystals have been investigated under pressure. From these results it's clear that van Der Waals force play a critical role in the correct description of these systems, and thanks to the stress it has been possible

to calculate the compressibility of these two materials, results in good agreement with experimental results.

The the second extension we proposed in the thesis is the formulation of a new non-local functional derived from the work of Vydrov and Van Voorhis. In 2010 these authors proposed a remarkably accurate form of non-local density functional, called VV10, with impressive results on several benchmark sets commonly used in this field, such as the S22. This new functional unfortunately cannot be expressed in a way suitable for the RPS interpolation scheme, and the computational cost involved in any plane-wave DFT code makes this approximation manageable only for very small systems.

We presented a revision of the VV10 functional, introducing a simple approximation that keeps the same functional behavior and precision, with an analytics form that is separable as dependent on two identical functions of $\mathbf{r}$ and $\mathbf{r}'$. The new functional, rVV10, can be interpolated with the efficient RPS scheme and it has been implemented in the Quantum-ESPRESSO package. Several examples have been reported showing the accuracy of this new functional, on the same set S22 and on graphite, compared both with highly accurate quantum chemistry results and experimental ones when available.

The final development presented in the thesis is focused on Density Functional Perturbation Theory, with its particular application in phonon calculations. Vibrational properties of soft material are becoming of great interest for many applications in the recent years, and DFPT represent the most efficient and practical theoretical framework to account for vibrational properties, with respect to the usual frozen phonon approach or similar techniques.

An extension of DFPT has been developed to account for non-local functionals, both in a general formalism and in the specific cases of *vdW-DF*-type and *rVV10*-type functionals. This new development require some new derivatives to be computed, but the computational cost is of the order of the potential calculation, and an efficient code has been developed for the Quantum ESPRESSO suite. As an example we report the first fully *ab-initio* calculations of soft phonons in graphite with non-local

functional, showing the great accuracy of these new approach in the prediction of the experimental results.

All these developments represent important advancements in the non-local density functional theory and offer some fundamental tools for material discovery and characterization. With the stress formulation, a new accurate non-local functional and the ability to compute phonons in an efficient way the theory is now complete for complex and sophisticated analysis and researches. Nevertheless a lot of work needs to done, and several open questions have to be addressed in future research, from a spin resolved extension of these functionals to a rigorous integration in their contribution in the construction of pseudo-potentials now still missing. There and other topics are under active investigation and they'll be the focus of our future research.

Appendix A

Moka: MOdeling pacKage for Atomistic simulations

In this chapter we introduce Moka (MOdeling pacKage for Atomistic simulations), an open-source modeling GUI that offers editing, visualization and execution features built specifically for *ab-initio* calculations. Based on Java programming language and build with state-of-the-art open source libraries, Moka is an extensible and modular software implemented originally for Quantum ESPRESSO and now available to the community through the Quantum ESPRESSO Foundation.

A.1 Introduction

In the recent years *ab-initio* atomistic simulations are becoming a fundamental resource for new material characterization and discovery. Once limited only to simple systems counting very few atoms, modern softwares implementing accurate theoretical methods at the level of quantum mechanics, such as Density Functional Theory or other post-Hartree-Fock *ab-initio* quantum chemistry methods (Configuration Interaction, Coupled Cluster, Møller-Plesset perturbation theory and others), are nowadays used for simulations of extend systems; from catalytic processes[124] to long molecular dynamics[125], complicated biological molecules and crystals comprising several hundreds or thousands atoms.

This achievements have been possible only thanks to both sophisticated parallel programming techniques and the ever growing computational power available on large scale High Performance Computing clusters. Calculations once considered unfeasible are now common objective in numerical atomistic simulations, and entirely new approaches can be investigated. In particular high-throughput techniques[126, 127], consisting in structural optimization through configuration-space searches and combinatorial substitutions, are becoming promising tools for new materials discovery, giving already interesting results that only few years ago seemed decades away[128, 129].

These new possibilities, "thousands atoms"-size systems and execution of massive batches of atomic configurations, pose new challenges in the numerical simulation field that have to be addressed with novel and ad-hoc solutions. While the science behind a small-size system and a big-size one is absolutely identical, the numerical challenges of the latter are effectively becoming the most complex aspect of this research. For simplicity we can split these challenges in two different domains: ones involving issues on the scaling of the simulation codes (parallel programming techniques, hardware infrastructure efficiency, etc.), and others including the preparation, management and execution of these simulations.

While code scaling techniques, and technologies are a very active field of research since several years, moving from peta-scale to exa-scale objectives, solutions on how to handle these new simulations emerged as an important issue only very recently[130, 131]. In this work we present a new program we developed to address these issues, called Moka (MOdeling pacKage for Atomistic simulations) and built from the beginning to lower the complexity in the preparation and execution of big-size and massively parallel simulations.

A brief summary on GUIs for atomistic simulations

Moka is essentially a modeling graphical user interface (GUI) for atomistic simulations, targeted to researchers and experts in the numerical simulations of matter. GUIs have a very long history in this field, and with modeling we refer to a complex set of features in the past addressed usually independently. In general "modeling"

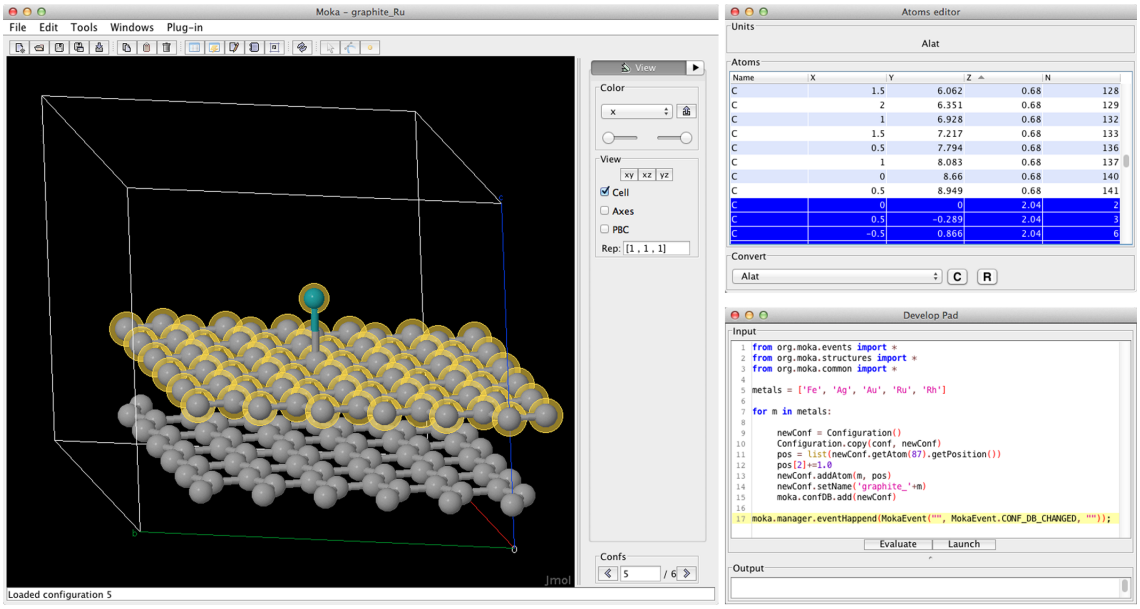

Figure A-1: Moka GUI in the initial configuration. On the left the main window, with the visualization frame in the center showing one atomic substrate, explained later in the example, with some selected atoms in yellow. On the window's right there's the modeling toolbar, divided in three tabs, and the configuration selector at the bottom of it. On the figure's right, at the top the Atoms Editor windows is displayed, where all the atoms in the configuration can be edited in all the details (in blue the selected atoms identified in the visualization). On the figure's right at the bottom the Development Pad with the script shown in List. A.3.

consist of four main tasks:

- **Structure definition**. This is the very beginning of any numerical simulations. In consist in the definition of the structure we want to study, from the atomic positions to the chemical composition of each atom, and possible cell parameters (or space groups) for crystal structures. Even if this step can be in principle reduced to the simple enumeration of positions and chemical symbols for each configuration, modern softwares have to be able to import structures from input and output file of other programs, or from public and private databases. In the years an enormous amount of work has been dedicated to engineer efficient data structures (and formats) to define atomistic configurations, and several database are present collecting hundred thousands different materials, such as the Inorganic Crystal Structure Database[132] or Cambridge Structural Database[133]

The ability to import structures from different sources and in many formats is a fundamental feature for an efficient modeling GUI.

- **Visualization**. Once the configuration is defined the ability to interact with the structure under analysis is highly empowered by the visualization techniques available. Starting from the famous "ball-and-stick" and "space-filling" representations of the Dreiding and Corey-Pauling-Koltun mechanical models [134], visualization tools are now an impressively fast-growing field in scientific research. To handle structures with hundreds or thousand of atoms efficiently new tools are needed, with features helping to lower the complexity of handling these systems, such as shortcuts to immediately find some species, or the possibility to switch-off some part of the system when working on small local details, shading techniques to let the user see through several layers and many others. A flexible visualization sometimes plays a crucial role in a modeling software, and due to the high computational effort involved in visualization and rendering this aspect became of critical importance.

- **Structure elaboration**. At the core of any modeling software, the structure elaboration represent the very toolbox for material discovery. Starting from an initial configuration, a surface for example, researches sometimes need to add new parts, molecules or atoms either build from scratch or imported from other sources. Atoms need to be moved, rotated, deleted or substituted with other chemical species, sometimes it's useful to duplicate parts, or cut others along planes and axes. These and many other functions are things that makes a modeling software a real plus in atomistic simulations. Moreover, most of the times modeling tools are needed in a programmatic way, using scripts to to replicate and iterate the operations among hundreds or thousands of difference configurations; something usually done with ad-hoc scripts and code snippets, an impractical solution that rapidly shows its limits with the growing size of the problem.

- **Execution of the simulation**. The modeling usually concludes with a nu-

merical simulation, today possible with tens of *ab-initio* codes available, from open-source distributions [29], [135] to commercial and closed source ones [136]. Most of these codes can be run in serial mode, for small and simple calculations, or in parallel mode on modern High Performance Computing (HPC) clusters, where more interesting applications and big-size calculations are the possibility. Modern *ab-initio* codes can run on this infrastructures with remarkable efficiency, and this will be the main application target we're going to discuss in this work. HPC clusters are sometimes complicated architectures with queue management systems and special configurations necessary to correctly use the I/O resource and the computing nodes. The modeling GUI should in principle help the researcher to overcome this complexity, offering a simple way to interact and launch one, or thousands, simulations in a seamless way.

This four groups of functions are all essential building blocks for a complete modeling GUI able to support researches with highly complex simulations and structures. Nowadays several GUIs are present on the market, most of them freely available and open-sourced by the authors, implementing some of the main features just discussed. We'll shortly review some of the most important cases, focusing only on open-source codes. This choice is motivated both because we believe open-source is by far the best option for scientific community and because, since the internal procedures used by closed-source codes are not known, it's hard to comment with sufficient precision on this alternatives.

The most basic GUIs are focused only on input parsing and conversion, with Open Babel [137] probably the most comprehensive one available. Capable of handling more than 100 different configuration formats, from XYZ to CIF[138], from legacy formats to standards such as Chemical Markup Language [139], several GUIs have been built upon this software library, offering only the automatic conversion procedures between the various formats. Even if some very basic modeling functions have been recently implemented, such as hydrogen bond addition and removal, these packages in general do not interface with any configuration databases and miss all the other three features listed above, visualization, modeling and execution.

Some more evolved GUIs are the structure visualization packages, such as Visual Molecular Dynamics (VMD)[140], Jmol [141] and XCrysDen [142]. With this codes some basic input parsing techniques are implemented, sometimes using OpenBabel as a library, and the core features are all about visualization of structures and properties. From static snapshots to dynamic molecular dynamics visualization, this packages evolved in the recent years as robust analytics tools. In most cases it's possible to visualize much more than the bare atomistic arrangement, plotting as well charge distributions, dipoles, forces and many other features derived from external codes. VMD in particular has been able to extend it's initial visualization functions thanks to an efficient plug-in infrastructure and a vibrant community of users, but even if some modeling extensions have been developed, both VMD as well in all the other visualization packages the modeling features are limited to the very essential ones, where mouse dragging is most of the times the only way to interact with atoms.

A final class of softwares we like to cite in this short review is comprised of packages that implements almost all the features described before, where VESTA [143] and Avogadro [144] are in our opinion the most interesting cases. In these packages, inputs, visualization and modifications of atomic structures are implemented in a very efficient way, giving the user a very broad range of possibilities. In particular Avogadro, with the flexible plug-in infrastructure developed by the authors and the Python scripting interface, covers all of the first three classes of features we listed as necessary for a modern atomistic modeler. Nevertheless, the execution of the simulation is most of the times left to the user, and these packages offer only partial input generation for specific codes, hard to extend and maintain.

To conclude we'd like to point the reader to a recent implementation we think covers in a very efficient and flexible way most of the requirements for atomistic modeling, Atomic Simulation Environment (ASE) [145]. As a set of libraries originally build for the Python scripting environments, visualization features are limited only to simple asynchronous image rendering, but the modeling functions and the general management of the configurations offered are remarkably efficient and flexible. As a library, ASE can in principle be integrated in other environments implementing a

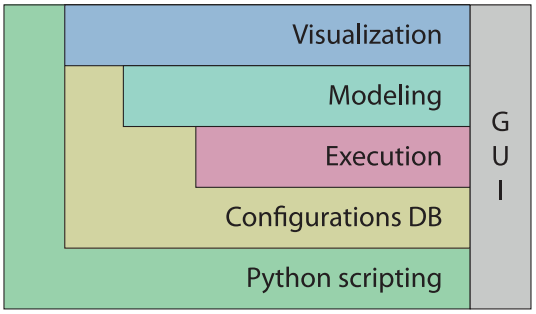

Figure A-2: Moka modular architecture. Through the GUI a user can interact with all the modules, while scripting can be decoupled from visualization and GUI as well giving the best performance and flexibility.

Python engine such as Moka[1].

A.2 The Moka program

Moka is a GUI build to cover all the four features previously discussed. Started in late 2011 as an experimental tool for some specific use cases, the project gained traction in the Quantum ESPRESSO development team and became a flagship project of the Quantum ESPRESSO Foundation in mid 2012. With this work we present the first version available for developers to download, that will be followed in next months by a public release for end users.

The code has been build with a modular approach, as shown in schema of Fig. A-2, where all the modules offer APIs to the rest of the code for integration and management, while a sophisticated event handling mechanism is implemented to keep in sync information in all the environment. The user can interact with the core modules only through the GUI or the scripting environment, depending on the research need, and special features have been implemented to give both the approaches the best performance possible [2].

[1] ASE integration with Moka as successfully achieved, as reported in the Moka home site

[2] With the GUI all the code responds to give the best fluid experience for the user, with all the modules and windows lively updated. With the scripting environment the code renounces to the live updates and synchronicity to overcome possible bottlenecks with batch executions of scripts and favor speed and computational power.

Configuration DB

The first block, the Configurations DB, is where all the input and structure representation takes place. Using OpenBabel as the input library, Moka can read more then 100 input formats that are represented in memory with a very efficient object structure, the so called DB. Each entry in the DB is called configuration, and since Moka has been developed for periodic structures, a configuration is defined by both a cell (a set of three 3-dimensional arrays) and a list of atoms identified by a name, a chemical type and a position in space. For each configuration the metric can be absolute (in atomic units or Angstroms), or relative with respect to the lattice.

The DB structure is a hybrid implementation of in-memory and local-disk storage, able to let the user store thousands of configuration in a seamless way between rapid in-memory access and disk-access; the recently used configuration will be kept in memory and the old ones will be dumped in the local-storage automatically. All the primitive functions to load a configuration in memory and interact with its elements such as addition or deletion of atoms, modification of cell properties and positions, selection of atoms (an inner property of atoms in Moka) and many others are offered by this module for all the applications.

Some note worthy implementations are the procedures to copy& paste of atoms between configurations, with automatic conversion of the metric, copy& paste of configuration, refolding of atoms in the cell with periodic boundaries conditions, the automatic generation of structures starting from the Whyckoff definitions and the implementation of direct queries on several crystallographic databases such as the ICSD and the CSD [3].

All the *Configuration DB* functions are present in the GUI both in the toolbar and through specific menus, as shown in Fig. A-1, while the other modules interact with the DB through its APIs and the event lister approach previously discussed.

[3]For external database connections authentication is necessary to access the service, parameters that can be modified from the GUI

Visualization

An evident part of the GUI in Fig. A-1 is the Visualization module. The visualization of atomic structures is a formidable complex problem, especially if code efficiency and rendering speed are important. Thanks to the open-source nature of the Moka code we decided to integrate the powerful visualization library Jmol [141], integrated with the rest of the code with the addition of a middle layer that handles event listeners and APIs, converting them to Jmol instructions.

The event listeners handle both side of the communication, for example when an atom is selected in the viewer (Jmol event) a Moka event for atom selection is broadcasted, while when the same selection happens in the GUI an event is received from the middle layer and converted to a specific Jmol instruction. This happens for all the events, atoms and cell modifications, configuration change in the DB, an so on. The middle layer does not add any computational cost, and the redundancy is limited to the single configuration visualized that is stored both in Jmol and Moka, a very low memory footprint in all the cases.

Thanks to this integration in Moka there are all the advanced visualization functions offered by Jmol, seamlessly integrated with the rest of the code, accessible both from the GUI and the scripting engine and some specific APIs added to the middle layer to simplify the visualization of periodic crystal cells.

Modeling

The Modeling module is the core set of functions that allows the user to interact with a specific configuration. Once a configuration is loaded the entire set of modeling functions are available through the GUI with simple buttons and input interfaces.

To list the most important ones, a user can add and remove groups of atoms, translate them along crystal axes by user defined vectors, rotate them around a point or a line, mirror atoms over planes, generate supercells, change the metric from absolute to relative, modify the crystal cell with scaling functions or directly modifying the basic axes. More sophisticated features, such as removal of atoms along

Miller planes, generation of subcells and configuration merging are illustrated in the documentation and are not discusses here for brevity.

Thanks to the event dispatching architecture, all the Moka modules will react to the modeling events, so that the visualization will be updated in sync with the events as well the atomic positions tables and all the other GUI features. To give an example, atom-atom distance indicators added in the viewer will be automatically refreshed after each atom translation applied during modeling giving the user a real-time feedback on his modifications.

Execution

The execution engine is one of the most innovative feature present in Moka, and its detailed analysis would require a long and technical discussion we believe it's not of interest for the reader in this context. We discuss in this section the execution implementation strategy, showing the main advantages present for the user and we point the reader to the Moka home site for a more details documentation.

The execution engine in composed of two parts, an Execution module present in Moka and a small Execution Daemon to install on the computing machines preferred by the user. The Execution Module, represented in Fig. A-2 and available to the user through main window's top menu and toolbar, offers a step-by-step user interface covering both input parameters definition and simulations execution.

When a structure is ready to be simulated, with the help of visualization and modeling functions, only a small part of the problem is solved. Every *ab-initio* code in fact needs a long and software-specific list of parameters to be able to function properly. This would in principle require a specific GUI implementation for each code, implying an enormous effort by the developers to keep the GUI updated with all the *ab-initio* codes updates.

To solve this issue we implemented a simple solution capable of handling and visualizing in a flexible way any kind of input parameter list, suitable to work in principle with input form and based on two external files for each ab-intio code, an input descriptor and a python script. All the parameters for a specific code are

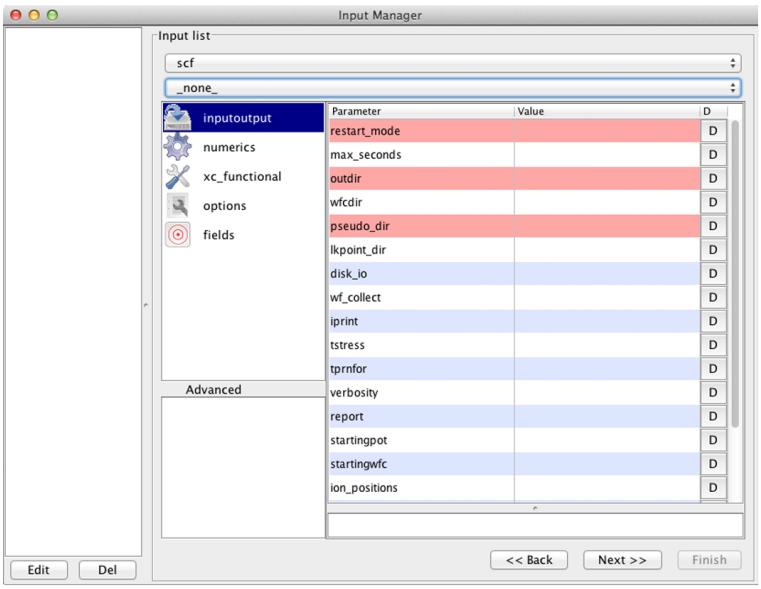

Figure A-3: Moka input GUI generated from the Quantum-ESPRESSO input descriptor. In top combo menu the type of simulation can be selected (scf, nscf, relax, ecc..) and in the central part all the inputs are shown to edit, grouped following the descriptor's rules. Red parameters are mandatory for the simulations, an in the bottom window helper description of the selected input is shown to the user for support.

described in an external XML descriptors following a specific scheme; each parameters type (integer, real, string, external file, matrix, etc.) can be defined with a name, a possible default value and an helper text for the user. When the user starts a simulations, Moka will present a list of input descriptors present in the Moka home directory and after the user selection a GUI window will be automatically generated following the descriptor definitions. The input window generated from the Quantum-ESPRESSO descriptor is reported in Fig. A-3

Once the user input is completed all the parameters are collected in a map and the python script specific for that *ab-initio* code will be called. In this script the materialization of the input will happen, following the very specific conditions and formats used by the developers, returning one or several input files needed to start the simulation. In this way each code can be integrated in Moka only with the definition of an input descriptor and a python script, a much better solution both for code updates and for future expansion.

The second part of the execution engine is the Moda Daemon, a small sever

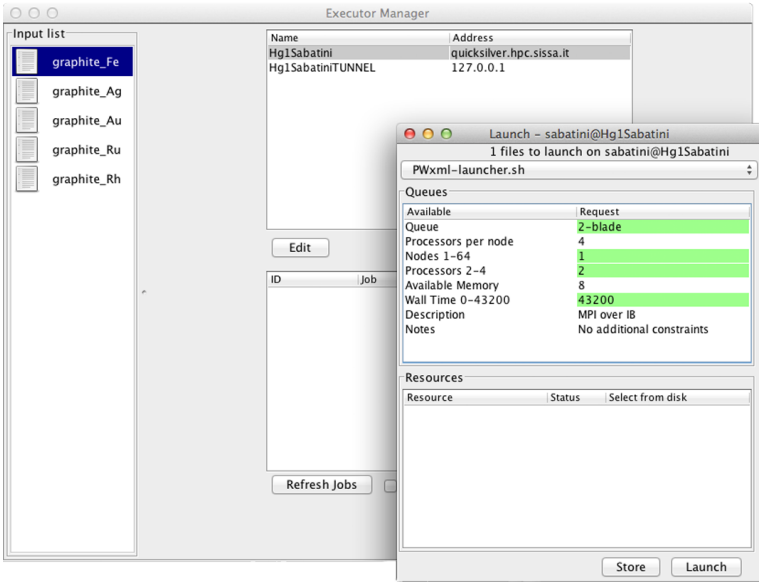

Figure A-4: Moka execution interface. In the bottom window all the input previously the simulation have to be executed. In the top window, appearing after a specific machine and set of inputs are selected, the user con define all the parameters for the configuration, a dynamical GUI built following the Moka Daemon responses on the specific remote machine's queue characteristics. In this figure results of the simple user case explained in the last section is reported.

interacting with Moka and installed in the user preferred computational unit. On modern HPC machines, usually give access to users only through interactive Secure Shell sessions, the Moka Daemon is a small software that abstract all the technical details of the specific HPC machine to a more general and simple level. That the user can copy the daemon in its own home directory using Moka initiate and manage the queue processes in a simple way.

With Moka the user can interact directly with the Moda Daemon installed on his account, sending hundreds of simulations at once and collecting back results. Interfaces to test the status of each run, and the possibility to open a file interactively on the cluster are features Moka implements, partially shown in Fig. A-4 and documented in the home site. This approach reduces the execution complexity of any numerical simulations to the sole input definition, where the scientific knowledge is fundamental, while leaving the technical details to be accounted by the Moka Daemon.

Scripting and GUI

The four main blocks described before, representing the core Moka's functionalities, are available to the user in two ways: through a visual GUI or a scripting interface. A snapshot of the GUI is reported in Fig. A-1, showing some of the main windows in use. On the left the main window showing up at the start, with several menus and toolbars on top of the Jmol visualization interface in the middle. At the right border of the main window a vertical contains all modeling tools described above, and at the bottom the configuration navigator lets the user scroll and move in the Configuration DB.

On the figure's right, the Atoms Editor (on top) shows the list of all the atoms present, giving the user the ability to select and modify all atoms properties (position, name and chemical element), and the Developer Pad (bottom) is the interface needed to interact with the scripting engine, an efficient way to use all the core functionalities, and some of the GUI ones, in a programmatic way.

The coexistence of GUI access and the scripting interface it's a fundamental characteristic of this package and gives the user a great flexibility in structure modeling. GUI access is mainly focused for single configuration details, when the assembly of the atoms is taking place. Adding clusters to a surface, packing molecules in a crystals, selecting specific configurations from a range of outputs, tilting or rotating some molecules in the systems; all these actions are better performed with the visual aid of the visualizer and the modeling commands present in the GUI.

On the other side, when automatism is necessary, the scripting engine works at best. Building extended systems with a simple repetitive pattern, such as nanotubes of graphite, generating variation of a specific configuration, such as compression or expansion, combinatorial substitution of elements and generation of trial structures for optimization algorithms or automatic generation of structures with different parameters. These and many more cases are perfect examples where a programmatic approach can be of great support. As we'll see in the next section, identical results can be obtained with both procedures and it's up to the user to chose the most adequate

one for his specific use case.

A.3 A simple use case

In this section we preset a simple example where Moka can be of great help. As we discussed the same results can be obtained with different approaches, and we present a mixed approach where both either the GUI or the scripting engine are used depending on their effectiveness.

Building graphite

Supported metallic clusters on graphite are a very interesting system under active investigation in the recent years[146, 147, 148] showing unique conductibility and catalytic properties that attracted the attention of both scientific and industrial players. Several *ab-initio* numerical simulations have been conducted in the years, and this structures are a perfect candidate to show the power of Moka modeling features.

There are several ways to build graphite in Moka. The first one we explain uses only the GUI tools, starting with a new empty configuration (File → New). The graphite crystal cell has to be set (Edit → Cell) with the alat parameters (for graphite $a = 4.65 a.u.$ and $c = 12.65 a.u.$) and all the tree cell axes $a_1 = [1/2,\ sqrt(3)/2,\ 0]$, $a_2 = [-1/2,\ sqrt(3)/2,\ 0]$, $a_3 = [0,\ 0,\ 4 \cdot c/a]$ (the 4 mutiplying the natural cell dimension is due to the fact we want some distance between periodic replicas in the z direction). Notice that all the input texts in Moka are connected to a mathematical parsers, and inputs like $sqrt(3)/2$ are automatically transformed in their numerical value. After this step the four atoms in the unit cell have to be added (Edit → Atoms → Add) and positioned using the Atoms Editor table, in this case we'll have four basis atoms in $[0,\ 0,\ 1/4(c/a)]$, $[1/2,\ sqrt(3)/6,\ 1/4(c/a)]$, $[0,\ 0,\ 3/4(c/a)]$ and $[1/2,\ -sqrt(3)/6,\ 3/4(c/a)]$.

Graphite unitary cell is now ready, and we can produce a larger supercell (Tools → Cell Tools → Make Supercell) of $6 \times 6 \times 1$. Now we conclude the GUI part by selecting, in the viewer or with the Atoms Editor, a specific carbon atom on the upper

graphite layer to host a metallic adatom on top, in our example the atom number 87 positioned.

Using script for automation

The objective of this simple example is building a set of configurations composed of two graphite planes with different metallic adatoms of top of a carbon atoms. To do this we can copy and paste this initial configuration just edited (Edit → Configurations → Copy / Paste) and adding the single metallic atom at a preferred position with the GUI, or we can use the scripting environment to automatize this process.

In List. A.3 we report a short script for the Moka Development Pad that generates all the final configurations with selected metallic adatoms positioned of top of carbon atom number 87. In the script, after the library imports, in the main loop (line 7), iterating over the metals array (line 5), the active configuration in Moka is cloned (lines 9 and 10), the 87th atom position is extracted (line 11) and modified (line 12) to let the adatom have some distance from the substrate. A new atom is added in the modified position (line 13) and the configuration is added to the DB with a new name (lines 14 and 15). After the loop a new event is generated re-synchronizing all the modules with the new DB changes (line 17).

After the script execution the new configurations are also available in the GUI, and the execution engine can be launched to set the input parameters and send the simulations to the cluster. For the sake of brevity we skip this last passage, described in the documentation on the Moka home site.

Even in this simple example the power of this hybrid approach is evident: having both the GUI and the scripting engine helps the user to have the best experience in any use case, an interactive approach in the buildup of the main structure and a faster one for repetitive tasks.

```
from org.moka.events import *
from org.moka.structures import *
from org.moka.common import *

metals = ['Fe', 'Ag', 'Au', 'Ru', 'Rh']

for m in metals:

 newConf = Configuration()
 Configuration.copy(conf, newConf)
 pos = list(newConf.getAtom(87).getPosition())
 pos[2]+=1.0
 newConf.addAtom(m, pos)
 newConf.setName('graphite_'+m)
 moka.confDB.add(newConf)

moka.manager.eventHappend(MokaEvent("", MokaEvent.CONF_DB_CHANGED, ""));
```

A.4 Remarks

In this chapter we presented Moka, a new software which aims to be an exhaustive package for atomistic modeling, with a particular focus for *ab-initio* simulations. Covering all the necessary features we believe a modern modeler should offer to the user, such as a flexible input engine, visualization and modeling tools and an execution management infrastructure, this first version of the code is already a powerful solution to handle research activities on complex materials and with large scale necessities.

Right now Moka is distributed by the Quantum ESPRESSO Foundation as an open-source code with a BSD license, allowing developers and researchers to modify, add and extend the original code to cover more specific needs and add new functionalities.

Appendix B

Stress derivation details

As we previously said the stress tensor $\sigma_{\alpha\beta}$ is defined as the derivative of the energy over the strain tensor $\epsilon_{\alpha\beta}$.

$$\sigma_{\alpha\beta} = -\frac{1}{\Omega}\frac{\partial E}{\partial \epsilon_{\alpha\beta}} \tag{B.1}$$

In density functional theory the energy is defined as a functional of the charge, and to calculate derive the stress we use a simple procedure proposed by Nielsen and Martin[149]. In this appendix we'll summaries the basic derivation for the stress for LDA, GGA and non-local DFT functionals, and we refer the reader to other works for the remaining terms of the energy functional[70].

$$\begin{cases} r \rightarrow & \tilde{r} = (1+\epsilon)r \\ G \rightarrow & \tilde{G} = (1-\epsilon)r \\ \Omega \rightarrow & \tilde{\Omega} = |1+\epsilon|\Omega \\ \Psi(r) \rightarrow & \tilde{\Psi}(r) = \frac{1}{|1+\epsilon|^{1/2}}\Psi\left((1-e)\tilde{r}\right) \\ n(r) \rightarrow & \tilde{n}(r) = \frac{1}{|1+\epsilon|}n\left((1-e)\tilde{r}\right) \\ \nabla_\alpha n(r) \rightarrow & \nabla_\alpha \tilde{n}(r) = \frac{1}{|1+\epsilon|}\nabla_\beta\left(n\left((1-\epsilon)r\right)\right)\cdot(1-\epsilon)_{\beta\alpha} \end{cases} \tag{B.2}$$

The calculations proceed as follow: we first apply and homogeneous expansion as defined by the relations in Eq.B.2 and then we rescale the density and the wavefunc-

tions. The differential of the energy thus obtained defines in a simple way the stress tensor.

Stress in LDA

In this case the exchange and correlations functional is defined as

$$E_{xc} = \int_{\Omega} n \cdot F_{xc}\left(n\right)\, d^3r \tag{B.3}$$

We apply the stress variation

$$E'_{xc} = \int_{(1+\epsilon)\Omega} \frac{n\left(\left(1-\epsilon\right)r'\right)}{|1+\epsilon|} \cdot F_{xc}\left(\frac{n\left(\left(1-\epsilon\right)r'\right)}{|1+\epsilon|}\right)\, d^3r' \tag{B.4}$$

and the rigid rescaling

$$E'_{xc} \xrightarrow{r' \to (1+\epsilon)r} \int_{\Omega} n(r) \cdot F_{xc}\left(\frac{n(r)}{|1+\epsilon|}\right)\, d^3r \tag{B.5}$$

We know calculate the differential of the energy, that defines the stress tensor

$$\begin{aligned}
\delta E'_{xc} &= \int_{\Omega} n \frac{\partial F_{xc}}{\partial n}\, n \left(-\sum_{\alpha} \epsilon_{\alpha\alpha}\right)\, d^3r = -\sum_{\alpha} \epsilon_{\alpha\alpha} \int n^2\, \frac{\partial F_{xc}}{\partial n}\, d^3r \\
&= -\sum_{\alpha} \epsilon_{\alpha\alpha} \int n \left[\frac{\partial\left(F_{xc}\, n\right)}{n} - F_{xc}\right]\, d^3r \\
&= \sum_{\alpha} \epsilon_{\alpha\alpha} \left[E_{xc} - \int n \cdot v_{xc}\, d^3r\right]
\end{aligned} \tag{B.6}$$

Stress in GGA

In this case the exchange and correlations functional is defined as

$$E_{xc} = \int_{\Omega} F_{xc}\left(n(r), |\nabla n|\right) d^3r \tag{B.7}$$

As before, we apply the stress variation

$$E'_{xc} = \int_{(1+\epsilon)\Omega} \frac{n\left((1-\epsilon)\,r\right)}{|1+\epsilon|} \cdot F_{xc}\left(\frac{n\left((1-\epsilon)\,r\right)}{|1+\epsilon|}, \frac{1}{|1+\epsilon|}\left|\nabla n\left((1-\epsilon)r\right)\left((1-\epsilon)\right)\right|\right) d^3r \tag{B.8}$$

and the rigid rescaling

$$E'_{xc} \xrightarrow{r\to(1+\epsilon)r} \int_{\Omega} n\left(r\right) \cdot F_{xc}\left(\frac{n\left(r\right)}{|1+\epsilon|}, \frac{1}{|1+\epsilon|}\left|\nabla n\left((1-\epsilon)\right)\right|\right) \tag{B.9}$$

Using $\left|\nabla n\left((1-\epsilon)\right)\right| = \sqrt{\left|\nabla n\right|^2 - \sum_{\alpha\beta} 2\nabla_\alpha n \epsilon_{\alpha\beta} \nabla_\beta n + O(\epsilon^2)}$ we can calculate the differential (some straightforward algebraic manipulations are omitted for brevity)

$$\delta E'_{xc} = -\sum_{\alpha} \epsilon_{\alpha\alpha} \int_{\Omega} n(r) \left[\frac{\partial F_{xc}}{\partial n} n + \frac{\partial F_{xc}}{\partial\left|\nabla n\right|}\left|\nabla n\right|\right] - \sum_{\alpha\beta} \epsilon_{\alpha\beta} \left[\int_{\Omega} n(r) \frac{\partial F_{xc}}{\partial\left|\nabla n\right|} \frac{\nabla_\alpha n \cdot \nabla_\beta n}{|\nabla n|}\right] \tag{B.10}$$

Noting that $\frac{\partial F_{xc}}{\partial n} n = \left(\frac{\partial (F_{xc} n)}{\partial n} - F_{xc}\right)$ and $|\nabla n| = \frac{\nabla n^2}{|\nabla n|}$ we can recast the GGA stress term in a much simpler form (here as well some straightforward algebraic manipulations are omitted for brevity)

$$\delta E'_{xc} = \sum_{\alpha} \epsilon_{\alpha\alpha} \underbrace{\left[E_{xc} - \int_{\Omega} n \cdot v_{xc}\right]}_{\text{LDA-like}} - \sum_{\alpha\beta} \epsilon_{\alpha\beta} \left[\int_{\Omega} n(r) \frac{\partial F_{xc}}{\partial\left|\nabla n\right|} \frac{\nabla_\alpha n \cdot \nabla_\beta n}{|\nabla n|}\right] \tag{B.11}$$

Stress in non-local functionals

Non local functionals, as described in Chap.3 depend on n,n',$|\nabla n|$,$|\nabla n'|$ and $|r-r'|$. Calculation are involved, but nothing more that mere algebraic manipulations are necessary to follow the derivation. For the sake of brevity we split the derivation in three steps, showing the different steps needed to obtain the final result.

We first we consider the restricted case of a functional defined as $F_{xc} \equiv F_{xc}(|r-r'|)$. Following the same derivation used for LDA and GGA we obtain, skipping the intermediary steps,

$$\delta E_{xc}^{|r-r'|} = \frac{1}{2}\sum_{\alpha\beta}\epsilon_{\alpha\beta}\int_\Omega d^3r\int_\Omega d^3r' n\, n'\,\frac{\partial F_{xc}}{\partial\,|r-r'|}\frac{(r-r')_\alpha\cdot(r-r')_\beta}{|(r-r')|} \tag{B.12}$$

Now we analyze the results for a generic functional of the form $F_{xc} \equiv F_{xc}(n, n')$, obtaining

$$\delta E'_{xc} = -\sum_\alpha \epsilon_{\alpha\alpha}\left[\int_\Omega n\cdot v_{xc} - 2E_{xc}\right] = \sum_\alpha \epsilon_{\alpha\alpha}\left[2E_{xc} - \int_\Omega n\cdot v_{xc}\right] \tag{B.13}$$

The unusual factor 2 multiplying the energy will vanish when we'll keep account for all the other terms. A similar results is obtained when we finally consider the restricted case of $F_{xc} \equiv F_{xc}(|\nabla n|\,, |\nabla n'|)$, where the results is expressed by

$$\delta E'_{xc} = \sum_\alpha \epsilon_{\alpha\alpha}\left[2E_{xc} - \int n\cdot v_{xc}\right] - \sum_{\alpha\beta}\epsilon_{\alpha\beta}\int\int n\, n'\cdot\frac{\partial F_{xc}}{\partial\,|\nabla n|}\frac{\nabla_\alpha n\cdot\nabla_\beta n}{|\nabla n|} \tag{B.14}$$

We now have all the terms to express the final results, defining the stress tensor for a generic non-local functional

$$\begin{aligned}\delta E'_{xc} = &\sum_\alpha \epsilon_{\alpha\alpha}\left[E_{xc} - \int_\Omega n\cdot v_{xc}\right] - \sum_{\alpha\beta}\epsilon_{\alpha\beta}\left[\int\int n\, n'\cdot\frac{\partial F_{xc}}{\partial\,|\nabla n|}\frac{\nabla_\alpha n\cdot\nabla_\beta n}{|\nabla n|}\right] \\ &+\sum_{\alpha\beta}\epsilon_{\alpha\beta}\left[E_{xc}\cdot\delta_{\alpha\beta} + \frac{1}{2}\int\int n\, n'\,\frac{\partial F_{xc}}{\partial\,|r-r'|}\frac{(r-r')_\alpha\cdot(r-r')_\beta}{|(r-r')|}\right]\end{aligned} \tag{B.15}$$

Written in this form, the stress is defined as the already existing LDA and GGA terms plus a correction that is non-zero only in the vdW case.

Appendix C

Phonons derivation details

Tn Chap.3 we generalized as mush as possible the theoretical extension of DFPT for non-local functional, but functional specific calculations are needed to obtain useful formulas to compute. Our analysis is focused on non-local functionals that can be expressed with the RPS interpolation scheme, and the differences among them can only be limited either in the Θ functions or in the kernel Φ.

In the next sections we'll present details calculations for the vdW-DF class of functionals, and the rVV10 functional introduces in Chap.5. Since the DFPT extension does not include any new derivations of the kernel Ψ, we'll present only Θ functions of these implementations, leaving the reader to the original sources for more informations on how to implement the full extension.

Phonons in vdW-DF

In vdW-DF we have a little involved definition of Θ functions, and specifically the q, reported here

$$\Theta = n\, P[q_0(q(r))] \tag{C.1}$$

and

$$q = k_F + L_1 \ln\left(1 + \frac{1}{L_2}\right) + G_c \tag{C.2}$$

with

$$
\begin{aligned}
k_F &= \left(3\pi^2 n\right)^{\frac{1}{3}} \\
G_c &= \frac{-Z_{ab}}{36 k_F n^2} |\nabla n|^2 \\
L_1 &= \frac{8\pi}{3} \left(L_A \left(L_{a1} r_s + 1\right)\right) \\
L_2 &= 2 L_A \left(L b_1 \sqrt{r_s} + L b_2 r_s + L b_3 r_s \sqrt{r_s} + L b_4 r_s^2\right)
\end{aligned}
\tag{C.3}
$$

where L_A, Lb_1, Lb_2, Lb_3 and Lb_4 are parameters and r_s is the Fermi radius. We now introduce first the necessary derivatives for the final formulations, first for the Θ functions,

$$
\frac{\partial \Theta}{\partial n} = P + \frac{\partial P}{\partial q_0} \frac{\partial q_0}{\partial q} \left(\frac{\partial q}{\partial n} n\right) \tag{C.4}
$$

$$
\frac{\partial \Theta}{\partial |\nabla n|} \frac{1}{|\nabla n|} = \frac{\partial P}{\partial q_0} \frac{\partial q_0}{\partial q} \left(\frac{\partial q}{\partial |\nabla n|} \frac{n}{|\nabla n|}\right) \tag{C.5}
$$

$$
\begin{aligned}
\frac{\partial^2 \Theta}{\partial n^2} = \Bigg[& \frac{\partial P}{\partial q_0} \frac{\partial q_0}{\partial q} \left(\frac{\partial q}{\partial n} n\right) + \frac{\partial^2 P}{\partial q_0^2} \left(\frac{\partial q_0}{\partial q}\right)^2 \left(\frac{\partial q}{\partial n} n\right)^2 + \\
& \frac{\partial P}{\partial q_0} \frac{\partial^2 q_0}{\partial q^2} \left(\frac{\partial q}{\partial n} n\right)^2 + \frac{\partial P}{\partial q_0} \frac{\partial q_0}{\partial q} \left(\frac{\partial}{\partial n} \left(\frac{\partial q}{\partial n} n\right) n\right) \Bigg] \frac{1}{n}
\end{aligned}
\tag{C.6}
$$

$$
\begin{aligned}
\frac{\partial}{\partial n} \left(\frac{\partial \Theta}{\partial |\nabla n|} \frac{1}{|\nabla n|}\right) = \Bigg[& \frac{\partial^2 P}{\partial q_0^2} \left(\frac{\partial q_0}{\partial q}\right)^2 \left(\frac{\partial q}{\partial n} n\right) \left(\frac{\partial q}{\partial |\nabla n|} \frac{n}{|\nabla n|}\right) + \\
& \frac{\partial P}{\partial q_0} \frac{\partial^2 q_0}{\partial q^2} \left(\frac{\partial q}{\partial n} n\right) \left(\frac{\partial q}{\partial |\nabla n|} \frac{n}{|\nabla n|}\right) - \frac{4}{3} \frac{\partial P}{\partial q_0} \frac{\partial q_0}{\partial q} \left(\frac{\partial q}{\partial |\nabla n|} \frac{n}{|\nabla n|}\right) \Bigg] \frac{1}{n}
\end{aligned}
\tag{C.7}
$$

$$\frac{\partial}{\partial|\nabla n|}\left(\frac{\partial\Theta}{\partial|\nabla n|}\frac{1}{|\nabla n|}\right)\frac{1}{|\nabla n|}=\left[\frac{\partial^2 P}{\partial q_0^2}\left(\frac{\partial q_0}{\partial q}\right)^2\left(\frac{\partial q}{\partial|\nabla n|}\frac{n}{|\nabla n|}\right)^2+\frac{\partial P}{\partial q_0}\frac{\partial^2 q_0}{\partial q^2}\left(\frac{\partial q}{\partial|\nabla n|}\frac{n}{|\nabla n|}\right)^2+\frac{\partial P}{\partial q_0}\frac{\partial q_0}{\partial q}\left(\frac{\partial}{\partial|\nabla n|}\left(\frac{\partial q}{\partial|\nabla n|}\frac{n}{|\nabla n|}\right)\frac{n}{\partial|\nabla n|}\right)\right]\frac{1}{n} \tag{C.8}$$

$$\frac{\partial}{\partial|\nabla n|}\left(\frac{\partial\Theta}{\partial n}\right)\frac{1}{|\nabla n|}=\left[-\frac{4}{3}\frac{\partial P}{\partial q_0}\frac{\partial q_0}{\partial q}\left(\frac{\partial q}{\partial|\nabla n|}\frac{n}{|\nabla n|}\right)+\frac{\partial^2 P}{\partial q_0^2}\left(\frac{\partial q_0}{\partial q}\right)^2\left(\frac{\partial q}{\partial|\nabla n|}\frac{n}{|\nabla n|}\right)\left(\frac{\partial q}{\partial n}n\right)+\frac{\partial P}{\partial q_0}\frac{\partial^2 q_0}{\partial q^2}\left(\frac{\partial q}{\partial|\nabla n|}\frac{n}{|\nabla n|}\right)\left(\frac{\partial q}{\partial n}n\right)\right]\frac{1}{n} \tag{C.9}$$

The all the previous equations some algebraic manipulations have been used to simplify the formulas, possible only for these specific functional form. Now we report the q derivatives, with the derivatives of all the terms necessary to completely define this extensions to DFPT,

$$\begin{aligned}
&q=k_F+L_1\ln\left(1+\frac{1}{L_2}\right)+G_c\\
&\frac{\partial q}{\partial|\nabla n|}\frac{n}{|\nabla n|}=\frac{-Z_{ab}}{18k_F n}\\
&\frac{\partial q}{\partial n}n=\frac{1}{3}k_F+\left(-\frac{7}{3}G_c\right)+\left(n\frac{\partial L_1}{\partial n}\right)\ln\left(1+\frac{1}{L_2}\right)+L_1\frac{-1}{L_2\left(1+L_2\right)}\left(n\frac{\partial L_2}{\partial n}\right)\\
&\frac{\partial}{\partial n}\left(\frac{\partial q}{\partial n}n\right)n=\frac{1}{9}k_F+\left(\frac{49}{9}G_c\right)+\left(n\frac{\partial L_1}{\partial n}\right)\ln\left(1+\frac{1}{L_2}\right)+\left(n^2\frac{\partial^2 L_1}{\partial n^2}\right)\ln\left(1+\frac{1}{L_2}\right)+\\
&\qquad 2\left(n\frac{\partial L_1}{\partial n}\right)\left(\frac{-1}{L_2\left(1+L_2\right)}\right)\left(n\frac{\partial L_2}{\partial n}\right)+\\
&\qquad L_1\frac{1+2L_2}{L_2^2\left(1+L_2\right)^2}\left(n\frac{\partial L_2}{\partial n}\right)^2+L_1\left(\frac{-1}{L_2\left(1+L_2\right)}\right)\left(n\frac{\partial L_2}{\partial n}\right)+\\
&\qquad L_1\left(\frac{-1}{L_2\left(1+L_2\right)}\right)\left(n^2\frac{\partial^2 L_2}{\partial n^2}\right)
\end{aligned} \tag{C.10}$$

and finally

$$
\begin{aligned}
&\frac{\partial k_F}{\partial n} = \frac{1}{3n} k_F \\
&\frac{\partial G_c}{\partial |\nabla n|} = \frac{2}{|\nabla n|} Gc \\
&\frac{\partial G_c}{\partial n} = -\frac{7}{3n} Gc \\
&\frac{\partial L_1}{\partial n} n = -\frac{8\pi}{9} L_A L_{a1} r_s \\
&\frac{\partial^2 L_1}{\partial n^2} n^2 = \frac{32\pi}{27} L_A L_{a1} r_s \\
&\frac{\partial L_2}{\partial n} n = -2 L_A \left(\frac{Lb_1}{6} \sqrt{r_s} + \frac{Lb_2}{3} r_s + \frac{Lb_3}{2} r_s \sqrt{r_s} + \frac{2Lb_4}{4} r_s^2 \right) \\
&\frac{\partial^2 L_2}{\partial n^2} n^2 = 2 L_A \left(\frac{7Lb_1}{36} \sqrt{r_s} + \frac{4Lb_2}{9} r_s + \frac{3Lb_3}{4} r_s \sqrt{r_s} + \frac{10Lb_4}{9} r_s^2 \right)
\end{aligned}
\tag{C.11}
$$

Phonons in rVV10

In this case Θ functions are a little more complicated, while q functionals are much simpler,

$$\Theta = C n^{\frac{3}{4}} P[q_0(q(r))] \tag{C.12}$$

$$q = \frac{w_0}{k} \tag{C.13}$$

where C (and b in the following equations) is a parameter, and q is defined by

$$
\begin{aligned}
k &= 3\pi b \left(\frac{n}{9\pi} \right)^{\frac{1}{6}} \\
wp^2 &= \frac{4\pi n e^2}{m} \\
wg^2 &= \frac{C\hbar^2}{m^2} \left(\frac{|\nabla n|}{n} \right)^4 \\
w_0 &= \sqrt{wg^2 + \frac{wp^2}{3}}
\end{aligned}
\tag{C.14}
$$

We now introduce the derivatives for the Θ functions

$$\frac{\partial \Theta}{\partial n} = C n^{-\frac{1}{4}} \left[\frac{3}{4} P + \frac{\partial P}{\partial q_0} \frac{\partial q_0}{\partial q} \left(\frac{\partial q}{\partial n} n \right) \right] \tag{C.15}$$

$$\frac{\partial \Theta}{\partial |\nabla n|} \frac{1}{|\nabla n|} = C n^{-\frac{1}{4}} \left[\frac{\partial P}{\partial q_0} \frac{\partial q_0}{\partial q} \left(\frac{\partial q}{\partial |\nabla n|} \frac{n}{|\nabla n|} \right) \right] \tag{C.16}$$

$$\begin{aligned} \frac{\partial^2 \Theta}{\partial n^2} =& C n^{-\frac{1}{4}} \left[-\frac{3}{16} P + \frac{1}{2} \frac{\partial P}{\partial q_0} \frac{\partial q_0}{\partial q} \left(\frac{\partial q}{\partial n} n \right) + \frac{\partial^2 P}{\partial q_0^2} \left(\frac{\partial q_0}{\partial q} \right)^2 \left(\frac{\partial q}{\partial n} n \right)^2 + \right. \\ & \left. \frac{\partial P}{\partial q_0} \frac{\partial^2 q_0}{\partial q^2} \left(\frac{\partial q}{\partial n} n \right)^2 + \frac{\partial P}{\partial q_0} \frac{\partial q_0}{\partial q} \left(\frac{\partial}{\partial n} \left(\frac{\partial q}{\partial n} n \right) n \right) \right] \frac{1}{n} \end{aligned} \tag{C.17}$$

$$\begin{aligned} \frac{\partial}{\partial n} \left(\frac{\partial \Theta}{\partial |\nabla n|} \frac{1}{|\nabla n|} \right) =& C n^{-\frac{1}{4}} \left[-\frac{1}{4} \frac{\partial P}{\partial q_0} \frac{\partial q_0}{\partial q} \left(\frac{\partial q}{\partial |\nabla n|} \frac{n}{|\nabla n|} \right) + \right. \\ & \frac{\partial^2 P}{\partial q_0^2} \left(\frac{\partial q_0}{\partial q} \right)^2 \left(\frac{\partial q}{\partial n} n \right) \left(\frac{\partial q}{\partial |\nabla n|} \frac{n}{|\nabla n|} \right) + \\ & \frac{\partial P}{\partial q_0} \frac{\partial^2 q_0}{\partial q^2} \left(\frac{\partial q}{\partial n} n \right) \left(\frac{\partial q}{\partial |\nabla n|} \frac{n}{|\nabla n|} \right) + \\ & \left. \frac{\partial P}{\partial q_0} \frac{\partial q_0}{\partial q} \left(\frac{\partial}{\partial n} \left(\frac{\partial q}{\partial |\nabla n|} \frac{n}{|\nabla n|} \right) n \right) \right] \frac{1}{n} \end{aligned} \tag{C.18}$$

$$\begin{aligned} \frac{\partial}{\partial |\nabla n|} \left(\frac{\partial \Theta}{\partial |\nabla n|} \frac{1}{|\nabla n|} \right) \frac{1}{|\nabla n|} =& C n^{-\frac{1}{4}} \left[\frac{\partial^2 P}{\partial q_0^2} \left(\frac{\partial q_0}{\partial q} \right)^2 \left(\frac{\partial q}{\partial |\nabla n|} \frac{n}{|\nabla n|} \right)^2 + \right. \\ & \frac{\partial P}{\partial q_0} \frac{\partial^2 q_0}{\partial q^2} \left(\frac{\partial q}{\partial |\nabla n|} \frac{n}{|\nabla n|} \right)^2 + \\ & \left. \frac{\partial P}{\partial q_0} \frac{\partial q_0}{\partial q} \left(\frac{\partial}{\partial |\nabla n|} \left(\frac{\partial q}{\partial |\nabla n|} \frac{n}{|\nabla n|} \right) \frac{n}{|\nabla n|} \right) \right] \frac{1}{n} \end{aligned} \tag{C.19}$$

and finally we report the q derivatives to complete the calculations

$$
\begin{aligned}
&\frac{\partial q}{\partial n} n = q\left[\frac{1}{2w_0^2}\left(\frac{16\pi n}{3} - 4wg^2\right) - \frac{1}{6}\right] \\
&\frac{\partial q}{\partial |\nabla n|}\frac{n}{|\nabla n|} = \left(\frac{2}{w_0}\frac{wg^2}{|\nabla n|^2}\right)\frac{n}{k} \\
&\frac{\partial}{\partial n}\left(\frac{\partial q}{\partial n} n\right) n = \left(\frac{\partial q}{\partial n} n\right)\left(\frac{n}{w_0}\frac{\partial w_0}{\partial n} - \frac{1}{6}\right) + q\left(\frac{-2n^2}{w_0^2}\left(\frac{\partial w_0}{\partial n}\right)^2 + \frac{n}{w_0}\frac{\partial w_0}{\partial n} + \frac{10}{w_0^2} wg^2\right) \\
&\frac{\partial}{\partial |\nabla n|}\left(\frac{\partial q}{\partial |\nabla n|}\frac{n}{|\nabla n|}\right)\frac{n}{|\nabla n|} = \left(\frac{\partial q}{\partial |\nabla n|}\frac{n}{|\nabla n|}\right)\left[\frac{2n}{|\nabla n|^2} - \frac{n}{w_0}\left(\frac{\partial w_0}{\partial |\nabla n|}\frac{1}{|\nabla n|}\right)\right] \\
&\frac{\partial}{\partial n}\left(\frac{\partial q}{\partial |\nabla n|}\frac{n}{|\nabla n|}\right) n = \left(\frac{\partial q}{\partial |\nabla n|}\frac{n}{|\nabla n|}\right)\left(\frac{5}{6} - \frac{n}{w_0}\frac{\partial w_0}{\partial n} - 4\right)
\end{aligned}
\tag{C.20}
$$

with

$$
\begin{aligned}
&\frac{\partial w_0}{\partial n} = \frac{1}{2w_0}\left(\frac{16}{3}\pi - \frac{4wg^2}{n}\right) \\
&\frac{\partial w_0}{\partial |\nabla n|}\frac{1}{|\nabla n|} = \frac{1}{2w_0}\frac{4wg^2}{|\nabla n|^2}
\end{aligned}
\tag{C.21}
$$

Bibliography

[1] P. Hohenberg and W. Kohn, "Inhomogeneous Electron Gas," *Physical Review*, vol. 155, no. 1962, 1964.

[2] W. Kohn and L. J. Sham, "Self-Consistent Equations Including Exchange and Correlation Effects," *Physical Review*, vol. 140, pp. A1133–A1138, Nov. 1965.

[3] U. von Barth and L. Hedin, "A local exchange-correlation potential for the spin polarized case. i," *Journal of Physics C: Solid State Physics*, vol. 5, pp. 1629–1642, July 1972.

[4] H. Xiao, J. Tahir-Kheli, and W. A. Goddard, "Accurate Band Gaps for Semiconductors from Density Functional Theory," *The Journal of Physical Chemistry Letters*, vol. 2, pp. 212–217, Feb. 2011.

[5] J. Perdew, K. Burke, and Y. Wang, "Generalized gradient approximation for the exchange-correlation hole of a many-electron system," *Physical Review B*, vol. 54, pp. 16533–16539, Dec. 1996.

[6] E. D. E. Murray, K. Lee, and D. C. Langreth, "Investigation of Exchange Energy Density Functional Accuracy for Interacting Molecules," *Journal of Chemical Theory and Computation*, vol. 5, no. 10, pp. 2754–2762, 2009.

[7] J. P. Perdew, J. A. Chevary, S. H. Vosko, K. A. Jackson, M. R. Pederson, D. J. Singh, and C. Fiolhais, "Atoms, molecules, solids, and surfaces: Applications of the generalized gradient approximation for exchange and correlation," *Physical Review B*, vol. 46, no. 11, p. 6671, 1992.

[8] E. E. Dahlke and D. G. Truhlar, "Improved density functionals for water.," *The journal of physical chemistry. B*, vol. 109, pp. 15677–83, Aug. 2005.

[9] A. Thiess, R. Zeller, M. Bolten, P. Dederichs, and S. Blügel, "Massively parallel density functional calculations for thousands of atoms: KKRnano," *Physical Review B*, vol. 85, p. 235103, June 2012.

[10] I. E. Dzyaloshinskii, E. M. Lifshitz, and L. P. Pitaevskii, "General theory of van der Waals' forces," *Soviet Physics Uspekhi*, vol. 4, no. 2, p. 153, 1961.

[11] J. Harris and R. O. Jones, "The surface energy of a bounded electron gas," *Journal of Physics F: Metal Physics*, vol. 4, pp. 1170–1186, Aug. 1974.

[12] H.-V. Nguyen and S. de Gironcoli, "Efficient calculation of exact exchange and RPA correlation energies in the adiabatic-connection fluctuation-dissipation theory," *Physical Review B*, vol. 79, pp. 205114–, May 2009.

[13] J. P. Perdew, M. Ernzerhof, and K. Burke, "Rationale for mixing exact exchange with density functional approximations," *The Journal of Chemical Physics*, vol. 105, p. 9982, Dec. 1996.

[14] A. D. Becke, "A new mixing of HartreeFock and local density-functional theories," *The Journal of Chemical Physics*, vol. 98, p. 1372, Jan. 1993.

[15] S. Grimme, "Accurate description of van der Waals complexes by density functional theory including empirical corrections.," *Journal of computational chemistry*, vol. 25, pp. 1463–73, Oct. 2004.

[16] S. Grimme, J. Antony, S. Ehrlich, and H. Krieg, "A consistent and accurate ab initio parametrization of density functional dispersion correction (DFT-D) for the 94 elements H-Pu.," *The Journal of chemical physics*, vol. 132, p. 154104, Apr. 2010.

[17] Y. Andersson, D. Langreth, and B. Lundqvist, "van der Waals interactions in density-functional theory.," *Physical review letters*, vol. 76, pp. 102–105, Jan. 1996.

[18] C. Richardson and N. Ashcroft, "Dynamical local-field factors and effective interactions in the three-dimensional electron liquid," *Physical Review B*, vol. 50, pp. 8170–8181, Sept. 1994.

[19] M. Dion, H. Rydberg, E. Schröder, D. C. Langreth, and B. I. Lundqvist, "Van der Waals Density Functional for General Geometries," *Physical Review Letters*, vol. 92, pp. 22–25, June 2004.

[20] K. Lee, D. Murray, L. Kong, B. I. Lundqvist, and D. C. Langreth, "A Higher-Accuracy van der Waals Density Functional ," no. 1, pp. 1–9, 2010.

[21] D. J. Carter and A. L. Rohl, "Noncovalent Interactions in SIESTA Using the vdW-DF Functional: S22 Benchmark and Macrocyclic Structures," *Journal of Chemical Theory and Computation*, vol. 8, pp. 281–289, Jan. 2012.

[22] A. Mø gelhøj, A. K. Kelkkanen, K. T. Wikfeldt, J. Schiø tz, J. J. r. Mortensen, L. G. M. Pettersson, B. I. Lundqvist, K. W. Jacobsen, A. Nilsson, and J. K. Nø rskov, "Ab initio van der waals interactions in simulations of water alter structure from mainly tetrahedral to high-density-like.," *The journal of physical chemistry. B*, vol. 115, pp. 14149–60, Dec. 2011.

[23] V. Cooper, "Van der Waals density functional: An appropriate exchange functional," *Physical Review B*, pp. 1–4, 2010.

[24] O. a. Vydrov and T. Van Voorhis, "Nonlocal van der Waals density functional: the simpler the better.," *The Journal of chemical physics*, vol. 133, p. 244103, Dec. 2010.

[25] S. Baroni and S. D. Gironcoli, "Phonons and related crystal properties from density-functional perturbation theory," *Reviews of Modern ...*, vol. 73, no. April, 2001.

[26] B. F. Putnam, L. L. Van Zandt, E. W. Prohofsky, and W. N. Mei, "Resonant and localized breathing modes in terminal regions of the DNA double helix.," *Biophysical journal*, vol. 35, pp. 271–87, Aug. 1981.

[27] J. Eyster and E. Prohofsky, "Soft modes and the structure of the DNA Double Helix," *Physical Review Letters*, vol. 38, no. 7, 1977.

[28] J. Brookes, F. Hartoutsiou, a. Horsfield, and a. Stoneham, "Could Humans Recognize Odor by Phonon Assisted Tunneling?," *Physical Review Letters*, vol. 98, pp. 1–4, Jan. 2007.

[29] P. Giannozzi, S. Baroni, N. Bonini, M. Calandra, R. Car, C. Cavazzoni, D. Ceresoli, G. L. Chiarotti, M. Cococcioni, I. Dabo, A. Dal Corso, S. de Gironcoli, S. Fabris, G. Fratesi, R. Gebauer, U. Gerstmann, C. Gougoussis, A. Kokalj, M. Lazzeri, L. Martin-Samos, N. Marzari, F. Mauri, R. Mazzarello, S. Paolini, A. Pasquarello, L. Paulatto, C. Sbraccia, S. Scandolo, G. Sclauzero, A. P. Seitsonen, A. Smogunov, P. Umari, and R. M. Wentzcovitch, "QUANTUM ESPRESSO: a modular and open-source software project for quantum simulations of materials.," *Journal of physics. Condensed matter : an Institute of Physics journal*, vol. 21, p. 395502, Sept. 2009.

[30] M. Born and R. Oppenheimer, "Zur Quantentheorie der Molekeln," *Annalen der Physik*, vol. 389, no. 20, pp. 457–484, 1927.

[31] J. P. Perdew, "Self-interaction correction to density-functional approximations for many-electron systems," *Physical Review B*, vol. 23, pp. 5048–5079, May 1981.

[32] J. P. Perdew and Y. Wang, "Accurate and simple analytic representation of the electron-gas correlation energy," *Physical Review B*, vol. 45, pp. 13244–13249, June 1992.

[33] P. Haas, F. Tran, and P. Blaha, "Calculation of the lattice constant of solids with semilocal functionals," *Physical Review B*, vol. 79, pp. 085104–, Feb. 2009.

[34] D. Langreth and J. Perdew, "Exchange-correlation energy of a metallic surface: Wave-vector analysis," *Physical Review B*, vol. 15, pp. 2884–2901, Mar. 1977.

[35] O. Gunnarsson and B. Lundqvist, "Exchange and correlation in atoms, molecules, and solids by the spin-density-functional formalism," *Physical Review B*, vol. 13, no. 10, pp. 4274–4298, 1976.

[36] J. F. Dobson, K. McLennan, A. Rubio, J. Wang, T. Gould, H. M. Le, and B. P. Dinte, "Prediction of Dispersion Forces: Is There a Problem?," *Australian Journal of Chemistry*, vol. 54, no. 8, pp. 513–527.

[37] H. Nyquist, "Thermal Agitation of Electric Charge in Conductors," *Physical Review*, vol. 32, pp. 110–113, July 1928.

[38] D. Langreth and J. Perdew, "The exchange-correlation energy of a metallic surface," *Solid State Communications*, vol. 17, pp. 1425–1429, Dec. 1975.

[39] M. Fuchs and X. Gonze, "Accurate density functionals: Approaches using the adiabatic-connection fluctuation-dissipation theorem," *Physical Review B*, vol. 65, pp. 23–26, 2002.

[40] S. Kurth and J. Perdew, "Density-functional correction of random-phase-approximation correlation with results for jellium surface energies," *Physical Review B*, vol. 59, pp. 10461–10468, Apr. 1999.

[41] J. Tao, J. Perdew, V. Staroverov, and G. Scuseria, "Climbing the Density Functional Ladder: Nonempirical MetaGeneralized Gradient Approximation Designed for Molecules and Solids," *Physical Review Letters*, vol. 91, pp. 146401–, Sept. 2003.

[42] A. D. Becke, "Density-functional thermochemistry. III. The role of exact exchange," *The Journal of Chemical Physics*, vol. 98, p. 5648, Apr. 1993.

[43] X. Xu, Q. Zhang, R. P. Muller, and W. A. Goddard, "An extended hybrid density functional (X3LYP) with improved descriptions of nonbond interactions and thermodynamic properties of molecular systems.," *The Journal of chemical physics*, vol. 122, p. 14105, Jan. 2005.

[44] J. Paier, M. Marsman, K. Hummer, G. Kresse, I. C. Gerber, and J. G. Angyán, "Screened hybrid density functionals applied to solids.," *The Journal of chemical physics*, vol. 124, p. 154709, Apr. 2006.

[45] V. N. Staroverov, G. E. Scuseria, J. Tao, and J. P. Perdew, "Comparative assessment of a new nonempirical density functional: Molecules and hydrogen-bonded complexes," *The Journal of Chemical Physics*, vol. 119, p. 12129, Dec. 2003.

[46] C. Adamo and V. Barone, "Exchange functionals with improved long-range behavior and adiabatic connection methods without adjustable parameters: The mPW and mPW1PW models," *The Journal of Chemical Physics*, vol. 108, p. 664, Jan. 1998.

[47] Y. Zhao and D. Truhlar, "The M06 suite of density functionals for main group thermochemistry, thermochemical kinetics, noncovalent interactions, excited states, and transition elements: two new functionals and systematic testing

of four M06-class functionals and 12 other function," *Theoretical Chemistry Accounts: Theory, Computation, and Modeling (Theoretica Chimica Acta)*, vol. 120, no. 1, pp. 215–241, 2008.

[48] Y. Zhao and D. G. Truhlar, "How well can new-generation density functional methods describe stacking interactions in biological systems?," *Physical chemistry chemical physics : PCCP*, vol. 7, pp. 2701–5, July 2005.

[49] J. Tao and J. P. Perdew, "Test of a nonempirical density functional: short-range part of the van der Waals interaction in rare-gas dimers.," *The Journal of chemical physics*, vol. 122, p. 114102, Mar. 2005.

[50] X. Xu and W. A. Goddard, "The X3LYP extended density functional for accurate descriptions of nonbond interactions, spin states, and thermochemical properties," *Proceedings of the National Academy of Sciences of the United States of America*, vol. 101, no. 9, pp. 2673–2677, 2004.

[51] A. D. Becke and E. R. Johnson, "A density-functional model of the dispersion interaction.," *The Journal of chemical physics*, vol. 123, p. 154101, Oct. 2005.

[52] A. D. Becke and E. R. Johnson, "Exchange-hole dipole moment and the dispersion interaction.," *The Journal of chemical physics*, vol. 122, p. 154104, May 2005.

[53] A. Tkatchenko and M. Scheffler, "Accurate Molecular Van Der Waals Interactions from Ground-State Electron Density and Free-Atom Reference Data," *Physical Review Letters*, vol. 102, p. 073005, Feb. 2009.

[54] L. a. Burns, A. Vázquez-Mayagoitia, B. G. Sumpter, and C. D. Sherrill, "Density-functional approaches to noncovalent interactions: a comparison of dispersion corrections (DFT-D), exchange-hole dipole moment (XDM) theory, and specialized functionals.," *The Journal of chemical physics*, vol. 134, p. 084107, Feb. 2011.

[55] P. L. Silvestrelli, "Van der Waals Interactions in DFT Made Easy by Wannier Functions," *Physical Review Letters*, vol. 100, p. 053002, Feb. 2008.

[56] I.-C. Lin, O. A. von Lilienfeld, M. D. Coutinho-Neto, I. Tavernelli, and U. Rothlisberger, "Predicting noncovalent interactions between aromatic biomolecules with London-dispersion-corrected DFT.," *The journal of physical chemistry. B*, vol. 111, pp. 14346–54, Dec. 2007.

[57] G. A. DiLabio, "Accurate treatment of van der Waals interactions using standard density functional theory methods with effective core-type potentials: Application to carbon-containing dimers," *Chemical Physics Letters*, vol. 455, pp. 348–353, Apr. 2008.

[58] Y. Y. Sun, Y.-H. Kim, K. Lee, and S. B. Zhang, "Accurate and efficient calculation of van der Waals interactions within density functional theory by local atomic potential approach.," *The Journal of chemical physics*, vol. 129, p. 154102, Oct. 2008.

[59] O. A. Vydrov and T. V. Voorhis, "Nonlocal Van Der Waals Density Functionals Based on Local Response Models," in *Lecture Notes in Physics, Berlin Springer Verlag* (M. A. L. Marques, N. T. Maitra, F. M. S. Nogueira, E. K. U. Gross, and A. Rubio, eds.), vol. 837 of *Lecture Notes in Physics, Berlin Springer Verlag*, p. 443, 2012.

[60] T. Thonhauser, A. Puzder, and D. C. Langreth, "Interaction energies of monosubstituted benzene dimers via nonlocal density functional theory," *The Journal of Chemical Physics*, vol. 124, no. 16, p. 164106, 2006.

[61] A. Bil, B. Kolb, R. Atkinson, D. Pettifor, T. Thonhauser, and A. Kolmogorov, "van der Waals interactions in the ground state of Mg(BH_{4})_{2} from density functional theory," *Physical Review B*, vol. 83, June 2011.

[62] T. Thonhauser, V. R. Cooper, S. Li, A. Puzder, P. Hyldgaard, and D. C. Langreth, "Van der Waals density functional: Self-consistent potential and the nature of the van der Waals bond," *Physical Review B*, vol. 76, Sept. 2007.

[63] J. White and D. Bird, "Implementation of gradient-corrected exchange-correlation potentials in Car-Parrinello total-energy calculations," *Physical Review B*, vol. 50, pp. 4954–4957, Aug. 1994.

[64] O. Vydrov and T. V. Voorhis, "Dispersion interactions from a local polarizability model," *Physical Review A*, vol. 81, p. 62708, June 2010.

[65] P. Jurecka, J. Sponer, J. Cerny, and P. Hobza, "Benchmark database of accurate (MP2 and CCSD(T) complete basis set limit) interaction energies of small model complexes{,} DNA base pairs{,} and amino acid pairs," *Phys. Chem. Chem. Phys.*, vol. 8, no. 17, pp. 1985–1993, 2006.

[66] R. K. Nesbet, "Local response model of the generalized polarization potential," *Phys. Rev. A*, vol. 56, pp. 2778–2783, Oct. 1997.

[67] G. Román-Pérez and J. Soler, "Efficient Implementation of a van der Waals Density Functional: Application to Double-Wall Carbon Nanotubes," *Physical Review Letters*, vol. 103, Aug. 2009.

[68] D. Lu, H.-V. Nguyen, and G. Galli, "Power series expansion of the random phase approximation correlation energy: The role of the third- and higher-order contributions," *The Journal of Chemical Physics*, vol. 133, no. 15, p. 154110, 2010.

[69] J. F. Dobson, A. White, and A. Rubio, "Asymptotics of the Dispersion Interaction: Analytic Benchmarks for van der Waals Energy Functionals," *Phys. Rev. Lett.*, vol. 96, p. 73201, Feb. 2006.

[70] O. Nielsen and R. Martin, "Quantum-mechanical theory of stress and force," *Physical Review B*, vol. 32, pp. 3780–3791, Sept. 1985.

[71] P. Giannozzi, S. Baroni, N. Bonini, M. Calandra, R. Car, C. Cavazzoni, D. Ceresoli, G. L. Chiarotti, M. Cococcioni, I. Dabo, and E. al., "QUANTUM ESPRESSO: a modular and open-source software project for quantum simulations of materials," *Journal of Physics: Condensed Matter*, vol. 21, p. 395502, Sept. 2009.

[72] Y. Iitaka, "The crystal structure of γ-glycine," *Acta Crystallographica*, vol. 14, pp. 1–10, Jan. 1961.

[73] Y. Iitaka, "The crystal structure of β-glycine," *Acta Crystallographica*, vol. 13, pp. 35–45, Jan. 1960.

[74] P. G. Jönsson and A. Kvick, "Precision neutron diffraction structure determination of protein and nucleic acid components. III. The crystal and molecular structure of the amino acid α-glycine," *Acta Crystallographica Section B Structural Crystallography and Crystal Chemistry*, vol. 28, pp. 1827–1833, June 1972.

[75] G. Perlovich, L. Hansen, and A. Bauer-Brandl, "The Polymorphism of Glycine. Thermochemical and structural aspects," *Journal of Thermal Analysis and Calorimetry*, vol. 66, no. 3, pp. 699–715, 2001.

[76] S. Chongprasert, S. A. Knopp, and S. L. Nail, "Characterization of frozen solutions of glycine," *Journal of Pharmaceutical Sciences*, vol. 90, pp. 1720–1728, Nov. 2001.

[77] K. Park, J. M. B. Evans, and A. S. Myerson, "Determination of Solubility of Polymorphs Using Differential Scanning Calorimetry," *Crystal Growth & Design*, vol. 3, pp. 991–995, Nov. 2003.

[78] H. Sakai, H. Hosogai, T. Kawakita, K. Onuma, and K. Tsukamoto, "Transformation of α-glycine to γ-glycine," *Journal of Crystal Growth*, vol. 116, pp. 421–426, Feb. 1992.

[79] E. S. Ferrari, R. J. Davey, W. I. Cross, A. L. Gillon, and C. S. Towler, "Crystallization in Polymorphic Systems: The Solution-Mediated Transformation of β to α Glycine," *Crystal Growth & Design*, vol. 3, pp. 53–60, Jan. 2003.

[80] E. V. Boldyreva, S. N. Ivashevskaya, H. Sowa, H. Ahsbahs, and H.-P. Weber, "Effect of High Pressure on Crystalline Glycine: A New High-Pressure Polymorph," *Doklady Physical Chemistry*, vol. 396, pp. 111–114, May 2004.

[81] A. Dawson, D. R. Allan, S. A. Belmonte, S. J. Clark, W. I. F. David, P. A. McGregor, S. Parsons, C. R. Pulham, and L. Sawyer, "Effect of High Pressure on the Crystal Structures of Polymorphs of Glycine," *Crystal Growth & Design*, vol. 5, pp. 1415–1427, July 2005.

[82] H. J. Simpson and R. E. Marsh, "The crystal structure ofL-alanine," *Acta Crystallographica*, vol. 20, pp. 550–555, Apr. 1966.

[83] J. D. Dunitz and R. R. Ryan, "Refinement of theL-alanine crystal structure," *Acta Crystallographica*, vol. 21, pp. 617–618, Oct. 1966.

[84] M. S. Lehmann, T. F. Koetzle, and W. C. Hamilton, "Precision neutron diffraction structure determination of protein and nucleic acid components. I. Crystal and molecular structure of the amino acid L-alanine," *Journal of the American Chemical Society*, vol. 94, pp. 2657–2660, Apr. 1972.

[85] A. M. R. Teixeira, P. T. C. Freire, A. J. D. Moreno, J. M. Sasaki, A. P. Ayala, J. Mendes Filho, and F. E. A. Melo, "High-pressure Raman study of l-alanine crystal," *Solid State Communications*, vol. 116, pp. 405–409, Oct. 2000.

[86] J. S. Olsen, L. Gerward, P. T. C. Freire, J. Mendes Filho, F. E. A. Melo, and A. G. Souza Filho, "Pressure-induced phase transformations in l-alanine crystals," *Journal of Physics and Chemistry of Solids*, vol. 69, pp. 1641–1645, July 2008.

[87] N. A. Tumanov, E. V. Boldyreva, B. A. Kolesov, A. V. Kurnosov, and R. Quesada Cabrera, "Pressure-induced phase transitions in L-alanine, revisited," *Acta Crystallographica Section B Structural Science*, vol. 66, pp. 458–471, Aug. 2010.

[88] J. P. Perdew, K. Burke, and M. Ernzerhof, "Generalized Gradient Approximation Made Simple [Phys. Rev. Lett. 77, 3865 (1996)]," *Physical Review Letters*, vol. 78, p. 1396, Feb. 1997.

[89] Y. Zhang and W. Yang, "Comment on Generalized Gradient Approximation Made Simple," *Physical Review Letters*, vol. 80, p. 890, Jan. 1998.

[90] M. Dion, H. Rydberg, E. Schröder, D. Langreth, and B. Lundqvist, "Erratum: Van der Waals Density Functional for General Geometries [Phys. Rev. Lett. 92, 246401 (2004)]," *Physical Review Letters*, vol. 95, Sept. 2005.

[91] A. Ahmed Adllan and A. Dal Corso, "Ultrasoft pseudopotentials and projector augmented-wave data sets: application to diatomic molecules," *Journal of Physics: Condensed Matter*, vol. 23, p. 425501, Oct. 2011.

[92] H. J. Monkhorst and J. D. Pack, "Special points for Brillouin-zone integrations," *Physical Review B*, vol. 13, pp. 5188–5192, June 1976.

[93] J. P. Legros and A. Kvick, "Deformation electron density of α-glycine at 120 K," *Acta Crystallographica Section B Structural Crystallography and Crystal Chemistry*, vol. 36, pp. 3052–3059, Dec. 1980.

[94] A. Kvick, W. M. Canning, T. F. Koetzle, and G. J. B. Williams, "An experimental study of the influence of temperature on a hydrogen-bonded system: the crystal structure of γ-glycine at 83 K and 298 K by neutron diffraction," *Acta Crystallographica Section B Structural Crystallography and Crystal Chemistry*, vol. 36, pp. 115–120, Jan. 1980.

[95] G. Román-Pérez and J. Soler, "Efficient Implementation of a van der Waals Density Functional: Application to Double-Wall Carbon Nanotubes," *Physical Review Letters*, vol. 103, pp. 1–4, Aug. 2009.

[96] O. A. Vydrov, Q. Wu, and T. Van Voorhis, "Self-consistent implementation of a nonlocal van der Waals density functional with a Gaussian basis set," *The Journal of Chemical Physics*, vol. 129, no. 1, p. 14106, 2008.

[97] O. A. Vydrov and T. Van Voorhis, "Vydrov and Van Voorhis Reply:," *Physical Review Letters*, vol. 104, Mar. 2010.

[98] T. Thonhauser, V. Cooper, S. Li, and A. Puzder, "Van der Waals density functional: Self-consistent potential and the nature of the van der Waals bond," *Physical Review B*, pp. 1–11, 2007.

[99] R. Sabatini, E. Küçükbenli, B. Kolb, T. Thonhauser, and S. de Gironcoli, "Structural evolution of amino acid crystals under stress from a non-empirical density functional," *Journal of Physics: Condensed Matter*, vol. 24, no. 42, p. 424209, 2012.

[100] R. Podeszwa, K. Patkowski, and K. Szalewicz, "Improved interaction energy benchmarks for dimers of biological relevance.," *Physical chemistry chemical physics : PCCP*, vol. 12, pp. 5974–9, July 2010.

[101] T. Takatani, E. G. Hohenstein, M. Malagoli, M. S. Marshall, and C. D. Sherrill, "Basis set consistent revision of the S22 test set of noncovalent interaction energies," *The Journal of Chemical Physics*, vol. 132, no. 14, p. 144104, 2010.

[102] K. Lee, E. D. Murray, L. Kong, B. I. Lundqvist, and D. C. Langreth, "A Higher-Accuracy van der Waals Density Functional," *Physical Review B*, vol. 82, no. 8, p. 14, 2010.

[103] N. Marom, A. Tkatchenko, M. Rossi, V. V. Gobre, O. Hod, M. Scheffler, and L. Kronik, "Dispersion Interactions with Density-Functional Theory: Benchmarking Semiempirical and Interatomic Pairwise Corrected Density Functionals," *Journal of Chemical Theory and Computation*, vol. 7, pp. 3944–3951, Dec. 2011.

[104] H.-V. Nguyen and G. Galli, "A first-principles study of weakly bound molecules using exact exchange and the random phase approximation.," *The Journal of chemical physics*, vol. 132, p. 044109, Jan. 2010.

[105] R. A. Aziz, "A highly accurate interatomic potential for argon," *The Journal of Chemical Physics*, vol. 99, no. 6, p. 4518, 1993.

[106] J. Klimeš, D. Bowler, and A. Michaelides, "Van der Waals density functionals applied to solids," *Physical Review B*, vol. 83, May 2011.

[107] Z. Liu, J. Z. Liu, Y. Cheng, Z. Li, L. Wang, and Q. Zheng, "Interlayer binding energy of graphite: A mesoscopic determination from deformation," *Physical Review B*, vol. 85, pp. 1–5, May 2012.

[108] K. RoÅciszewski, B. Paulus, P. Fulde, and H. Stoll, "Ab initio coupled-cluster calculations for the fcc and hcp structures of rare-gas solids," *Physical Review B*, vol. 62, no. 9, pp. 6–9, 2000.

[109] G. Moyano, P. Schwerdtfeger, and K. Rosciszewski, "Lattice dynamics for fcc rare gas solids Ne, Ar, and Kr from ab initio potentials," *Physical Review B*, vol. 75, pp. 1–6, Jan. 2007.

[110] M. Lazzeri, C. Attaccalite, L. Wirtz, and F. Mauri, "Impact of the electron-electron correlation on phonon dispersion: Failure of LDA and GGA DFT functionals in graphene and graphite," *Physical Review B*, pp. 8–11, 2008.

[111] a. Gupta, G. Chen, P. Joshi, S. Tadigadapa, and P. C. Eklund, "Raman scattering from high-frequency phonons in supported n-graphene layer films.," *Nano letters*, vol. 6, pp. 2667–73, Dec. 2006.

[112] L. Vitali, M. Schneider, K. Kern, L. Wirtz, and A. Rubio, "Phonon and plasmon excitation in inelastic electron tunneling spectroscopy of graphite," *Physical Review B*, vol. 69, Mar. 2004.

[113] G. Kresse, J. Furthmüller, and J. Hafner, "Ab initio Force Constant Approach to Phonon Dispersion Relations of Diamond and Graphite," *Europhysics Letters (EPL)*, vol. 32, pp. 729–734, Dec. 1995.

[114] Y. Miyamoto, M. Cohen, and S. Louie, "Ab initio calculation of phonon spectra for graphite, BN, and BC2N sheets," *Physical Review B*, vol. 52, pp. 14971–14975, Nov. 1995.

[115] O. Dubay and G. Kresse, "Erratum: Accurate density functional calculations for the phonon dispersion relations of graphite layer and carbon nanotubes [Phys. Rev. B 67, 035401 (2003)]," *Physical Review B*, vol. 69, Feb. 2004.

[116] L. Wirtz and A. Rubio, "The phonon dispersion of graphite revisited," *Solid State Communications*, vol. 131, pp. 141–152, July 2004.

[117] P. Pavone, R. Bauer, K. Karch, and O. Schütt, "Ab initio phonon calculations in solids," *Physica B: Condensed ...*, vol. 220, pp. 439–441, 1996.

[118] M. Hasegawa and K. Nishidate, "Semiempirical approach to the energetics of interlayer binding in graphite," *Physical Review B*, vol. 70, Nov. 2004.

[119] N. Mounet and N. Marzari, "First-principles determination of the structural, vibrational and thermodynamic properties of diamond, graphite, and derivatives," *Physical Review B*, vol. 71, pp. 205214–, May 2005.

[120] M. Mohr, J. Maultzsch, E. Dobardžić, S. Reich, I. Milošević, M. Damnjanović, a. Bosak, M. Krisch, and C. Thomsen, "Phonon dispersion of graphite by inelastic x-ray scattering," *Physical Review B*, vol. 76, pp. 1–7, July 2007.

[121] J. Maultzsch, S. Reich, C. Thomsen, H. Requardt, and P. Ordejón, "Phonon Dispersion in Graphite," *Physical Review Letters*, vol. 92, pp. 1–4, Feb. 2004.

[122] R. Nicklow, N. Wakabayashi, and H. Smith, "Lattice dynamics of pyrolytic graphite," *Physical Review B*, 1972.

[123] N. Mounet and N. Marzari, "High-accuracy first-principles determination of the structural, vibrational and thermodynamical properties of diamond, graphite, and derivatives," 2006.

[124] S. Piccinin, C. Stampfl, and M. Scheffler, "Ag-Cu alloy surfaces in an oxidizing environment: A first-principles study," *SURFACE SCIENCE*, vol. 603, pp. 1467–1475, June 2009.

[125] F. L. Gervasio, P. Carloni, and M. Parrinello, "Electronic structure of wet DNA," *PHYSICAL REVIEW LETTERS*, vol. 89, Sept. 2002.

[126] S. Curtarolo, W. Setyawan, S. Wang, J. Xue, K. Yang, R. H. Taylor, L. J. Nelson, G. L. W. Hart, S. Sanvito, M. Buongiorno-Nardelli, N. Mingo, and O. Levy, "AFLOWLIB.ORG: A distributed materials properties repository from high-throughput ab initio calculations," *Computational Materials Science*, vol. 58, pp. 227–235, 2012.

[127] G. Hautier, A. Jain, and S. P. Ong, "From the computer to the laboratory: Materials discovery and design using first-principles calculations," *Journal of Materials Science*, vol. 47, no. 21, pp. 7317–7340, 2012.

[128] S. Wang, Z. Wang, W. Setyawan, N. Mingo, and S. Curtarolo, "Assessing the Thermoelectric Properties of Sintered Compounds via High-Throughput Ab-Initio Calculations," *Physical Review X*, vol. 1, no. 2, pp. 1–8, 2011.

[129] K. Yang, W. Setyawan, S. Wang, M. Buongiorno Nardelli, and S. Curtarolo, "A search model for topological insulators with high-throughput robustness descriptors," *Nature Materials*, vol. 11, no. 7, pp. 614–619, 2012.

[130] C. W. Glass, A. R. Oganov, and N. Hansen, "USPEXEvolutionary crystal structure prediction," *Computer Physics Communications*, vol. 175, pp. 713–720, Dec. 2006.

[131] S. Curtarolo, W. Setyawan, G. L. Hart, M. Jahnatek, R. V. Chepulskii, R. H. Taylor, S. Wang, J. Xue, K. Yang, O. Levy, M. J. Mehl, H. T. Stokes, D. O. Demchenko, and D. Morgan, "AFLOW: An automatic framework for high-throughput materials discovery," *Computational Materials Science*, vol. 58, pp. 218–226, June 2012.

[132] A. Belsky, M. Hellenbrandt, V. L. Karen, and P. Luksch, "New developments in the Inorganic Crystal Structure Database (ICSD): accessibility in support of materials research and design," *Acta Crystallographica Section B*, vol. 58, pp. 364–369, June 2002.

[133] F. H. Allen, "The Cambridge Structural Database: a quarter of a million crystal structures and rising," *Acta Crystallographica Section B*, vol. 58, pp. 380–388, June 2002.

[134] A. Leach, *Molecular Modelling: Principles and Applications (2nd Edition)*. Prentice Hall, 2001.

[135] X. Gonze, B. Amadon, P.-M. Anglade, J.-M. Beuken, F. Bottin, P. Boulanger, F. Bruneval, D. Caliste, R. Caracas, M. Côté, T. Deutsch, L. Genovese, P. Ghosez, M. Giantomassi, S. Goedecker, D. R. Hamann, P. Hermet, F. Jollet, G. Jomard, S. Leroux, M. Mancini, S. Mazevet, M. J. T. Oliveira, G. Onida, Y. Pouillon, T. Rangel, G.-M. Rignanese, D. Sangalli, R. Shaltaf, M. Torrent, M. J. Verstraete, G. Zerah, and J. W. Zwanziger, "ABINIT: First-principles approach to material and nanosystem properties," *Computer Physics Communications*, vol. 180, no. 12, pp. 2582–2615, 2009.

[136] G. Kresse and J. Hafner, "Ab initio molecular dynamics for liquid metals," *Phys. Rev. B*, vol. 47, p. 558, 1993.

[137] N. M. O'Boyle, M. Banck, C. a. James, C. Morley, T. Vandermeersch, and G. R. Hutchison, "Open Babel: An open chemical toolbox.," *Journal of cheminformatics*, vol. 3, p. 33, Jan. 2011.

[138] S. R. Hall, F. H. Allen, and I. D. Brown, "The crystallographic information file (CIF): a new standard archive file for crystallography," *Acta Crystallographica Section A Foundations of Crystallography*, vol. 47, pp. 655–685, Nov. 1991.

[139] S. Kuhn and T. Helmus, "Chemical Markup, XML, and the World Wide Web. 7. CMLSpect, an XML vocabulary for spectral data," *Journal of chemical ...*, vol. 47, no. 6, pp. 2015–34, 2007.

[140] W. Humphrey, A. Dalke, and K. Schulten, "VMD: visual molecular dynamics," *Journal of molecular ...*, vol. 14, pp. 33–38, 1996.

[141] R. M. Hanson, "Jmol a paradigm shift in crystallographic visualization," *Journal of Applied Crystallography*, vol. 43, pp. 1250–1260, Sept. 2010.

[142] a. Kokalj, "XCrySDen–a new program for displaying crystalline structures and electron densities.," *Journal of molecular graphics & modelling*, vol. 17, no. 3-4, pp. 176–9, 215–6, 2000.

[143] K. Momma and F. Izumi, "VESTA3 for three-dimensional visualization of crystal, volumetric and morphology data," *Journal of Applied Crystallography*, vol. 44, pp. 1272–1276, Oct. 2011.

[144] M. D. Hanwell, D. E. Curtis, D. C. Lonie, T. Vandermeersch, E. Zurek, and G. R. Hutchison, "Avogadro: An advanced semantic chemical editor, visualization, and analysis platform.," *Journal of cheminformatics*, vol. 4, p. 17, Aug. 2012.

[145] S. Bahn and K. Jacobsen, "An object-oriented scripting interface to a legacy electronic structure code," *Computing in Science & Engineering*, vol. 4, no. 3, pp. 56–66, 2002.

[146] F. G. Sen, Y. Qi, and A. T. Alpas, "Anchoring platinum on graphene using metallic adatoms: a first principles investigation," *Journal of Physics: Condensed Matter*, vol. 24, no. 22, p. 225003, 2012.

[147] G. Profeta, M. Calandra, and F. Mauri, "How to make graphene superconducting," *ArXiv e-prints*, May 2011.

[148] M. Amft, S. Lebègue, O. Eriksson, and N. V. Skorodumova, "Adsorption of Cu, Ag, and Au atoms on graphene including van der Waals interactions," *Journal of Physics: Condensed Matter*, vol. 23, no. 39, p. 395001, 2011.

[149] O. H. Nielsen and R. M. Martin, "First-Principles Calculation of Stress," *Physical Review Letters*, vol. 50, pp. 697–700, Feb. 1983.